2018

FINITE CONTROL SET MODEL PREDICTIVE CONTROL FOR RENEWABLE ENERGY CONVERSION SYSTEMS

AGUIRRE MARTÍNEZ, MATÍAS ALEJANDRO

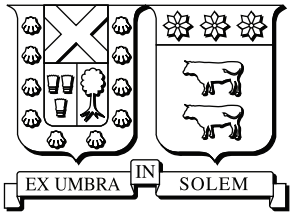

UNIVERSIDAD TECNICA
FEDERICO SANTA MARIA

REQUISITE FOR THE GRANT OF THE DOCTOR DEGREE IN ELECTRONIC ENGINEERING

Finite Control Set Model Predictive Control for Renewable Energy Conversion Systems

Author
Matías AGUIRRE

Supervisor
Dr. Samir KOURO

August 14, 2018

“I want to believe as many true things and as few false things as possible”

Matt Dillahunty

Acknowledgements

I would like to take some time to thank to everyone involved in this very long process.

In first place, my most deepest appreciation goes to my family, whose support all this year allowed me to remain strong through the difficult times that accompanied this work. Their encouragement and love has been vital to my development, and I am sure nothing could have been finished without them.

I also owe a special thanks to the POWERLAB group and AC3E, both the professors that built these groups as well as the students and people working there, that make up its soul. It hard to describe how much I appreciate the friendships that I formed in these groups and all the people that I met during these years. It is hard to imagine a better group with better people, both in the professional field as well as in the human one.

A particular thanks goes to my supervisor Samir, for all his patience and comprehension. His guidance has been invaluable and his support not only on the academic aspect but also in personal growth has no parallel.

I must finally thank to all the support given by the university and institutions that provides me with financial aid during this years. To "Qatar National Research Foundation" who, through the project "Advanced Model Predictive Control of Power Electronics Converters and Electric Drives" (NPRP 4-077-2-028) founded most of my time in this process. To "Conicyt" that provided financial aid through "Beca de Doctorado Nacional" (CONICYT-PCHA/Doctorado Nacional/2016-21161118). To the government of Canada, that allowed and funded my stay in Vancouver through the "Emerging Leaders of the Americas (ELAP) y Canada-Chile" program. To "Universidad Tecnica Federico Santa Maria" for all the support through the internal benefits for traveling to conferences and financial support.

Abstract

Model predictive control (MPC), and in particular Finite Control Set MPC (FCS-MPC), has shown many interesting characteristics that makes it suitable for multiple application of power conversion. Among these favorable traits are its high control speed response, easy implementation, the ability to include multiple non trivial control objectives into the strategy and the automatic selection of the output signals, among others. This characteristics makes FCS-MPC a suitable control strategy for renewable energy conversion systems, where a fast control response on multiple objectives permits a more flexible integration to the mains.

One of the main drawbacks of FCS-MPC strategy so far is the high variability of the switching frequency of the semiconductors. This variability leads to many problems, such as switching losses due to excessive amount of commutations, undesired resonance stimulation due to the wide voltage spectrum and uneven power distribution among the semiconductor devices. These problems are specially relevant in medium and high power generation systems, where low efficiency translates in major power losses, leading to high temperatures and fast degradation of the electronic components. Two main approaches are studied in this work to address these issues.

The first approach consists on solving the issue of variable switching frequency. This is done through a change in the control objectives by not addressing the switching frequency, but the switching period, thus being named "Period Control". A new measurement is designed to allow FCS-MPC to monitor and control the switching period, as well as some changes in the control structure to allow this measurement to be effective. Some design elements for the weight factor and the period reference are studied to simplify its implementation. Simulation and experimental results are presented to validate the proposed approach, as well as a comparison against some alternatives available in the literature.

The second approach aims to embrace the frequency variability in order to improve the control performance in terms of switching power losses. This is achieved through the use of a switching penalization with variable weight factor, strengthening the this factor for high currents, and relaxing it for low currents. The performance is evaluated through a direct comparison between the switching power losses and the harmonic distortion induced

by the reduced switching frequency. Multiple functions are evaluated, through simulation, for this variable weight, and are compared against each other and against classic switching loss reduction strategies.

Resumen

Control predictivo (MPC por sus siglas en inglés), y en particular MPC de Estados de Control Finitos (FCS-MPC), ha demostrado características interesantes que la hacen adecuada para múltiples aplicaciones en el ámbito de conversión de potencia. Entre estas características están la alta velocidad de control, fácil implementación, facilidad para incluir objetivos de control no triviales, y la selección automática de las señales de actuación, entre otros. Estas características hacen de FCS-MPC una estrategia de control atractiva para sistemas de generación de energías renovables, donde la alta velocidad de control sobre múltiple objetivos permite una integración mas flexible con la red.

Una de las principales desventajas de FCS-MPC hasta ahora es la alta variabilidad de la frecuencia de conmutación en los semiconductores. Esta variabilidad lleva a múltiples problemas, tales como altas perdidas por conmutación, estimulación de resonancias indeseadas debido al amplio espectro de voltaje, y distribución desigual entre los semiconductores de un dispositivo de conversión. Estos problemas son especialmente relevantes en sistemas de media o alta tension, donde una baja eficiencia se traduce en perdidas importantes, resultando en altas temperaturas y una rápida degradación de los componentes electrónicos. En este trabajo dos estrategias son analizadas para abordar estos problemas.

La primera propuesta consiste en resolver el problema de frecuencia de conmutación variable. Esto se logra mediante un cambio en los objetivos de control, no abordando el problema desde la frecuencia, si no a través del periodo de conmutación, siendo bautizada como “Period Control”. Para esto, una nueva medición es diseñada, lo que permite a FCS-MPC monitorear y controlar el periodo de conmutación, ademas de cambios en la estructura de control para permitir que esta medición sea efectiva. Algunos elementos de diseño para el factor de peso y la referencia de periodo son estudiado con el fin de simplificar su implementación. Simulaciones y resultados experimentales son presentados para validar la propuesta, además de comparaciones con alternativas previamente propuestas por la literatura.

La segunda propuesta apunta a disponer de esta frecuencia variables con el objeto de mejorar el desempeño de control en términos de las perdidas de potencia. Esto se logra mediante el uso de una penalización de la conmutación con un peso variable, fortaleciendo

este peso para altas corrientes, y relajándolo para corrientes bajas. El desempeño es evaluado mediante una comparación directa entre las perdidas causadas por la conmutación y la distorción armónica provocada por la reducción de las conmutaciones. Múltiples estrategias son evaluadas mediante simulación para este peso variables, y son comparadas entre ellas y contra estrategias clásicas de reducción de conmutaciones.

Contents

List of Figures

Chapter 1

Introduction

Since the early years of the Industrial Revolution the energy consumption around the globe has been increasing exponentially. This increased demand has been addressed through the consumption of mostly nonrenewable sources. One of these sources are the fossil fuels, such as coal, crude oil or natural gas, which are also the main cause of pollution and climate change around the globe. An alternative to the fossil fuels are the renewable energy sources, such as hydro, solar or wind power sources, which allow to reduce up to some point the negatives effects that fossil fuels generate on the environment.

1.1 Renewable Energies

In the last decades the development of alternative energy sources has been on the rise, allowing for multiple generation systems to be integrated to the mass market and electric grid, with their respective capabilities and limitations. This growth is caused both by the connection of high power generation plants, as well as the integration of distributed generation to the grid. This growth is especially noticeable for wind power and photovoltaic technologies, for which the price reduction and new battery developments had allowed a massive boost of their popularity. Though it is still a growing portion of the overall energy generation, as shown in figure 1.1 [1], its growth has been so important in the last years, and its effects in the emission of green house gasses so noticeable, that its makes it a fertile ground for new researches and development. Despite this growth, there is still much room to grow in terms of overall energy production, since, as shown in figure 1.2 [1], a big portion of the generation comes from non-renewable sources.

The particular situation of Chile, due to its geography, places it at a great advantage regarding the renewable energy potential. The Atacama desert presents the highest solar radiation on the world, there are strong winds through all Chilean longitude and a high

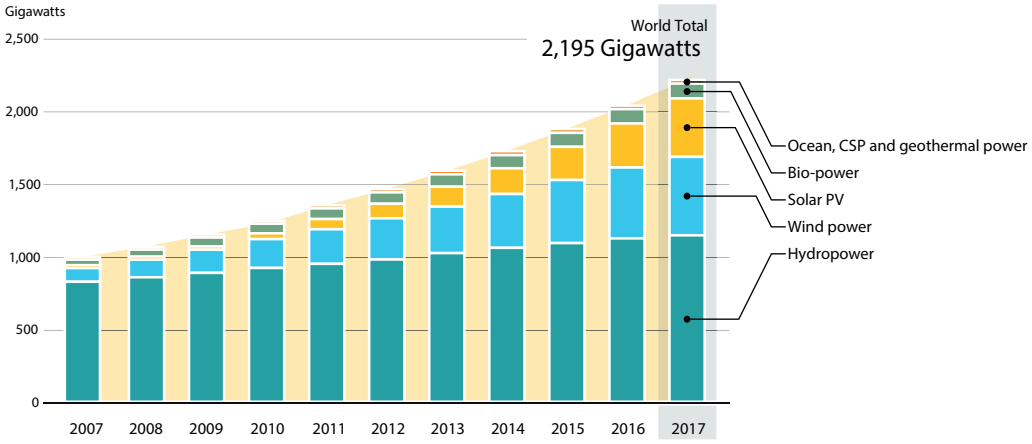

Figure 1.1: Global renewable power capacity [1]

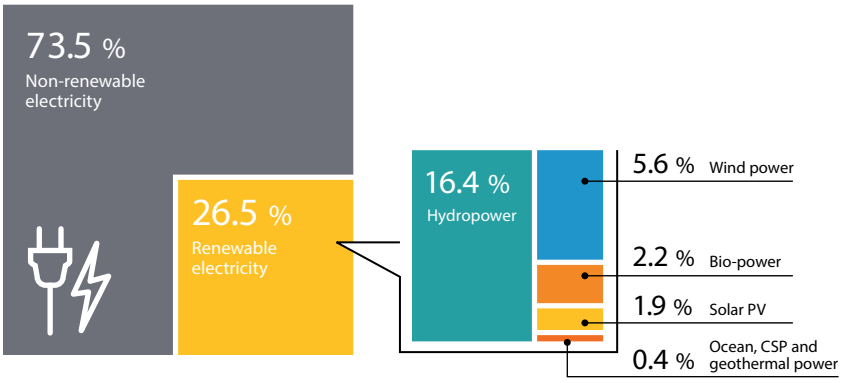

Figure 1.2: Estimated renewable energy share of global electricity production, End-2017 [1]

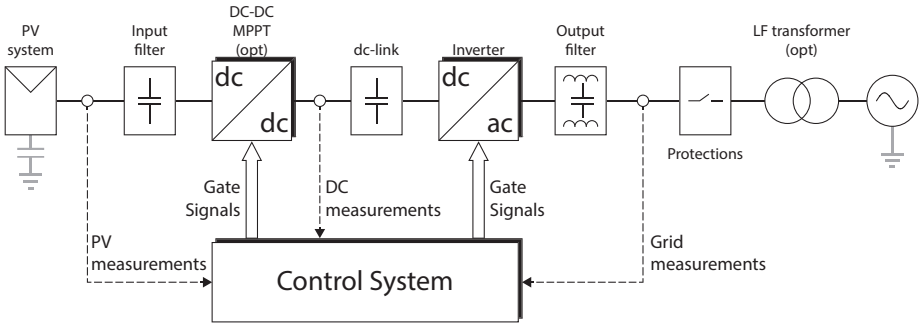

Figure 1.3: General structure of a PV generation system [2]

potential in wave and geothermal power [3, 4]. This potential, along with the energy demand, had lead to multiple projects to increase the generated power output using renewable sources, as well as increasing the research funding for these areas.

1.2 Power Conversion Systems

One of the most important elements in the electric power generation is the power converter. This device is the responsible of adapting the electric output from its raw source into a more manageable form. For photo-voltaic (PV) systems this may translate into isolating the voltage of the PV panels from the rest of the systems, or generating the sinusoidal current for the connection to the mains, while for wind power systems means reshaping the output voltage in phase and magnitude to reach a proper connection while managing a proper speed control.

1.2.1 PV Systems

Figure 1.3 illustrates the general structure used for the connection of a PV system to the mains. The PV system illustrated here can be composed of a single module, a string of modules connected in series or an array of parallel connected strings, as required by the power output and power converters. The possible configurations for an array of PV panels and the respective converters used for its connection to the grid is illustrated in figure 1.4. The main criteria used to select which configuration has to be used are the power generation levels, the required flexibility and the efficiency of the setup.

The centralized configuration is the most widely used for large scale PV plants, usually in the range of over 1.6 MW. It has the advantages of being fairly simple in design and

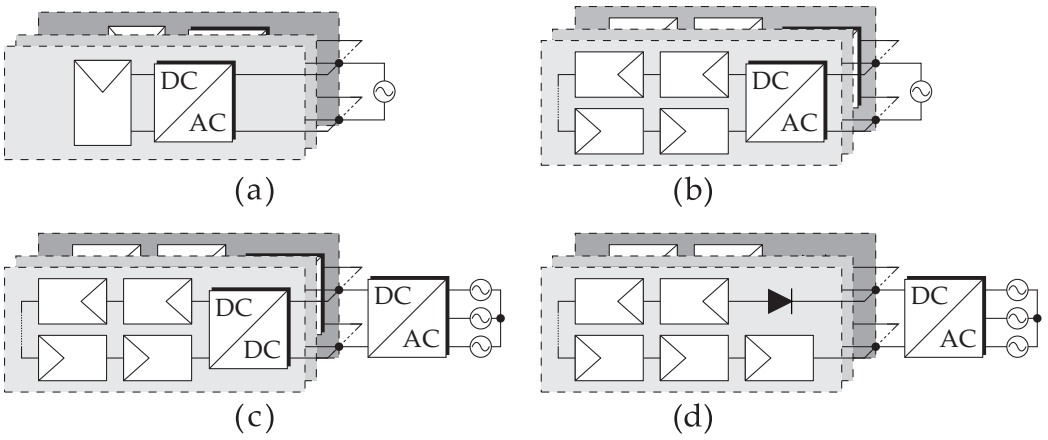

Figure 1.4: PV system configurations: (a) AC-module configuration, (b) String configuration, (c) Multi- string configuration and (d) Centralized configuration [2]

control, as well as being of low cost per watt installed. Nonetheless it lacks the capability of optimizing each string independently, thus reducing its efficiency when part of the array is shaded or misbehaving. The mains connection for this configuration is commonly implemented through a 3-phase DC-AC converter. Some of the most used topologies for three phase mains connection are presented in figure 1.5 [2]. The criteria for the selection of one over the other goes in line with the requirements of the system, such as harmonic distortion, maximum dc-voltage limits, reduction of switching or conduction power losses, etc. In general, the higher amount of semiconductors goes in line with a better waveform, but tends to be more expensive and harder to control.

The string configuration, usually implemented for less than 10 kW systems, allows to split the MPPT for a smaller string of PV panels, thus increasing the energy output per panel installed. Since it only connects one PV string at a time it is better suited for low power systems, such as rooftop. Some common converter topologies used for this PV configuration are presented in figure 1.6 [2]. An important criteria for the design and control of these converters is the mitigation of the leakage current through the parasitic capacitor, shown in grey in figure 1.3 [2]. The source of this current is the high frequency switching voltage at the PV panel, which leads the capacitor to present a small impedance, allowing for conduction between the PV panel and the ground [5]. This can be solved through the use of galvanic isolation, as shown in 1.6(e-f), or through the use of additional semiconductors, 1.6(a-d), to propose alternative paths to the currents and voltages.

The multi-string configuration works as an alternative between the two previous, allowing for a dedicated MPPT for each string, while managing high power levels, usually

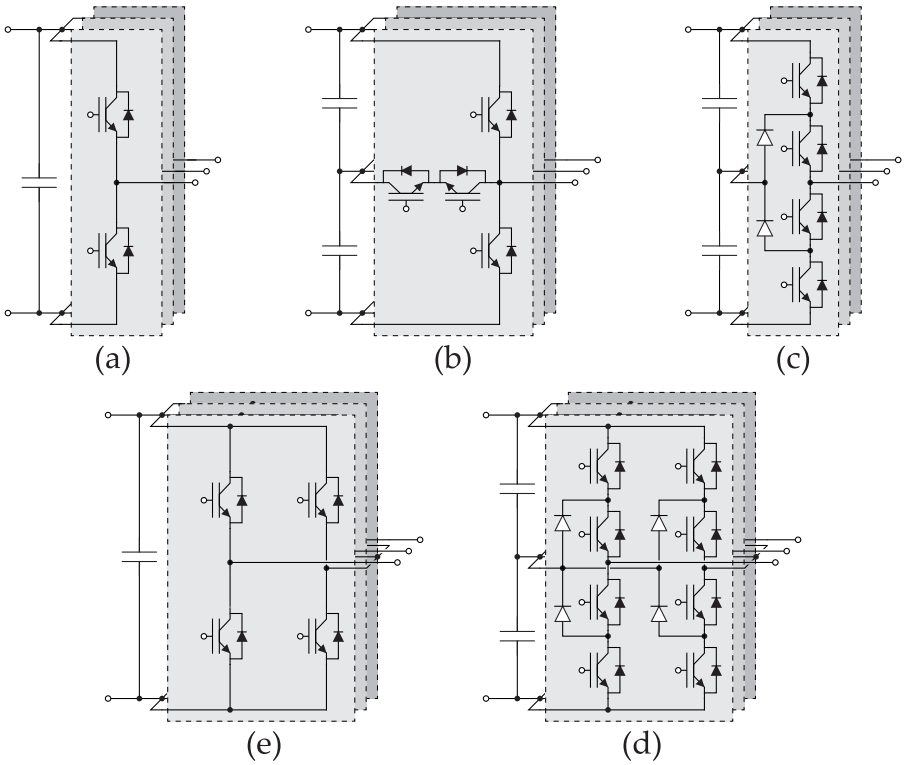

Figure 1.5: Common 3-phase DC-AC power converters: (a) 2-level converter, (b) T-Type converter, (c) NPC Converter, (d) H-Bridge Converter and (e) H-Bridge NPC Converter

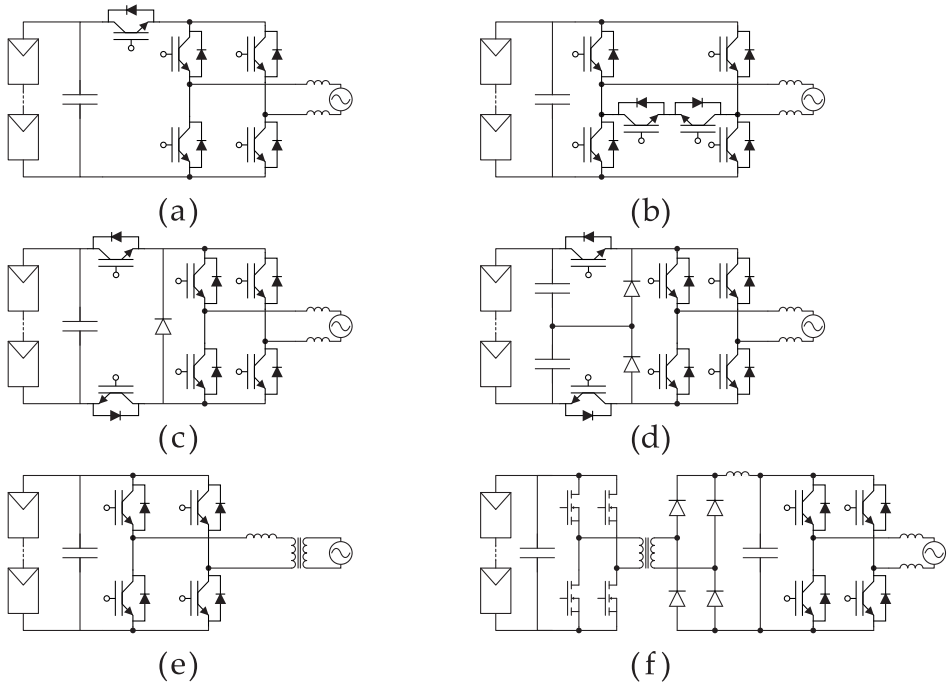

Figure 1.6: Common DC-AC converters for PV systems: (a) H5 converter, (b) HERIC converter, (c) H6D1 converter, (d) Full-bridge DC bypass (FB-DCBP) converter, (e) H-bridge with low frequency isolation and (f) DC-DC stage with high frequency isolation

up to 500 kW. Since the PV strings and the converter are decoupled by the dc-link it is possible to achieve a robust control to the mains while extending the PV modules operating range. The modular nature of this configuration makes its operation more robust to failure or weather conditions, as well as being fairly easy to disconnect some modules for maintenance or replacement. This configuration can be constructed as a three-phase or single phase system, sweeping through a wide range of power levels. The most common DC-DC converters for this configuration is the Boost converter, for non-isolated connection, or a high frequency galvanic isolated H-bridge, similar to the DC part in 1.6(f).

Finally, the AC-module configuration makes use of a dedicated converter for each PV module, thus being also known as micro-converter configuration. The power level for this configuration is around 300W, and due to its dedicated converter and control system, it is the most expensive per watt produced. Nonetheless, it is the mos efficient system in terms of power capture, since the dedicated MPPT permits the extraction of the maximum available power. Due to the low voltage level of a PV module, the converter requires a mandatory elevation stage, commonly implemented through a boost-converter or variations of it [6] or flyback converter [2]. A common trend for this dc-dc stage is the use of interleaved converters, which allow better waveforms with less switching frequency per semiconductor, though at the expense of and increased count of semiconductors

1.2.2 Wind Power Systems

A particular consideration in the design of wind power generation systems is the power scale for the wind turbine. Unlike many power sources that may extract energy at a wide variety of power levels, wind power thrives mostly at high power. This is due to the nature of the power transfer form the blades to the main generator, where the power extracted form the wind increases linearly with the covered area, and not the size of the blades. This permits a substantial growth in the harnessed power from small increments in the wind turbine system size, thus being of the interest of the producer to account for the biggest possible blades.

Illustrated in figure 1.7 are the most common converter structures used in the power conversion of wind turbine systems (WTS), for the most common electric machines used for them. Due to the lack of technology in the early years of WTS, many of these systems allowed for partial or no control of the turbine speed through the simple connection of the machine to the mains. These machines behave like high inductive loads, thus requiring capacitor banks to address the reactive power. This is illustrated in figure 1.7(b). Along with this problem, was the fact that due to the lack or restriction of rotation speed control, it was not possible to achieve the maximum power extraction for variable wind conditions, rendering the power transfer somewhat inefficient. In current times the best established

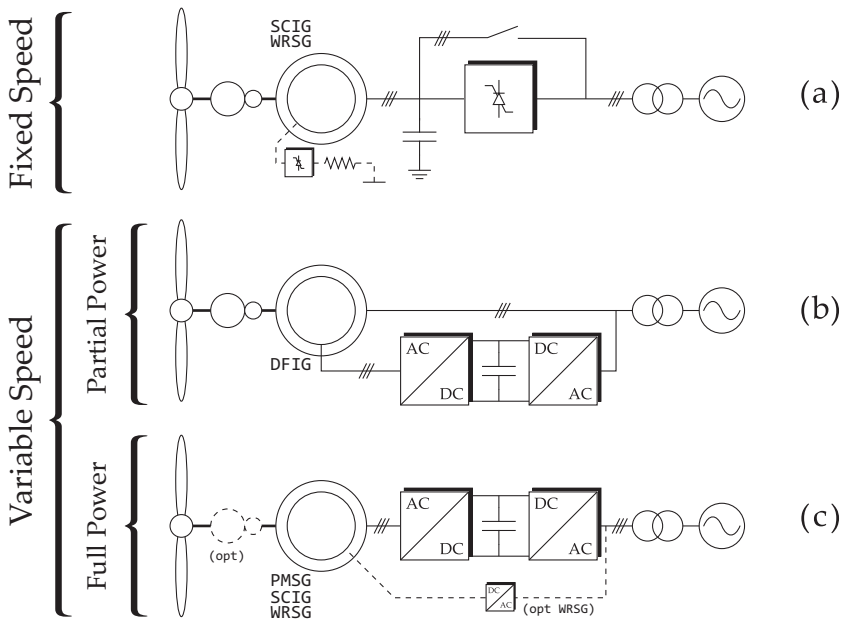

Figure 1.7: Common wind energy conversion systems (WECS) configurations: (a) Fixed speed configuration, (b) Partial power configuration for doubly fed induction generator, (b) Full power configuration

solution is the variable speed wind turbine, that allows to properly control of the rotation speed, thus being able to reach the maximum power extraction from the wind.

The partial power configuration 1.7(a) is implemented for doubly fed induction machines. This configuration allows to control the speed of the machine by controlling the rotor field, which allows to control the electric torque. The main advantage of this configuration is that the rotor field control requires much less current for the power transfer than the whole system, up to 30%, which allows the use of smaller semiconductors to manage a much larger generation. With this configuration it is possible to manage a proper control of the current generated by the converter, thus allowing a direct connection of the machine to the mains. The main disadvantage of this configuration lays in the challenging control problem that raises in the case of grid faults. Another problem is the absolute requirement of slip ring in the electric machine, which demand a higher maintenance cost.

Another alternative for WTS is the use of a full scale power converter configuration, as shown in 1.7(b). Since this configuration permits a full control of the currents, frequency and phase, a full power control becomes available. This permits the use of any kind of electric machine, such as Asynchronous Generator (AS), Permanent Magnet Synchronous

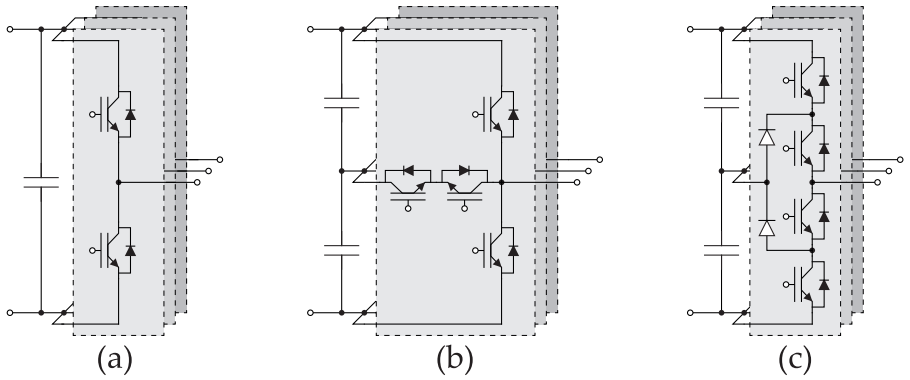

Figure 1.8: Common 3-phase DC-AC power converters for WECS: (a) 2-level converter, (b) T-Type converter, (c) NPC Converter

Generator (PMSG) and Wound Rotor Synchronous Generator (WRSG). The lack of need for slip rings in the machine permits a much more robust mechanical system, while the full control over the electric variables allow a higher pole count for PMSG and WRSG, which permits a simpler or even removed gearbox. Both the lack of slip rings and the higher pole count allow a less costly maintenance. The main disadvantage of this configuration lays on the higher cost of its components since the converter is bound to stand all 100% of the power flow.

The power converters used for either of these configurations are usually build as 3-phase DC-AC converters, in a back-to-back configuration. The DC-AC converters most popular in the industry are illustrated in figure 1.8. An important factor in the design of these converters is the fact that the DC link voltage is limited to levels that allow a connection to the mains. This means a minimum value of 600(V), and a maximum of no more than 1000(V). This limitation, along with the high power levels that this systems need to mange, lead to very high current values. Though new technologies allow better and more powerful semiconductor devices, the most straight forward solution is the use of multiple identical converters in an interleaved configuration. This allows not only to spread the transferred power between multiple converters, but also improve the output waveform, thanks to a proper use of the additional semiconductors.

1.3 Converter Control

The control of power converters have been a thriving research topic in the field of power electronics. This interest in the area rises form the multitude of topologies used in

the power conversion process, either for low, medium or high power applications, as well as the multitude of control objectives that may be addressed [7–9].

Among control strategies, the most commonly used by the industry belong to the pulse width modulated based control (PWM). These strategies are widely used thanks to the low technology requirement for its implementation, demanding in many cases only analog control loops, which rendered them the only option when the microprocessor technology was not developed enough. Among the most common requirements for the control of power converters are the low switching frequency, low harmonic distortion and fast dynamic response, which cannot be simultaneously satisfied by PWM [10], which calls for a different approach to control problem. Today most control strategies are implemented in digital platforms, as an industry standard [8], which opens the door for more complex variables to be analyzed and controlled.

1.3.1 Control Requirements for Renewable Energy Systems

One of the critical characteristics of renewable energy sources is its unreliability in terms of power output. This can be seen for the case of PV power, where the state of the weather can severely hinder the generated power, and even in the best conditions its limited to a varying output during the day. In a similar way wind power generation is constrained by the weather, and can be turned inoperative for either too weak or too strong winds. The power output for multiple conditions is illustrated in figures 1.9 for PV cells, and 1.10 for wind turbines.

In order to allow the best possible power extraction against multiple weather conditions, the implemented control strategy must aim for the optimization of either the voltage, in case of PV, or the rotor speed, for the WTS. This is achieved by a Maximum Power Point Tracking (MPPT) algorithms, which can take many forms in accordance to the requirements of the system and the available control platforms [11]. An important point to notice from these graphs is that for both systems a very careful control has to be implemented to reach the best possible performance.

In the case of PV systems, the temperature is a fairly stable variable along a day. Nonetheless, the irradiation can change dramatically in very short time spans. This can occur due to the presence of clouds, bird activity in the area or some terrain feature, all of which may cause obstruction to the panels. The faster and more accurate is the MPPT strategy, the better is the power generation.

The same conclusion can be extracted for WECS, though for a different cause. As can be seen in figure 1.10, when properly controlling the rotor speed to reach the MPP the relation between wind speed and power extracted is of third order. This means that a small fall in the wind speed leads to a big dip in power. This can be appreciated in the

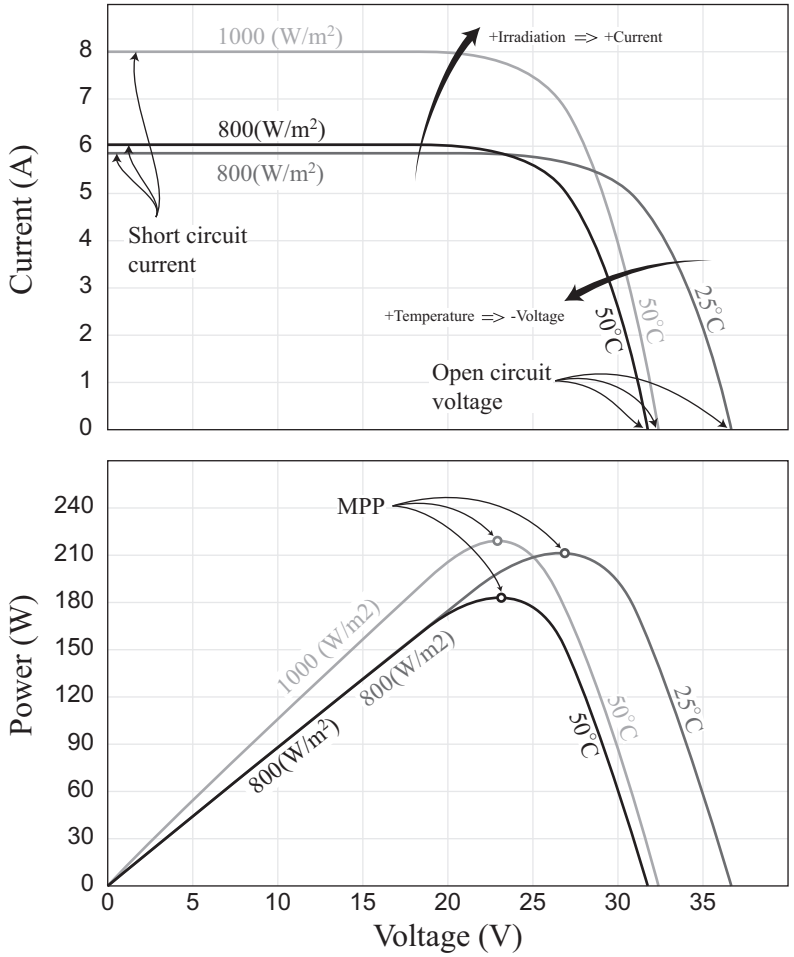

Figure 1.9: Current and Power curves for a photo-voltaic cell

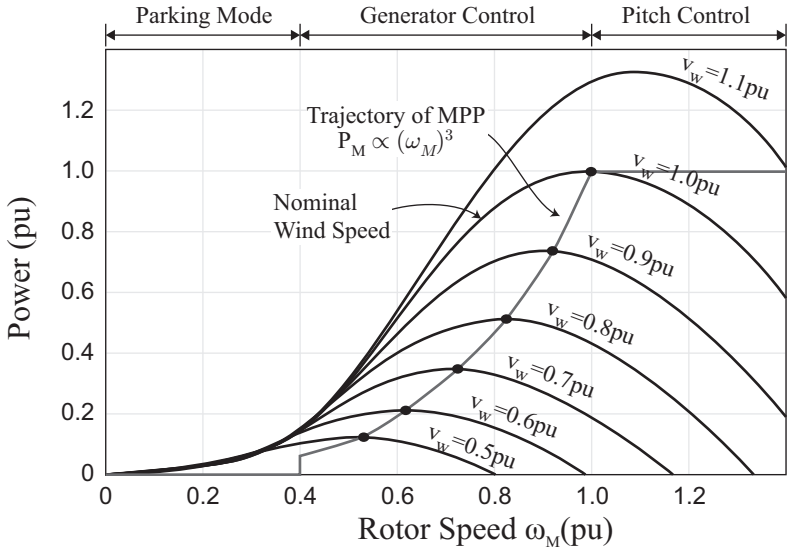

Figure 1.10: Wind turbine power-speed curves and maximum power point (MPP)

difference between the curves for nominal wind speed and 80% wind speed, where the extracted power is less than half. This also is the reason why bellow 40% the nominal wind speed it is no longer feasible to remain operating, since the available power is less than 10% of the system capability.

Along with the search of the maximum power point, any system connected to the mains is bound to certain restrictions, in particular for the power generation system. Though these restrictions are mostly defined by each country through their own regulation, many have established some common criteria that a power generation system should abide to.

One of these criteria is the possibility of reactive power injection up to certain limits. This means that the generation systems must by oversize, albeit slightly, to be able to provide the extra current required by the mains.

Another requirement is the proper fault ride through response, where the grid voltage drops bellow a critical level, which may be caused by a major failure in the grid. A proper fault response is such that the system is still capable to provide electric power to the mains when the voltage drop is small or fast, suggesting just a dip in grid stability, instead of a black out.

1.3.2 Voltage Oriented Control

To date, one of the most widely used control strategies for the control of grid connected power converters is Voltage Oriented Control (VOC), illustrated in figure 1.11. The base of this strategy is the synchronization of the control system with the mains voltage through the use of a PLL algorithm. For the 3-phase controller it is possible to describe the system as a static one by rotating the variables with the voltage. This rotation permits the use of simple PI controllers in a cascade structure, addressing current control in the inner loops, and voltage control in the outer loops, as shown in figure 1.12. An important aspect of this rotation is the need of a decoupling factor between d and q current controllers in order to fully split their controllers. A similar structure can be achieved for a single phase controller, through the use of resonant PI controllers (PR), since rotation is not possible in single phase systems.

In both cases the output of the controller is the voltage that the converter must generate, and this is given to the PWM module for its conversion to gate signals. These signals are then given to the converter to close the control loops.

An important issue with these strategies is the fact that a cascaded structure is bound to have bandwidth limits. This limits rise from the need of the external control loops to wait for the internals loops to properly reach their control objectives. A common criteria for the relation between loops is the use of a factor of 10 in the respective bandwidths. This way, if the voltage control needs to reach up to 300 (Hz), then the internal current control has to function properly up to 3(kHz) to not disturb each other. Therefore, this control structure forces either a high frequency bandwidth on the internal loop, or a low bandwidth on the external loop. A high frequency internal loop is not always feasible due to limitations in the semiconductors, and a low frequency external loop may allow undesired behavior in the control performance to appear along with slow control speed. Therefore, it is desirable to have a control strategy that permits a fast control performance without the need of a cascaded control structure.

1.4 Predictive Control

Thanks to the explosive development of digital signal processing theory and technologies, more complex techniques have become available for both research and industry implementation. Among these strategies are, as an example, fuzzy control, sliding mode and a whole family of predictive controllers. In most commercial systems, these new control strategies have shown improvements on either particular applications, or approaching different control objectives [7]. Due to their relative recent history when compared with more classic and mature controllers, and thanks to the technological advancements, these strate-

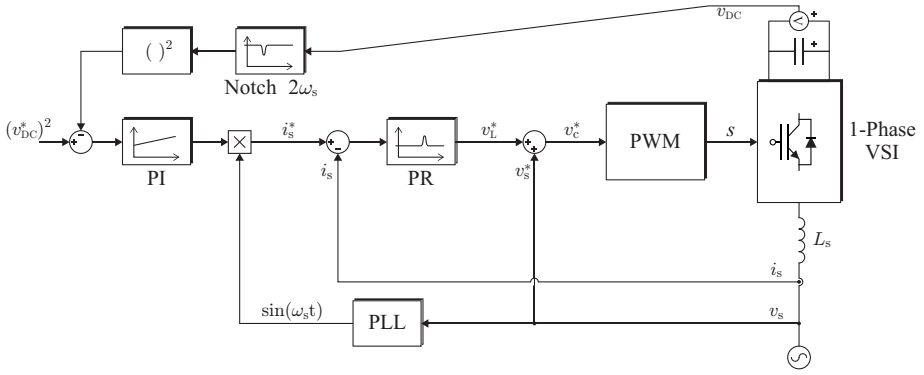

Figure 1.11: Single phase voltage oriented control diagram

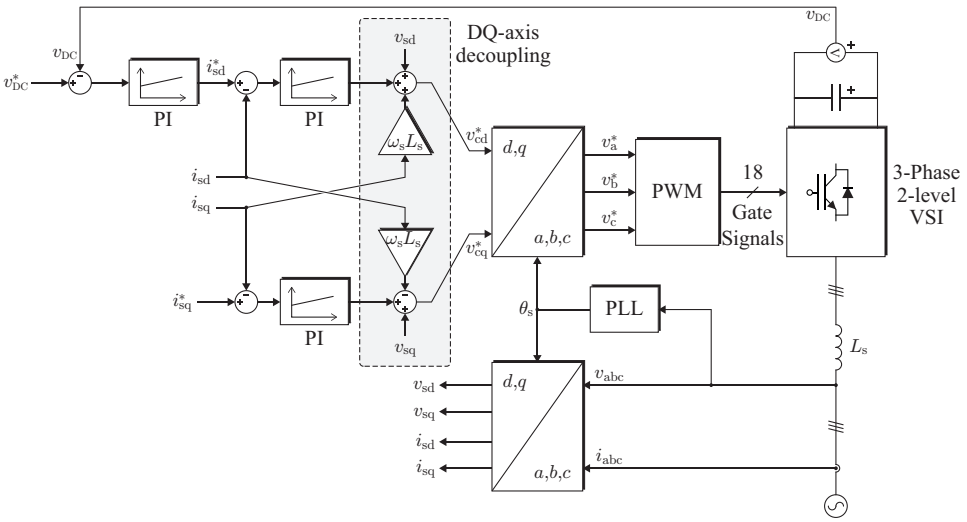

Figure 1.12: Three phase voltage oriented control diagram

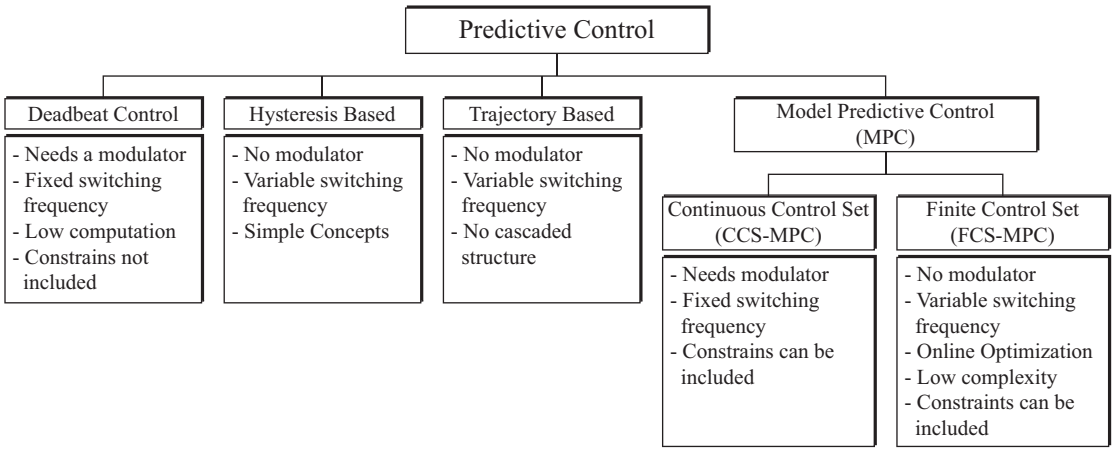

Figure 1.13: Predictive control methods use in power electronics

gies show much room for improvement and become a fairly attractive research area. The main improvement these new strategies provide over classic control system is the possibility of including non-linear control objectives, such as constrains, parameter variations, non-linear functions, etc, as well as including all control objectives in a single control loop. Is in this context that Model Predictive Control (MPC) appear as an attractive alternative to classic control thanks to its many features.

Predictive control, as a family of strategies, has been in development for quite some time already. The first applications of predictive control were in slow and highly complex industrial plants. Its first appearances in power electronics are in the control of nonlinear system, such as electric machines, where classic controllers lack on either the required speed or the flexibility to perform a satisfactory control [12].

Predictive control belongs to the family of optimal control strategies. This family of controllers is characterized by the use of a functional in charge of establishing the quality that a control action has on the system. The functional may take various control objectives, such as the system's state error, settling time, output ripple over some variables, etc, as well as a combination of these. Independent of the strategy, all members of this control family need a goal that is followed by an optimization algorithm. Some show advantages with nonlinear systems, while others present better response time and control speed. A brief overview of the main classification of optimal controllers frequently used in power converters is sumarized in figure 1.13 [13].

1.4.1 Dead Beat Control

Dead Beat control is a discrete time strategy that focuses on reaching a desired state of the system in the shortest time possible. This strategy uses the model of the system to compute a set of input actions that allows the system to arrive to its reference as fast as possible. The omptimality in this strategy comes then from the required time to reach the reference. For a linear time-invariant system (LTI), an unconstrained input can be chosen to make the state follow the reference as fast as the systems order in sampling periods. This means that a second order system can be forced to arrive to its reference in as few as 2 samples.

One of the main disadvantages of this strategy is its strong dependence of the model. As the system model is being used to find the optimal input, any mistake in the modeling can transform into a big over or under actuation, which will not arrive to the reference in the desired time. In some cases this mistakes in modeling can cause instability or undesired resonances. Another disadvantage is the difficulty of including nonlinearities or constrains, since the controller tries to produce an exact and intense actuation that would lead the system to its objective.

1.4.2 Hysteresis Based

The main goal of Hysteresis Based controllers is to keep the system inside a set of boundaries. The optimization process that gives this algorithm the characteristic of optimal controller occurs when the state of the system reaches a boundary. At this instant, the controller evaluates the different input possibilities in order to find the one that provides the longer time inside the limits. The goal of this decision is to reduce the switching frequency to the minimum such that the boundaries are respected. Some publications had shown this method and some strategies to improve its computation time [14].

1.4.3 Trajectory Based

The main goal of this control strategy is to force the system variables into predefined trajectories. As shown in [12], the actuation is chosen based on predefined state curves that the system would follow as a function of the present state. As a result, when the system cross an objective curve, a modification in the actuation state will be performed in order to follow it. When the system arrives to the reference, or a nearby region, the controller makes the actuation force the system to follow trajectories that surround this reference as could be with an Hysteresis controller. Similar to deadbeat control, this method is extremely sensitive to parameter deviations, since the chosen trajectories only reach the desired state if all the computation is correct.

1.4.4 Continuous Control Set Model Predictive Control

CCS-MPC makes use of the model of the system to provide an optimal control action according to a predefined cost function. With CCS-MPC, the computation for this actuation can be not performed online, but obtained previously as a function of the state. This allows the controller to quickly choose the optimal control action based on affine function that takes different forms in the state space. The chosen actuation is usually implemented as a PWM signal, where the reference is provided by the controller, but the semiconductor is switched accordingly. The main drawback of this strategy is the intensive mathematical background required for its implementation, which make it an unfriendly strategy for newcomers.

1.5 Finite Control Set Model Predictive Control

The particular optimal control configuration to be studied in this document is Finite Control Set Model Predictive Control (FCS-MPC). This strategy is especially suited for its use in power converters, where the possible control actions are limited by the amount of feasible semiconductor states [8, 15]. Though explained in more detail in following chapters, the core idea behind this control strategy is to establish a model of the system to be controlled and use this model to compute the system's future state, that is, predict its behavior. These predictions are evaluated and the optimal action is chosen as the one that leads to the best available predicted state. As long as the model of the system is properly constructed, it is possible to include multiple control objectives without adding major complexity to the control structure.

So far in the literature FCS-MPC has been successfully implemented in a wide variety of applications, and addressing multiple control objectives. From power quality regulation [16–18], machine drive control [19–24], grid connected systems [25, 26] and power supplies [27, 28], the possibilities for predictive control are ever expanding. Thanks to this feature, it becomes quite easy to include all the control objectives involved in the power generation for renewable energies, which makes FCS-MPC an atractive alternative to classic controllers.

The main disadvantage of this control strategy is the variable switching frequency generated by the controller. As the nature of the strategy is to aim for the best state according to the designed cost function, if no action is taken to control the switching events, then the controller would completely disregard it as an issue. Aside from the high frequency, there is the problem of variability in the switching patterns, which means an almost flat frequency spectrum, which is not a permissible characteristic of grid connected systems due to the stimulation of resonant modes.

So far in the literature the most successful solution for the issue of variable switching frequency comes in the form of modulated strategies that apply the principles of predictive control to compute the times each state should remain active [29–33]. This strategy, though effective in controlling the switching frequency, is not as easy to implement as FCS-MPC due to the details involved in the computation of the optimal actuation. Also, since the actuation is now continuous in time by choosing the time at which this takes place, now a modulator is mandatory for the proper control of the system, which is an unnecessary step in FCS-MPC.

Other proposed strategies aim to extend the prediction horizon, or fraction the sampling time to generate a discrete modulation. Nonetheless, these strategies are bound to a fixed predefined switching frequency, require the use of a modulator, are harder to construct, harder to include non linearities and constrains, and do not make use of the flexibility that FCS-MPC can allow to the control.

1.6 Hypothesis

Regarding FCS-MPC, some alternatives have been proposed that address the issue of switching frequency without the use of a modulation. Nonetheless, none so far have been able, up to the author knowledge, to produce a stable switching pattern that allow both a low and stable switching frequency with a clean frequency spectrum, and a proper tracking of other control objectives.

The main objective of this document is to present a new alternative to the switching frequency control that permits a clean spectrum and a very stable switching frequency along with the proper control of other control objectives. This strategy should be compatible with the core of FCS-MPC design, that is, a simple to design and integrate control objective. The proposed strategy must also demand a low computational burden, due to the high sampling frequency commonly required for FCS-MPC.

Along the line of reducing the power losses in the converter, a new strategy is proposed in opposition to the use of a stable switching pattern, embracing the variable switching performance to allow a more ad-hoc switching pattern. This strategy makes use of the model of the switching power losses to better choosing the optimal switching state. The proposed strategy is to be evaluated against classic control and raw predictive control to highlight its performance.

1.7 Thesis Structure

Chapter 1: Introduction

An overview of renewable energy systems and their growth is presented in this chapter, with a special emphasis on the power converters that are commonly used for these systems, as well as the control objectives that these must comply. A brief summary of predictive control is presented, as well as an introduction to Finite Control Set Model Predictive Control. The hypothesis that drives this work is stated and the structure of the document is defined.

Chapter 2: Finite Control Set Model Predictive Control

The control strategy of FCS-MPC is explained in detail, reviewing its operating principle as well as its components. A summary of the most common discretization strategies used for the prediction stage is presented, along with the advantages and limitations of each. A small set of converters are analyzed as an example of different systems and their best suited discretization. The cost function is studied, in a similar fashion, evaluating the most commonly used alternatives and their characteristics. Finally a review of the documented strategies to address the switching frequency problem are presented.

Chapter 3: Period Control

This chapter presents one of the main contributions of this work. Here the strategy of Period Control is studied in detail, from its operating principle to the cost function design. The performance of Period control is analyzed and compared with PWM, to establish the similarities in their performance. An NPC converter and an Interleaved Boost converter are analyzed in more detail to exemplify some cases where Period Control, in its raw form, is not enough to achieve a proper control. Finally a few improvements are proposed to the basic strategy to achieve an even better performance.

Chapter 4: Experimental Results

The experimental set up used to validate the performance of Period Control is presented. The simulation performance is replicated in practice and reported. Later a comparison between Period Control and the other frequency control strategies is presented and the results are analyzed in detail, highlighting advantages and disadvantages of each.

Chapter 5: Switching Frequency Variable Weight

The strategy of Variable Weight factors is presented in this chapter. A brief summary of the work that inspired this contribution is presented and analyzed. The switching losses are discussed in detail, and the benchmark used to evaluate the performance of different strategies is presented. The Variable Weight factor is presented for a 3-phase system, along with the different alternatives to change this weight factor, and the fine tuning of a Shift constant. Finally, Period Control is combined with the Variable Switching factor and its performance studied

Chapter 6: Conclusions

In this last chapter, the main conclusions of this work are presented along with some possible future works that derive form this.

Chapter 2

Finite Control Set Model Predictive Control

As a control strategy, FCS-MPC is extremely versatile, being implemented in multiple systems, for various control objectives and for a wide range of converters.

2.1 Operating Principle

As with any control strategy, the goal of FCS-MPC is to establish an actuation that allows the system, in state $x(t_k)$, to reach a desired or reference state $x_r(t_k)$. For power converters and drives this actuation is the state of the n switches that compose the device, $S(t_k) = \{s_1(t_k), ..., s_n(t_k)\}$. Each of these switches can take up to two different states, either On or Off, and the collection of all the possible and allowed combinations corresponds to the control set, $\mathbf{S} = \{S_1, ..., S_m\}$. For many systems $m = 2^{n/2}$ since all switches are paired in their operation, and these pairs are independent from each other. Nonetheless, for some converters, like T-type or NPC converters, not every combination is available, reducing the options.

Since the amount of switches in a converter is finite, also are the states these can take. Therefore, it becomes possible to compute the future state of the system for each element in $\mathbf{S}$. For regularly sampled systems, this would be computing all predictions of the state of the system, $\mathbf{x}_p(t_{k+1}) = \{x_{p1}, ..., x_{pm}\}$, based on the data collected at time t_k. This can be done through the use of a prediction function $\mathbf{x}_p(t_{k+1}) = f_p\{x(t_k), \mathbf{S}\}$, that can be derived from the model and parameters of the system. To select the control action to be applied, a cost function, $\mathbf{J} = f_j\{x_r(t_{k+1}), \mathbf{x}_p\}$ is used to determine how close each of the predicted states is to the reference. The closer a prediction is to the reference the smaller the value it yields in the cost function. Thus, the control action that yields the prediction closest to

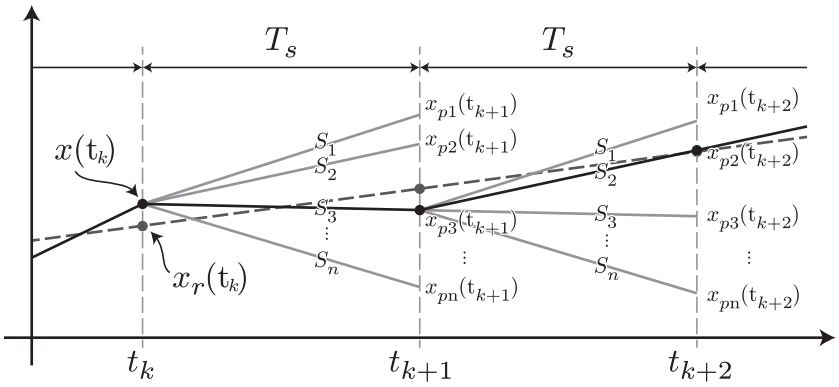

Figure 2.1: FCS-MPC operation

the reference is optimal, and is chosen to be applied in the next switching moment.

The whole process is illustrated in figure 2.1. At time t_k a measurement of the state of the system, $x(t_k)$, is taken. This measurement is used to compute the future state x_{pi}, for each possible control action S_i , $i \in \{1, ..., n\}$. Each of these predicted states is evaluated in the cost function J, searching for the one that yields the smallest tracking error. In this example S_3 leads to the state closest to the reference at time t_{k+1}, thus being chosen by the controller. This process is repeated at every sample time, always searching for the actuation that aims fastest to the reference for the next step. Figure 2.2 presents the step by step process of this control technique.

2.1.1 Delay Compensation

An important consideration in this algorithm is the fact that the time required to get the measurements form the system, to compute all the predictions and to evaluate the optimal output is not negligible, especially when the sampling time T_s is short, which is a desired trait in order to improve the control bandwidth. Since it is not possible to know the optimal state required for time t_k a two step prediction is implemented [34]. With this correction, the optimal actuation is not computed for the current time, t_k, but for the next one, t_{k+1}. Based on the example shown in figure 2.1, at time t_k the actuation S_3 is applied to the system and only the prediction of S_3 is computed, to obtain the new state $x_{p3}(t_{k+1})$. Then, is this new state is used a basis to compute all the predictions for time t_{k+2}. The optimal control action is selected, S_2 in this case, and stored to be used for the next step. At the next sample time, t_{k+1}, S_2 is selected and applied to the converter and the whole process repeats. Figure 2.3 illustrates the corrected algorithm, where measurement and actuation

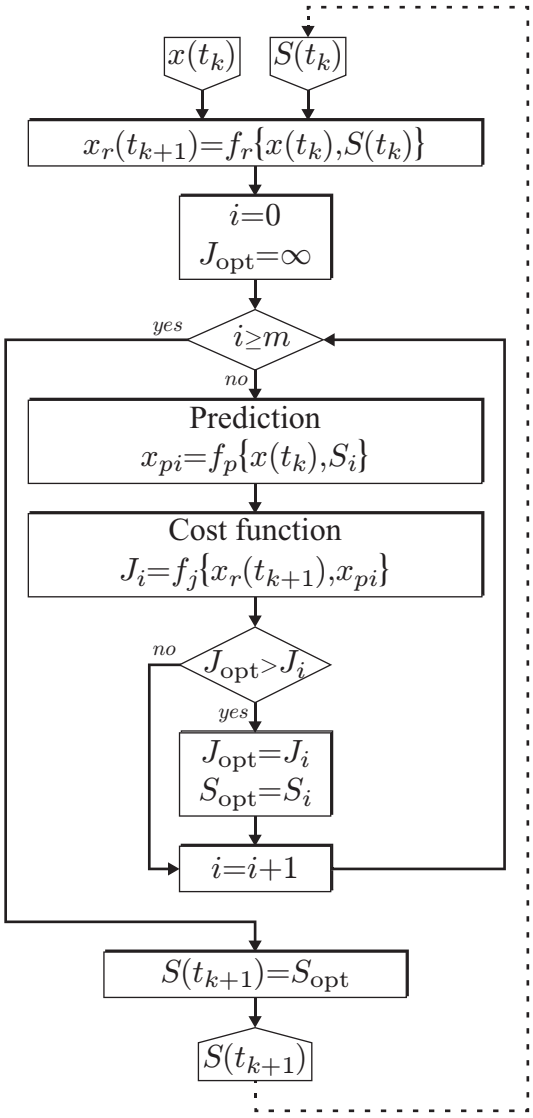

Figure 2.2: Flow diagram of finite control set model predictive control

takes place prior to the whole process at each sampling time.

It is important to note that the reference does not need to be constant nor linear as shown in 2.1. The only requirement for the reference is that it can be computed or defined prior to the instant it would be evaluated in the cost function. This way the two step algorithm can be properly applied to the system. Also, though the example presents a single control variable, the structure of FCS-MPC permits multiple variables to be included, as well as multiple control objectives, not necessarily included among the states of the system.

2.2 Model Discretization Strategies

The model of a system is the set of equations that describe its dynamics and constrains. For most systems, these equations arise from physical laws, such as Maxwell equations, conservation of energy or momentum, etc. These models are most commonly of the form of ordinary differential equations, described in continuous time, like

$$\frac{\partial \mathbf{x}}{\partial t} = f\left(\mathbf{x}, \mathbf{u}, t\right). \tag{2.1}$$

Due to the time discrete nature of FCS-MPC, the model of the system must be approximated by a time discrete version. This approximation process may lead to modeling errors that must be taken into account when evaluating the performance of the closed control loop.

In many cases, an accurate discretization can be cumbersome to compute or obtain, and often a high sampling frequency is enough to achieve a proper control performance, even with a simple discretization. On the other hand, in the case of some systems, it is required a minimum level of accuracy to be properly used in MPC [35]. These different situations forbid the possibility to choose one discretization strategy as the overall best, for any system.

The following section presents some of the most commonly used discretization strategies used in power electronics, its advantages and limitations.

2.2.1 Euler Method

The Euler discretization method takes the derivative term, in (2.1), and approximates it by the difference between two consecutive sampled values,

$$\frac{dx}{dt} = \frac{x(t_{k+1}) - x(t_k)}{T_s}. \tag{2.2}$$

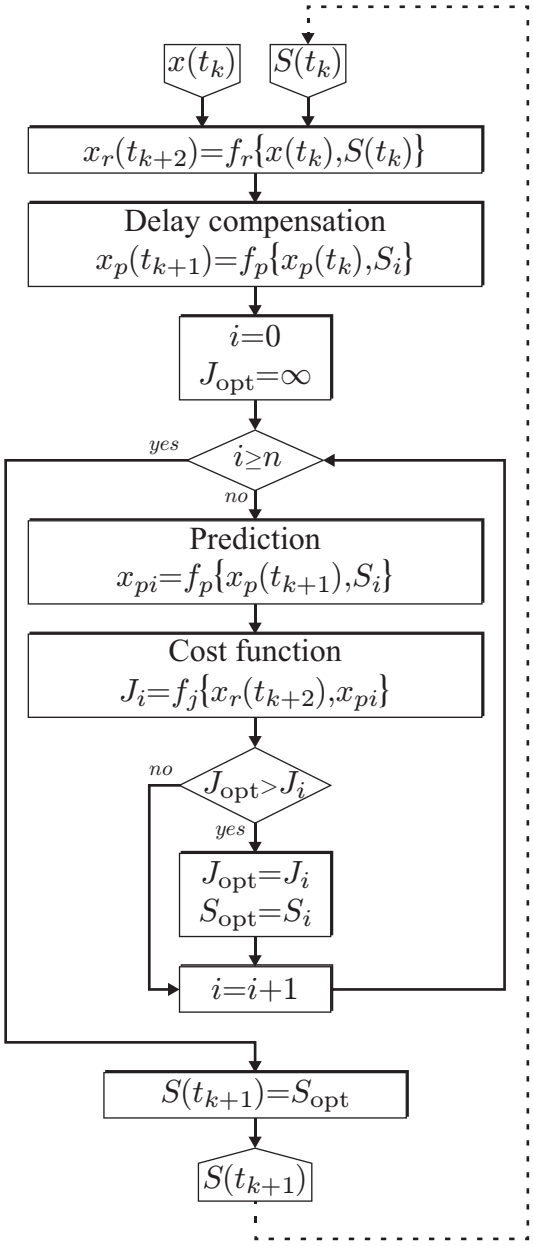

Figure 2.3: Flow diagram of finite control set model predictive control with delay compensation

For a regularly sampled system, the difference between two consecutive values of time is always equal to the sampling period T_s. The simplicity of this method permits quick implementation in multiple platforms, with little effort.

A particular case of this method can be seen in LTI systems, as described in (2.3), where the continuous transfer function, $G(s)$, can be expressed as

$$\dot{x} = Ax + Bu \quad , \quad y = Cx \; , \tag{2.3}$$

$$G(s) = \frac{Y(s)}{U(s)} = C(sI_n - A)^{-1}B. \tag{2.4}$$

$U(s)$ and $Y(s)$ are respectively the input and output of the system in the Laplace domain, and I_n is an Identity matrix of size n. The discrete form of this model using Euler transformation is achieved by the following approximation, where z is the delay operator, $s \approx \frac{z-1}{T_s}$,

$$G_d(z) = G\left(\frac{z-1}{T_s}\right) = C\left(\frac{z-1}{T_s}I_n - A\right)^{-1}B. \tag{2.5}$$

A problem related to this transformation is that some elements of $x(t_{k+1})$ might not be affected by the input signal. This happens in a system with a relative degree greater than one, as shown in the following example.

$$G(s) = \frac{b_0}{s^2 + a_1 s + a_0} \; , \tag{2.6}$$

$$\begin{aligned} G_d(z) &= \frac{b_0 T_s^2}{(z-1)^2 + a_1 T_s (z-1) + a_0 T_s^2} \; , \\ &= \frac{b_0 T_s^2}{(z^2 - 2z + 1) + a_1 T_s (z-1) + a_0 T_s^2} \; , \\ &= \frac{b_0 T_s^2}{z^2 + (a_1 T_s - 2)z + (a_0 T_s^2 - a_1 T_s + 1)} = \frac{Y(z)}{U(z)} \; , \end{aligned} \tag{2.7}$$

$$Y(z)(z^2 + (a_1 T_s - 2)z + (a_0 T_s^2 - a_1 T_s + 1)) = U(z) b_0 T_s^2 \; . \tag{2.8}$$

The delay operator works as a time shift function over a fixed time, which in the case of discrete time systems is the sampling time. Therefore, (2.8) can be written as

$$y(t_{k+2}) + (a_1 T_s - 2)y(t_{k+1}) - (a_0 T_s^2 - a_1 T_s + 1)y(t_k) = b_0 T_s^2 u(t_k) \; , \tag{2.9}$$

$$y(t_{k+2}) = b_0 T_s^2 u(t_k) - (a_1 T_s - 2)y(t_{k+1}) - (a_0 T_s^2 - a_1 T_s + 1)y(t_k) \; , \tag{2.10}$$

$$y(t_k) = b_0 T_s^2 u(t_{k-2}) - (a_1 T_s - 2)y(t_{k-1}) - (a_0 T_s^2 - a_1 T_s + 1)y(t_{k-2}) \; . \tag{2.11}$$

As shown in (2.11) the effect of the input signal over the output has a delay of a whole sample. In many applications of MPC the prediction horizon is of only one sample, which

means that for for this kind of system, any control action would yield the same prediction, rendering the strategy ineffective in choosing the optimal actuation. For these and other more complex systems, a better discrete approximation must be constructed.

2.2.2 Taylor Series

While Euler discretization is a simple strategy to construct the discrete model of a system, the Taylor Series Method presents a whole family of discretizations, all following the same expansive structure. This method makes use of Taylor series approximation over time, to produce a discrete model that is close to the continuous model only at the referred instant.

The full Taylor series expansion around time T of a function $f(t)$ has the structure

$$f(T+T_s) = f(T) + \frac{T_s}{1!}\left.\frac{\partial f(t)}{\partial t}\right|_T + \frac{T_s^2}{2!}\left.\frac{\partial^2 f(t)}{\partial t^2}\right|_T + \cdots = \sum_{m=0}^{\infty} \frac{T_s^m}{m!}\left.\frac{\partial^m f(t)}{\partial t^m}\right|_T . \quad (2.12)$$

The full series is composed by an infinite sum that exactly discretizes $f(t)$. To implement this method for a real control system, the series must be truncated, thus inducing some error in the discretized model. Nonetheless, this induced error is dampened exponentially for each new element. The level m at which the series is truncated is called the series order.

A special case of Taylor series rises when an order 1 is selected. This truncation leads exactly to an Euler discretization.

The advantage of this strategy is that it allows to discretize any model in a structured way and with any level of precision, provided that the continuous model is infinitely differentiable. This differentiablity condition is acomplished for most physical models, thus not being a critical condition. Semiconductors are a family of elements with a not infinitely differentiable model. In particular, the non-diferentiability occurs at the state change point of the semiconductor, from On to Off and vice versa. Nonetheless, since for FCS-MPC the state of the semiconductor is kept unchanged between samples, the inclusion of its model is neglected.

Even though this method can increase its accuracy indefinitely, it has the associated cost of increasing the computation demand. For linear systems the computation demand grows linearly with the chosen order, while for non-linear systems it can grow even faster. This computation demand might render this method unimplementable for high sampling frequencies, though there are some systems where this discretization is the only feasible option to achieve a proper control through FCS-MPC [22, 23].

2.2.3 Zero Order Hold

While Taylor series, and its special case of Euler discretization, produce a discrete approximation of a continuous system, they would never be able to produce an exact representation without infinite computation power. Nonetheless, it is possible to build an exact discrete model of a system, as long as this systems complies with being linear, as in (2.3), and A nonsingular. If these conditions are met, then the exact discrete model of the system is

$$A_d = e^{AT_s} \,, \tag{2.13}$$

$$B_d = \int_0^{T_s} e^{A\mu} B d\mu \,, \tag{2.14}$$

$$C_d = C. \tag{2.15}$$

Furthermore, if the system is also time invariant, the discrete matrix B_d can be computed as

$$B_d = A^{-1}(A_d - \mathbf{I})B \,, \tag{2.16}$$

where $\mathbf{I}$ is of the same size as A_d. This strategy is known as Zero Order Hold (ZOH), due to the assumption that the actuation u can be considered constant in between two consecutive samples. For power converters, this assumption is usually correct, since the actuation comes from the semiconductor states, which are expected to be constant.

A big disadvantage of this method is that the computation of the discrete matrices A_d and B_d requires the use of matrix exponential and matrix inversion. For small systems, of up to 3 variables, it is relatively easy to compute these functions. For higher order systems, these computations may demand a considerable amount of time. If the actual system is not constant in time and requires regular updates of the model to keep its accuracy, as would be the case for thermal-dependent or degrading elements, this computation time may be detrimental or simply prohibitive for the implementation.

The great advantage of this strategy, regardless of the computation time required to compute the matrices, is the complete exactitude of the discrete model achieved. This permits, in the absence o noise or disturbance, certainty that the discrete model would react exactly as the real system would, giving more precision to the control loop. This precision also permits low sampling time, since no major error would accumulate in the prediction due to discretization errors. A second advantage is the low computation demand required by the control system to perform the predictions, only surpassed by Euler discretization. This low computation time comes form the fact that, after computing the matrices A_d and B_d, the only operation required are sums and products. These two advantages permits the implementation of predictive control in low-end control systems without losing much control capability. Nonetheless, since it can only be used in linear systems, any non-linearity

of the system can not be considered in the systems model with the same performance in speed or precision.

2.2.4 Tustin Discretization

Tustin discretization, also known as bilinear transformation, is a simplification of ZOH, yet from another perspective. This method performs an approximation of the delay function (2.17), that uses a truncated form of the Taylor Series Linearization to replace the s term in the state-space model, choosing to end the series at the second element. Thus

$$z = e^{sT_s} = \frac{e^{sT_s/2}}{e^{-sT_s/2}} = \frac{1 + \frac{sT_s/2}{1} + \frac{(sT_s/2)^2}{2} + \dots}{1 - \frac{sT_s/2}{1} + \frac{(sT_s/2)^2}{2} + \dots} \approx \frac{1 + \frac{sT_s}{2}}{1 - \frac{sT_s}{2}} , \tag{2.17}$$

$$\therefore s \approx \frac{2}{T}\frac{z-1}{z+1} . \tag{2.18}$$

The main advantage of this method is that for a linear control system, this transformation allows to map any stable pole or zero inside the unit circle in the Nyquist diagram. This leads to a better approximation of the systems dynamics.

A problem that comes with this discretization is that the resulting transfer function has a relative degree equal to zero. This means that the effect of an input is computed on the output at the same sampling instant it is applied, having then an instantaneous response of the system, which is not the case for most physical systems. Nonetheless, since the discrete pole and zero location are close to the continuous ones, it is well suited for digital filters, that does not need to compute the future state, but to update the present one as a response to the new measurements

2.3 Discrete systems

Some systems that are commonly used in solar and wind power systems are modeled and discretized to be used for in the implementation of predictive control. The discretization strategy changes for each system, aiming to find the most efficient model.

The systems presented here are generic, in the sense that no analysis is given on the values used, but just the structure and the equations that govern each one. The differences between two systems may arise from either the load connected as well as the structure of the converter. Therefore, if a similar converter structure is used with different loads or there are changes in the way the converters are allowed to operate, then the proper analysis must take place to validate the discrete models.

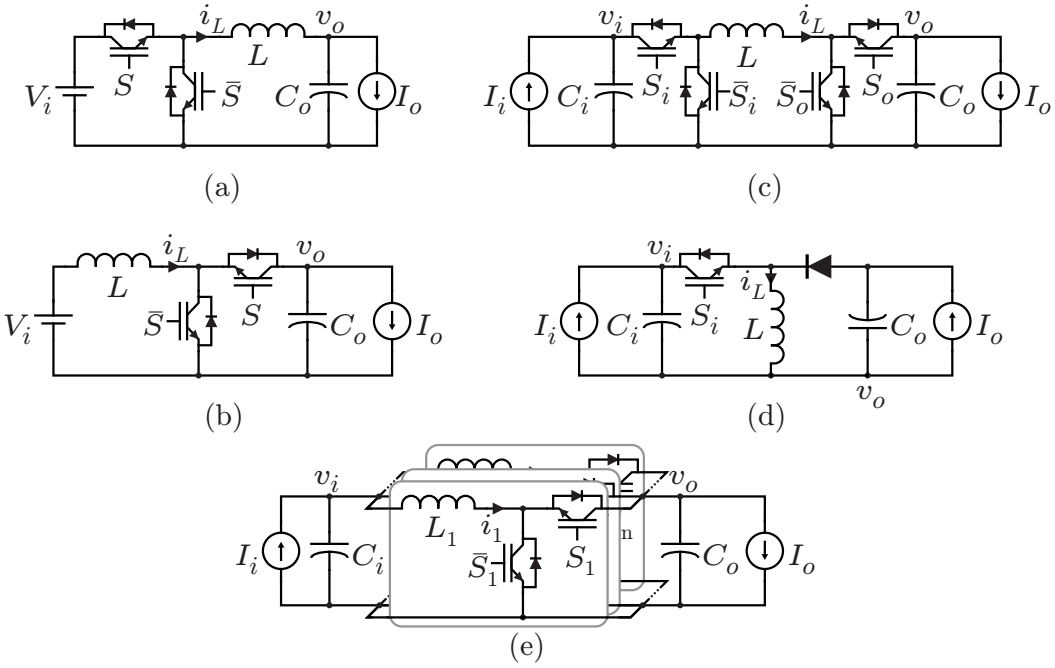

Figure 2.4: Commonly used DC-DC converters: (a)Buck converter, (b)Boost converter, (c)Buck/Boost without voltage inversion, (d)Buck/Boost with voltage inversion & (e)Interleaved Boost.

2.3.1 Boost & Buck Converters

Among the simplest converter topologies we have the DC/DC converters. Illustrated in figure 2.4 are the Buck converter (a), Boost converter (b), Buck/Boost without voltage inversion (c), Buck/Boost with voltage inversion (d) and an interleaved boost (e)

As a first step to obtain the model description and discretization, the basic equations involved in these converters are expressed in terms of the system variables. These equations describe the dynamics of the capacitors and inductors in a generic form, being these respectively

$$C\frac{dv_C(t)}{dt} = i_C(t) \quad , \quad v_C(t) = \int_0^t \frac{i_C(\tau)}{C}d\tau + v_C(0)\ , \tag{2.19}$$

$$L\frac{di_L(t)}{dt} = v_L(t) \quad , \quad i_L(t) = \int_0^t \frac{v_L(\tau)}{L}d\tau + i_L(0)\ . \tag{2.20}$$

$$\tag{2.21}$$

The next step in the discretization process is the selection of the discretization strategy to be used for each system.

Buck Converter

For the case of the Buck converter, the inductor and capacitor are both on the same side of the converter, meaning that they are not separated by semiconductors, so the continuous model of the system can be expressed as

$$\begin{bmatrix}\dot{i}_L \\ \dot{v}_o\end{bmatrix} = \begin{bmatrix}0 & -\frac{1}{L} \\ \frac{1}{C} & 0\end{bmatrix}\begin{bmatrix}i_L \\ v_o\end{bmatrix} + \begin{bmatrix}0 & \frac{1}{L} \\ -\frac{1}{C} & 0\end{bmatrix}\begin{bmatrix}I_o \\ SV_i\end{bmatrix} , \tag{2.22}$$

where the actuation u is partly dependent on the state of the semiconductors. This model follows the same structure as a time-invariant linear system, which can be expressed as

$$\dot{x} = Ax + Bu , \tag{2.23}$$

$$x = [i_L\ v_o]^T\ ,\ u = [I_o\ SV_i]^T\ , \tag{2.24}$$

$$A = \begin{bmatrix}0 & -\frac{1}{L} \\ \frac{1}{C} & 0\end{bmatrix} , B = \begin{bmatrix}0 & \frac{1}{L} \\ -\frac{1}{C} & 0\end{bmatrix} . \tag{2.25}$$

Since the model is linear and time invariant, a ZOH discretization can be used to compute an exact discrete model of the system as follows.

$$x(t_{k+1}) = A_d x(t_k) + B_d u(t_k) , \tag{2.26}$$

$$A_d = e^{A\tau} , B_d = A^{-1}(A_d - I)B . \tag{2.27}$$

Boost Converter

Unlike what can be done with Buck converter, the Boost converter can not be discretized using ZOH strategy. This is due to the fact that the semiconductors are in between the passive elements, which translates into a changing system (i.e. is not time invariant). This can be seen when presented in a variable state form

$$\begin{bmatrix}\dot{i}_L \\ \dot{v}_o\end{bmatrix} = \begin{bmatrix}0 & -\frac{S}{L} \\ \frac{S}{C} & 0\end{bmatrix}\begin{bmatrix}i_L \\ v_o\end{bmatrix} + \begin{bmatrix}0 & \frac{1}{L} \\ -\frac{1}{C} & 0\end{bmatrix}\begin{bmatrix}I_o \\ V_i\end{bmatrix} , \tag{2.28}$$

$$\dot{x} = A(S)x + Bu , \tag{2.29}$$

where the value of the matrix A changes with the state of the semiconductor, S. An alternative to ZOH is the discretization of each possible submodel with ZOH, thus computing

the predictions with a different model according to the desired semiconductor state. This is feasible for this system thanks to the low amount of possible switching states. For a more complex system, or one that has more semiconductors, this alternative may not be the appropriate due to the sheer amount of possible state combinations, that would lead to a heavy use of memory to store all the possible discrete models.

Buck-Boost Converter

For a more complex systems, where there are too many variables and too many semiconductor states to be tested, a better approach to its discretization is the use of Taylor series. Taylor series discretization requires the selection of the degree at which the series will be truncated, which defines, along with the sampling time (due to computation requirements), how accurate the discretization is.

For the case of the Buck-Boost converter, with inverted voltage, presented in figure 2.4(d), the continuous model equations are

$$\dot{v_i} = \frac{1}{C_i} I_i - \frac{S_i}{C_i} i_L \tag{2.30}$$

$$\dot{i_L} = \frac{S_i}{L} v_i - \frac{\bar{S}_i}{L} v_o \tag{2.31}$$

$$\dot{v_o} = \frac{\bar{S}_i}{C_o} i_L - \frac{1}{C_o} I_o \tag{2.32}$$

Since each variable in this system is directly linked to the actuation variable, it is possible to obtain a good enough discretizaion by using Taylor series truncated at the first degree. This leads to the following discrete model

$$v_i(t_{k+1}) = v_i(t_k) + \left(I_i(t_k) - i_L(t_k) S_i\right) \frac{\tau}{C_i} \,, \tag{2.33}$$

$$i_L(t_{k+1}) = i_L(t_k) + \left(v_i(t_k) S_i - i_L(t_k) \bar{S}_i\right) \frac{\tau}{L} \,, \tag{2.34}$$

$$v_o(t_{k+1}) = v_o(t_k) + \left(i_L(t_k) \bar{S}_i - I_o(t_k)\right) \frac{\tau}{C_o} \,. \tag{2.35}$$

A different situation takes place for the non inverting Buck-Boost, 2.4(c), where, though all variables are linked to at least one actuation, they are not directly linked to all, as follows

$$\dot{v_i} = \frac{1}{C_i} I_i - \frac{S_i}{C_i} i_L \,, \tag{2.36}$$

$$\dot{i_L} = \frac{S_i}{L} v_i - \frac{S_o}{L} v_o \,, \tag{2.37}$$

$$\dot{v_o} = \frac{S_o}{C_o} i_L - \frac{1}{C_o} I_i \,. \tag{2.38}$$

If this system were to be discretized with a first order Taylor discretization, then the capacitor voltages would be insensitive to the respective opposing control action. In a control

strategy that only takes into consideration a one step ahead prediction, such as the standard form of FCS-MPC studied here, this may induce control errors or undesired dynamics. This issue can be solved by either extending the prediction to more steps, incurring in the increased computation required for it, or by extending the discretization to a second degree. This way, the final discrete model is

$$\begin{aligned}
\left.\frac{dv_i}{dt}\right|_k &= \frac{1}{C_i}\left(I_i(t_k) - S_i i_L(t_k)\right) \ , \\
\left.\frac{di_L}{dt}\right|_k &= \frac{1}{L}\left(S_i v_i(t_k) - S_o v_o(t_k)\right) \ , \\
\left.\frac{dv_o}{dt}\right|_k &= \frac{1}{C_o}\left(S_o i_L(t_k) - I_i(t_k)\right) \ ,
\end{aligned} \tag{2.39}$$

$$\begin{aligned}
\left.\frac{d^2v_i}{dt^2}\right|_k &= \frac{1}{C_i}\left(S_i \frac{di_L(t_k)}{dt}\right) \ , \\
\left.\frac{d^2i_L}{dt^2}\right|_k &= \frac{1}{L}\left(S_i \frac{dv_i(t_k)}{dt} - S_o \frac{dv_o(t_k)}{dt}\right) \ , \\
\left.\frac{d^2v_o}{dt^2}\right|_k &= \frac{1}{C_o}\left(S_o \frac{di_L(t_k)}{dt}\right) \ ,
\end{aligned} \tag{2.40}$$

$$\begin{aligned}
v_i(t_{k+1}) &= v_i(t_k) + \left.\frac{dv_i}{dt}\right|_k \frac{\tau}{1} + \left.\frac{d^2v_i}{dt^2}\right|_k \frac{\tau^2}{2} \ , \\
i_L(t_{k+1}) &= i_L(t_k) + \left.\frac{di_L}{dt}\right|_k \frac{\tau}{1} + \left.\frac{d^2i_L}{dt^2}\right|_k \frac{\tau^2}{2} \ , \\
v_o(t_{k+1}) &= v_o(t_k) + \left.\frac{dv_o}{dt}\right|_k \frac{\tau}{1} + \left.\frac{d^2v_o}{dt^2}\right|_k \frac{\tau^2}{2} \ ,
\end{aligned} \tag{2.41}$$

Here it can be seen that through the effects of the second derivative (2.40), each control action can directly affect each of the variables, with more or less impact, allowing a better discretization.

Interleaved Boost Converter

In a similar fashion as with the previous models, the interleaved boost, as presented in figure 2.4(e), is modeled in continuous time

$$\dot{v_i} = \left(I_i - \sum_{x=1}^{n} i_x\right)\frac{1}{C_i} \ , \tag{2.42}$$

$$\dot{i_x} = \left(v_i - s_x v_o\right)\frac{1}{L_o} \ \ , \forall x \in \{1, ..., n\} \ , \tag{2.43}$$

$$\dot{v_o} = \left(\sum_{x=1}^{n} S_x i_x - I_o\right)\frac{1}{C_o} \ . \tag{2.44}$$

The model used here is mostly the same as with a boost converter. Nonetheless, since the input system for the converter is now a capacitor and a current source, the model has to have it into consideration.

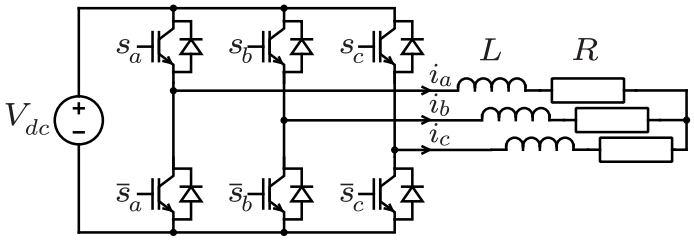

Figure 2.5: 2-level 3-Phase Voltage Source converter with RL Load

Table 2.1: 2-Level 3-Phase Converter States

Voltage	Switching State			Voltage $\alpha\beta$	
Vector	S_a	S_b	S_c	v_α	v_β
v_0	0	0	0	0	0
v_1	1	0	0	$\frac{2}{3}v_{dc}$	0
v_2	1	1	0	$\frac{1}{3}v_{dc}$	$\frac{1}{\sqrt{3}}v_{dc}$
v_3	0	1	0	$-\frac{1}{3}v_{dc}$	$\frac{1}{\sqrt{3}}v_{dc}$
v_4	0	1	1	$-\frac{2}{3}v_{dc}$	0
v_5	0	0	1	$-\frac{1}{3}v_{dc}$	$-\frac{1}{\sqrt{3}}v_{dc}$
v_6	1	0	1	$\frac{1}{3}v_{dc}$	$-\frac{1}{\sqrt{3}}v_{dc}$
v_7	1	1	1	0	0

It can be seen that the semiconductors are in between the dynamic elements, forcing to either have multiple ZOH discrete models for each possible state or have one less precise Taylor discretized model. In the case of a Taylor series discretization, an order 2 series is required to properly predict the system's future state. Therefore, the same steps used for the non inverting Buck-Boost must be followed to compute the discrete model of the interleaved boost.

2.3.2 3-Phase 2-Level Voltage Source converter

The most simple 3-phase converter is the 2-level 3-phase converter presented in figure 2.5. This device is build from the structure of an H-Bridge converter, where each phase corresponds to half a bridge. Unlike the previously presented DC/DC converters, this converter does not require an inductance or capacitor as a fundamental part of its structure, and can actually be connected to any structure, as long as the left part remains as DC and

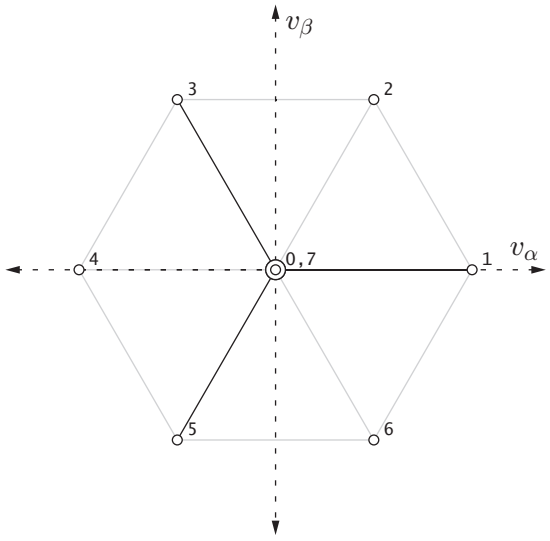

Figure 2.6: Voltage vectors in $\alpha\beta$ coordinates for a 3-phase 2-level converter

the right as 3-phase AC. This can be appreciated in figure 2.7. The possible states of this converter are presented in table 2.1 along the voltage generated to the AC side in $\alpha\beta$ coordinates, represented graphically in figure 2.6. These states are the ones that FCS-MPC would evaluate for the multiple predictions of the future state of the system.

The particular case presented in figure 2.5 corresponds to a DC voltage source and RL load and can be modeled as follows.

$$L\frac{di_x}{dt} = \left(s_x - \frac{s_a + s_b + s_c}{3}\right) V_{dc} - i_x R \ , \ \ \forall x \in \{a, b, c\} \ . \tag{2.45}$$

For a balanced load, this can be seen as two independent systems in $\alpha\beta$ coordinates.

$$\begin{aligned} L\frac{di_\alpha}{dt} &= -i_\alpha R + s_\alpha V_{dc} \ , \\ L\frac{di_\beta}{dt} &= -i_\beta R + s_\beta V_{dc} \ , \\ \begin{bmatrix} s_\alpha \\ s_\beta \end{bmatrix} &= \sqrt{\frac{2}{3}} \begin{bmatrix} 1 & -\frac{1}{2} & -\frac{1}{2} \\ 0 & \frac{\sqrt{3}}{2} & -\frac{\sqrt{3}}{2} \end{bmatrix} \begin{bmatrix} s_a \\ s_b \\ s_c \end{bmatrix} \ . \end{aligned} \tag{2.46}$$

Since this is a linear system and the state of the converter is kept constant between samples,

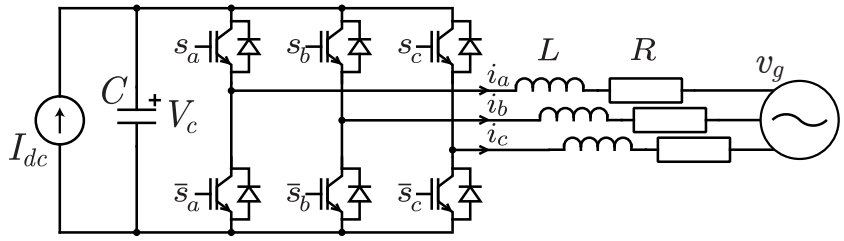

Figure 2.7: 2-level 3-Phase converter with C dc-link and RL grid conection

it is possible to get an exact discretization using ZOH discretization, as follows.

$$\begin{bmatrix} i_\alpha(t_{k+1}) \\ i_\beta(t_{k+1}) \end{bmatrix} = \mathbf{A}_d \begin{bmatrix} i_\alpha(t_k) \\ i_\beta(t_k) \end{bmatrix} + \mathbf{B}_d \begin{bmatrix} s_\alpha(t_k) \\ s_\beta(t_k) \end{bmatrix} V_{dc}(t_k) \,, \tag{2.47}$$

$$\mathbf{A}_d = e^{-T_s \frac{R}{L}} \,, \tag{2.48}$$

$$\mathbf{B}_d = \left(1 - e^{-T_s \frac{R}{L}}\right) / R \,. \tag{2.49}$$

By reducing this system to 2 variables, each component, α and β are independent of each other, thus allowing for a very simple discrete model.

A common situation for this system is the use of a capacitor as DC-Link, and to be connected to the grid, as illustrated in figure 2.7. This model helps to represent the system as part of a bigger power conversion scheme by simplifying the DC and AC ends. The addition of a new dynamic element calls for a different model of the system. The equations that define the systems dynamics are

$$L\frac{di_x}{dt} = \left(s_x - \tfrac{s_a+s_b+s_c}{3}\right) V_c - i_x R - v_{g,x} \;\;,\;\; \forall x \in \{a,b,c\} \,, \tag{2.50}$$

$$C\frac{dV_c}{dt} = I_{dc} - s_a i_a - s_b i_b - s_c i_c \,. \tag{2.51}$$

The nature of each of the dynamic elements is continuous and unchanging (at least for simulations), which would make this system suitable for ZOH discretization. Nonetheless, since there are elements at both side of the converter, each conduction state leads to a different effective system, thus being required 8 similar models. Though possible to execute, this is a very time consuming process. A better choice for a fast and accurate enough discrete model is the use of Euler discretization, as shown in (2.2). This strategy is good enough to discretize this system as long as the sampling time is much faster than any of

the systems dynamics. The final discrete model of the system is

$$i_x(t_{k+1}) = i_x(t_k) + \left(\left(s_x - \frac{s_a+s_b+s_c}{3}\right) V_c - i_x R - v_{g,x}(t_k)\right) \frac{T_s}{L} \ , \ \forall x \in \{a,b,c\} \ , \quad (2.52)$$

$$V_c(t_{k+1}) = V_c(t_k) + (I_{dc} - s_a i_a(t_k) - s_b i_b - s_c i_c) \frac{T_s}{C} \ . \quad (2.53)$$

As it can be seen, the state of the semiconductors becomes part of the model, and not just a control input. This is the main reason why the model of the system changes for each state, and why it is not suited for ZOH dicretization.

2.3.3 Induction Machine

Another common element in power system is the induction machine (IM), usually connected to other systems through an AC/DC converter. Regardless of the used converter, the voltage applied to the IM is kept constant through the sampling period. Thus, the relevant system to be analyzed is the IM itself. Unlike the system revised so far, IM presents a more complex analysis due to its non-linearities. For the purpose of this model, for any complex variable x, x_α and x_β are respectively its real and imaginary components. Thus, the continuous time model of the induction machine in complex variables is

$$\begin{aligned} \begin{bmatrix} \dot{i} \\ \dot{\psi} \end{bmatrix} &= \begin{bmatrix} -\frac{\rho_s+\gamma\rho_r}{\sigma} & \gamma\frac{\rho_r - j\omega_r}{L_m\sigma} \\ L_m\rho_r & -\rho_r + j\omega_r \end{bmatrix} \begin{bmatrix} i \\ \psi \end{bmatrix} + \begin{bmatrix} \frac{1}{L_s\sigma} \\ 0 \end{bmatrix} v_s \quad (2.54) \\ &= \begin{bmatrix} a_{11} & a_{12\alpha} + a_{12\beta}\omega_r \\ a_{21} & a_{22\alpha} + a_{22\beta}\omega_r \end{bmatrix} \begin{bmatrix} i \\ \psi \end{bmatrix} + \begin{bmatrix} b_1 \\ b_2 \end{bmatrix} v_s \ , \\ \dot{\omega} &= \frac{3}{2}\frac{L_m}{L_r}\frac{p}{J}\left(\psi_\alpha i_\beta - \psi_\beta i_\alpha\right) - \frac{T_L}{J} \quad (2.55) \\ &= c_1\left(\psi_\alpha(t_k) i_\beta(t_k) - \psi_\beta(t_k) i_\alpha(t_k)\right) - c_2 T_L \ , \end{aligned}$$

where $\rho_s = \frac{R_s}{L_s}$, $\rho_r = \frac{R_r}{L_r}$, $\gamma = \frac{L_m^2}{L_s L_r}$ and $\sigma = 1 - \gamma$, i is the stator current, ψ the rotor magnetic flux and ω the rotor electrical speed.

These nonlinearyties make ZOH and Tustin discretizations unsuitable for this system, thus requiring Taylor discretization. Due to the structure of IM dynamics, a minimum order of 2 in the Taylor series is required for this purpose [22]. With this choice, the

discrete IM model in α- β coordinates gets constructed as

$$\left.\frac{\partial i_\alpha}{\partial t}\right|_k = i'_\alpha(t_k) = a_{11} i_\alpha(t_k) + a_{12,\alpha}\psi_\alpha(t_k) - a_{12,\beta}\omega_k\psi_\beta(t_k) + b_1 v_\alpha(t_k)\ , \tag{2.56a}$$

$$\left.\frac{\partial i_\beta}{\partial t}\right|_k = i'_\beta(t_k) = a_{11} i_\beta(t_k) + a_{12,\alpha}\psi_\beta(t_k) + a_{12,\beta}\omega_k\psi_\alpha(t_k) + b_1 v_\beta(t_k)\ , \tag{2.56b}$$

$$\left.\frac{\partial \psi_\alpha}{\partial t}\right|_k = \psi'_\alpha(t_k) = a_{21} i_\alpha(t_k) + a_{22,\alpha}\psi_\alpha(t_k) - a_{22,\beta}\omega_k\psi_\beta(t_k) + b_2 v_\alpha(t_k)\ , \tag{2.56c}$$

$$\left.\frac{\partial \psi_\beta}{\partial t}\right|_k = \psi'_\beta(t_k) = a_{21} i_\beta(t_k) + a_{22,\alpha}\psi_\beta(t_k) + a_{22,\beta}\omega_k\psi_\alpha(t_k) + b_2 v_\beta(t_k)\ , \tag{2.56d}$$

$$\left.\frac{\partial \omega}{\partial t}\right|_k = \omega'_k = \tfrac{3}{2}\tfrac{L_m}{L_r}\tfrac{p^2}{J}\left(\psi_\alpha(t_k) i_\beta(t_k) - \psi_\beta(t_k) i_\alpha(t_k)\right) - T_L\tfrac{p}{J}\ , \tag{2.56e}$$

$$\left.\frac{\partial^2 i_\alpha}{\partial t^2}\right|_k = i''_\alpha(t_k) = a_{11} i'_\alpha(t_k) + a_{12,\alpha}\psi'_\alpha(t_k) - a_{12,\beta}\left(\omega_k\psi'_\beta(t_k) + \psi_\beta\omega'_k\right)\ , \tag{2.57a}$$

$$\left.\frac{\partial^2 i_\beta}{\partial t^2}\right|_k = i''_\beta(t_k) = a_{11} i'_\beta(t_k) + a_{12,\alpha}\psi'_\beta(t_k) + a_{12,\beta}\left(\omega_k\psi'_\alpha(t_k) + \psi_\alpha\omega'_k\right)\ , \tag{2.57b}$$

$$\left.\frac{\partial^2 \psi_\alpha}{\partial t^2}\right|_k = \psi''_\alpha(t_k) = a_{21} i'_\alpha(t_k) + a_{22,\alpha}\psi'_\alpha(t_k) - a_{22,\beta}\left(\omega_k\psi'_\beta(t_k) + \psi_\beta\omega'_k\right)\ , \tag{2.57c}$$

$$\left.\frac{\partial^2 \psi_\beta}{\partial t^2}\right|_k = \psi''_\beta(t_k) = a_{21} i'_\beta(t_k) + a_{22,\alpha}\psi'_\beta(t_k) + a_{22,\beta}\left(\omega_k\psi'_\alpha(t_k) + \psi_\alpha\omega'_k\right)\ , \tag{2.57d}$$

$$\left.\frac{\partial^2 \omega}{\partial t^2}\right|_k = \omega''(t_k) = \tfrac{3}{2}\tfrac{L_m}{L_r}\tfrac{p^2}{J}\left(\psi'_\alpha(t_k) i_\beta(t_k) + \psi_\alpha(t_k) i'_\beta(t_k) - \psi'_\beta(t_k) i_\alpha(t_k) - \psi_\beta(t_k) i'_\alpha(t_k)\right)\ , \tag{2.57e}$$

$$i_\alpha(t_{k+1}) = i_\alpha(t_k) + i'_\alpha(t_k)\tfrac{T_s}{1} + i''_\alpha(t_k)\tfrac{T_s^2}{2}\ , \tag{2.58a}$$

$$i_\beta(t_{k+1}) = i_\beta(t_k) + i'_\beta(t_k)\tfrac{T_s}{1} + i''_\beta(t_k)\tfrac{T_s^2}{2}\ , \tag{2.58b}$$

$$\psi_\alpha(t_{k+1}) = \psi_\alpha(t_k) + \psi'_\alpha(t_k)\tfrac{T_s}{1} + \psi''_\alpha(t_k)\tfrac{T_s^2}{2}\ , \tag{2.58c}$$

$$\psi_\beta(t_{k+1}) = \psi_\beta(t_k) + \psi'_\beta(t_k)\tfrac{T_s}{1} + \psi''_\beta(t_k)\tfrac{T_s^2}{2}\ , \tag{2.58d}$$

$$\omega(t_{k+1}) = \omega(t_k) + \omega'(t_k)\tfrac{T_s}{1} + \omega''(t_k)\tfrac{T_s^2}{2}\ . \tag{2.58e}$$

2.4 Cost Function

For a control strategy to be considered optimal it needs to involve a criterion to evaluate the performance and aim for the best possible result based on this criterion. The purpose of the cost function is to provide said evaluation that allows the control system to choose the best input alternative for the controlled system to reach a desired state.

For model predictive control the cost function correspond to a functional over the tracking error of the relevant variables. This means it provides a scalar value along the real numbers. In a system of n states and m inputs the cost function can be generalized as

$$e_x = x^* - x \ , \ e_u = u^* - u \ , \tag{2.59}$$

$$J(e_x, e_u) \mid \mathbb{R}^n \times \mathbb{R}^m \to \mathbb{R} \ , \tag{2.60}$$

where x and u are the state and actuation vectors, of length n and m respectively.

One of the main properties that must be fulfilled by the cost function is the convexity in its domain. This ensures that the minimum value of $J(x, u)$ exists and is unique inside the domain. A function $f(x)$ is said to be convex in its domain $D(f)$ if, for any pair of points $(x_1, f(x_1))$ and $(x_2, f(x_2))$, the segment generated between them lies either on or above $f(x)$,

$$f(x_1 + \alpha(x_2 - x_1)) \leq f(x_1) + \alpha(f(x_2) - f(x_1)) \ , \ \forall \, x_1, x_2 \in D(f) \ \ \& \ \ \alpha \in]0, 1[\ . \tag{2.61}$$

From this also comes the strictly convex definition, which follows the same structure but only applies for strictly above ($<$ instead of $\leq$) the curve.

For most systems, if the cost function structure is in itself convex, then the whole control system is so. Nevertheless, some nonlinear systems might generate a non-convex cost function.An example of these systems is a self driving car, which in the situation of turning in 180 degrees, has the choice of either go left or right. Both choices are equally valid, yet requires opposite actuation to reach the objective. This case does not creates a critical situation nor reaches a local minimum, but illustrates the fact the some systems might generate issues in the cost function that must be considered for a proper control.

The cost function provides a scalar value that evaluates the performance of a control action over the system. The main goal of this value is to find the control action that leads to its minimum value. Since the cost function only needs to find the point x for which $f(x)$ reaches the minimum, but does not care for the actual value reached, the following properties hold,

$$\min_{x \in D}(f(x)) = \min_{x \in D}(f(x) + K) \ \ , \ \forall \, K \in \mathbb{R} \ , \tag{2.62}$$

$$\min_{x \in D}(f(x)) = \min_{x \in D}(f(x) \cdot K) \quad , \ \forall \, K \in \mathbb{R} > 0 \ . \tag{2.63}$$

This means that if the whole function is shifted (2.62) or scaled (2.63), the minimum will remain in the same point.

2.4.1 Absolute value or Norm 1

One of the most common cost function used in literature for power systems is the absolute value of the tracking error. When the structure shown in (2.60) is replaced by the

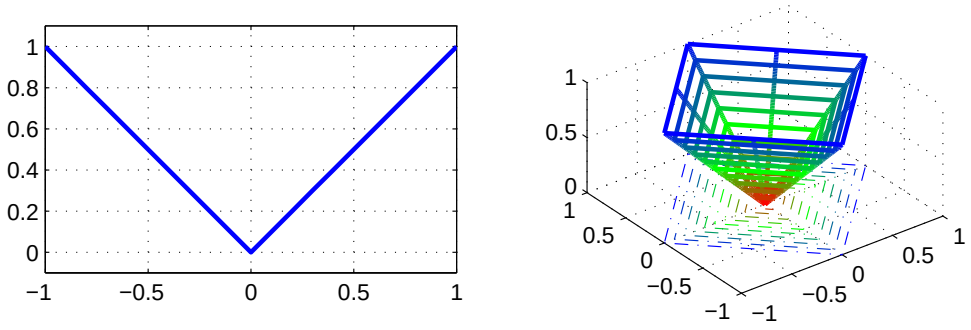

Figure 2.8: Abolute value cost function for one and two variables

absolute value function, the resulting structure is

$$J(e_x(t_k), e_u(t_k)) = \sum_{j=1}^{n} \lambda_j |e_{x,j}(t_k)| + \sum_{k=1}^{m} \gamma_k |e_{u,j}(t_k)| \ . \tag{2.64}$$

This cost function has the property of returning a lower value the closer is the predicted state to the reference. This way, by choosing the input that gives the lowest value of the cost function, the systems moves to the reference. Nevertheless, this structure does not fully comply the strictly convex requirement. This can be seen in figure 2.8 where a pair of points can be chosen to form a segment that is not above the curve. For the case of a single variable, if the chosen points are both bigger than 0, then the segment created matches the absolute value function. The same happens for 2 variables, when both point live in the same face of the pyramid. This logic, extended to an n variable system, can be stated as having two points that share sign at each of its composing elements for a segment that is not above the surface, that is,

$$x_1, x_2 \in \mathbb{R}^n \mid sign(x_{1,i}) = sign(x_{2,i}) \forall \ i \in \{1, ..., n\} \ . \tag{2.65}$$

Another drawback of this cost function comes from the fact that its slope is always the same and independent from the error, as long as there is no change in its sign. This means that the importance of an error correction is the same, regardless if the error is big or small.

2.4.2 Quadratic or Norm 2

The quadratic cost function, also known as Euclidean Norm or Norm 2, evaluates the square of the error instead of its absolute value. This method is widely used in many works

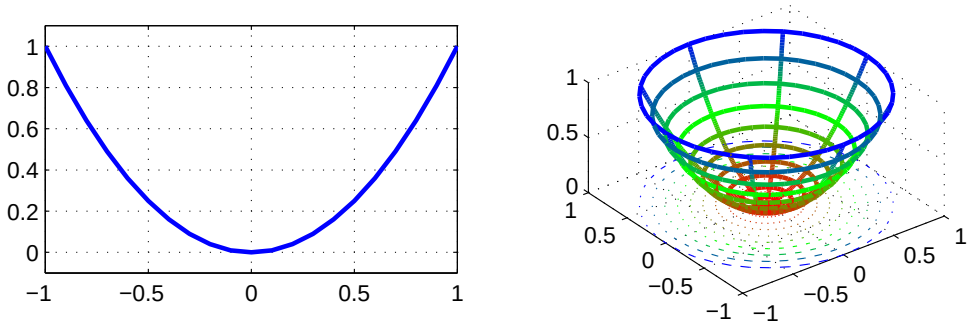

Figure 2.9: Quadratic cost function for one and two variables

related to the control area, since it is more tractable and easier to operate with for linear systems. The following equation (2.66) shows the basic structure of this cost function.

$$
\begin{aligned}
J(e_x(t_k), e_u(t_k)) =& \sum_{j=1}^{n} \lambda_j |e_{x,j}(t_k)|^2 + \sum_{k=1}^{m} \gamma_k |e_{u,j}(t_k)|^2 && (2.66)\\
=& |e_x(t_k)|_Q^2 + |e_u(t_k)|_R^2 \\
=& e_x'(t_k) Q e_x(t_k) + e_u'(t_k) R e_u(t_k) \ , && (2.67)\\
Q =& diag\left[\lambda_1 \ \lambda_2 \ \ldots \lambda_n\right] \ , && (2.68)\\
R =& diag\left[\gamma_1 \ \gamma_2 \ \ldots \gamma_m\right] \ , && (2.69)
\end{aligned}
$$

Unlike the absolute value structure, the convexity for the quadratic function does hold for any pair of points in the domain. This is proved as follows by the use of (2.61)

$$
\begin{aligned}
f(x_1 + \alpha(x_2 - x_1)) &< f(x_1) + \alpha(f(x_2) - f(x_1)) \ , && (2.70)\\
(x_1 + \alpha(x_2 - x_1))^2 &< x_1^2 + \alpha(x_2^2 - x_1^2) \ , && (2.71)\\
(x_1(1-\alpha) + \alpha x_2)^2 &< x_1^2(1-\alpha) + \alpha x_2^2, \\
x_1^2(1-\alpha)^2 + 2x_1x_2\alpha(1-\alpha) + \alpha^2 x_2^2 &< x_1^2(1-\alpha) + \alpha x_2^2 \ , \\
0 &< \alpha x_1^2(1-\alpha) - 2x_1x_2\alpha(1-\alpha) + \alpha x_2^2(1-\alpha) \ , && (2.72)\\
0 &< \alpha(1-\alpha)(x_1 - x_2)^2 \ . && (2.73)
\end{aligned}
$$

Since $\alpha \in]0,1[$ and $x_1, x_2 \in \mathbb{R}^n$, equation (2.73) is always truth.

Another major difference of the quadratic function in comparison with the absolute value is that the effect a variable has in the cost function is not only given by its scale

factor, but also by the magnitude of the error, as shown in (2.78).

$$\min_u J = \min_u \left(\sum_{j=1}^{n} \lambda_j (e_{x,j}(t_k, u))^2 \right) , \tag{2.74}$$

$$= \min_u \left(\sum_{j=1}^{n} \lambda_j (x_j(t_k)^* - x_j(t_{k-1}) - \Delta x(u))^2 \right) , \tag{2.75}$$

$$= \min_u \left(\sum_{j=1}^{n} \lambda_j (e_j(t_{k-1}) - \Delta x(u))^2 \right) , \tag{2.76}$$

$$= \min_u \left(\sum_{j=1}^{n} \lambda_j (e_j(t_{k-1})^2 - 2e_j(t_k)\Delta x(u) + \Delta x(u)^2) \right) , \tag{2.77}$$

$$= \min_u \left(\sum_{j=1}^{n} -\lambda_j 2e_j(t_{k-1})\Delta x(u) + \lambda_j \Delta x(u)^2 \right) . \tag{2.78}$$

It can be seen that when the error previous to any actuation, $e_j(t_{k-1})$, is bigger than the correction action $\Delta x(u)$, the cost function is mainly affected by $-\lambda_j 2e_j(t_{k-1})\Delta x(u)$. Thus, the weighting factor that ponder each deviation is no longer static, but increases with the current error, pondering with more strength the correction action over high error variables.

A particular consideration for this cost function is that the optimal solution can be computed for an unrestricted system. This means that for a continuous boundless system, the optimal solution is a function of the state, as follows, taking in consideration that the minimum is found where the first derivative of J over u is 0.

$$\dot{J} = -2((x^*(t_{k+1}) - \hat{A}x)'Q\hat{B} + u_k^{*\prime}R)\dot{u} + 2u'(\hat{B}'Q\hat{B} + R)\dot{u} , \tag{2.79}$$

$$0 = -2((x^*_{k+1} - \hat{A}x)'Q\hat{B} + u_k^{*\prime}R) + 2u'(\hat{B}'Q\hat{B} + R) , \tag{2.80}$$

$$\therefore\ u = (\hat{B}'Q\hat{B} + R)^{-1}(\hat{B}'Q(x^*_{k+1} - \hat{A}x) + Ru^*_k) . \tag{2.81}$$

In a restricted system this optimal input might not be possible to achieve but still provides an idea of where in the input space $\mathbb{R}^m$ the absolute optimal input is located. By having this information it becomes easier to find the optimal restricted input.

2.4.3 Norm-n

The general structure of the cost function aims to provide a measurement of how far the system is from the desired reference. In general, a cost function can be build as a Norm-n

of the error over its variables, properly weighted, as it is necessary in order to ponder the importance of each one. The Norm-n is the general form to describe this distance, and is defined as

$$Norm_n(x) = \sqrt[n]{\sum_j |x_j|^n} \, . \tag{2.82}$$

The most frequently used norms are 1, 2 and ∞ [36–38]. The infinity norm simply chooses the biggest value among x, working in a similar fashion as a the $\max$ function would.

$$J_\infty(e_x) = |e_x|^\infty = \max(e_x) \, . \tag{2.83}$$

2.4.4 Limits and Constrains

In most systems there are boundaries inside which the state of the system can move, but must not surpass. If the MPC cost function does not include these boundaries, the controller can try to reach an impossible or forbidden state of the system. In order to take these limits into account, they must be added into the cost function in a way that forces the system back to a permitted state.

The basic form of limiting a variable is by giving an infinite cost to any prediction that tries to pass over the limits. This way every time the system is near the boundaries, the controller will reject any input that might place it outside of the permitted zone. In a digital implementation the cost function is capped to a very high value instead of using infinite. Another way to implement the infinity it to simply not consider in the evaluation those inputs that move the system out of the boundaries.

A problem may occur with the infinite strategy when the system is capable of surpassing the limits and some noise makes the system state pass into a forbidden zone. In this situation, if the input is no capable of returning the system to a permitted state in one period, then all the inputs will lead to an unfeasible state. As all these predictions are forbidden, the value of the cost function would be the same for every input, which means that controlability would be lost. In order to face this issue, the boundary can be written as a ramp with a very high slope,

$$\Theta_{B,x} = \begin{cases} K(\hat{x} - L_{MAX})^2 & if \quad \hat{x} > L_{MAX} \\ 0 & if \quad L_{MAX} > \hat{x} > L_{min} \\ K(\hat{x} - L_{min})^2 & if \quad L_{min} > \hat{x} \end{cases} \, . \tag{2.84}$$

This way, even if the system is in a forbidden state, the different input alternatives will give different cost values and, because of the very high slope, the best one will always be the one that forces the system to approach the permitted zone.

2.5 Switching Frequency Control

Model predictive control, and in particular Finite Control Set (FCS-MPC), is well know for its many advantages when applied in the control of power converters. Among these advantages are the fast control response, robustness to noise and parameter mismatch, as well as its easy implementation. Nonetheless, these advantages are accompanied by some serious drawbacks, that might render FCS-MPC unsuitable for some systems.

The most critical disadvantages of FCS-MPC are the high computation demand, the difficulty of tuning the weight factors in an analytical way, and the high sampling and switching frequency required by the controller. The computation demand is a problem that will gradually become less prohibitive with the development of new technologies, and weight factor design is still fairly easy to tune manually for few control objectives. Nonetheless, the issue of switching frequency regulation presents itself as a non trivial problem. If no action is taken to address this issue, the device switching frequency typically presents a highly noisy behavior, usually ranging around the high frequencies. This is exemplified in figures 2.10 and 2.11 for a 2-level 3-phase converter, as presented in section 2.3.2. Here the sampling frequency is limited to 10 kHz, in order to bound the switching frequency up to 5 kHz. The average switching frequency for this simulation is around 1900 Hz.

When implemented in a voltage source converter, this high frequency variability translates into a wide voltage spectrum, with a strong tendency towards the high frequencies. Since the harmonic content of the voltage cannot be allocated to specific frequencies by design, as can be done with modulated control strategies, the design of filters becomes a complex or heuristic procedure, while power quality (specially sensitive in grid-connected applications) becomes a blinded guess from a design perspective. In addition, the lack of control over the switching frequency leads to an upper limit in this variable of up to half sampling frequency, which leads to undesired losses in the semiconductors.

Other MPC methods that can easily incorporate a modulator, such as deadbeat control [39], or modulated MPC [40], do not present these issues. Nonetheless, one of the advantages of FCS-MPC is the absence of a modulator, making it attractive for complex converter topologies, as it is not limited by the linear range of the modulator, and can achieve faster dynamic responses. Some solutions for the switching frequency problems have been addressed for FCS-MPC using a variety of approaches and tools, such as, simple penalization [41, 42], sliding window [43], and notch filter [13], which are further explained for comparison purposes later in this work. Although these solutions mitigate the switching frequency variability to some extent, they do not produce a stable switching patterns. For the purpose of this work, a stable switching pattern is considered to be similar to the ones achieved through modulators, with a characteristic commutation pattern

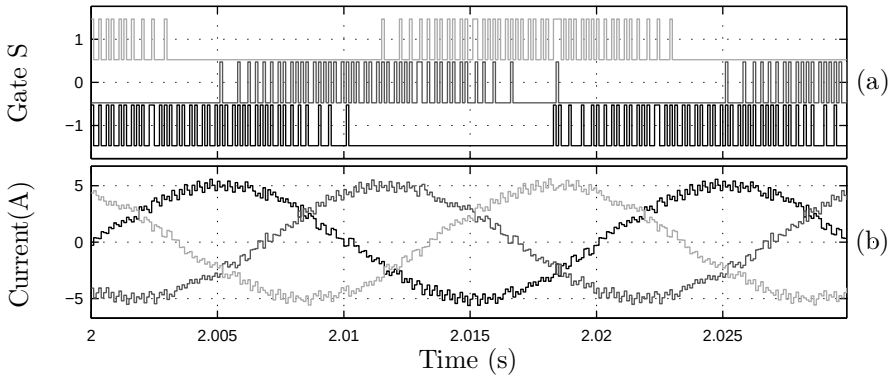

Figure 2.10: Performance 2-phase 3-level converter with RL load, with no switching frequency control: (a) Gate signal and (b) Output current for each phase

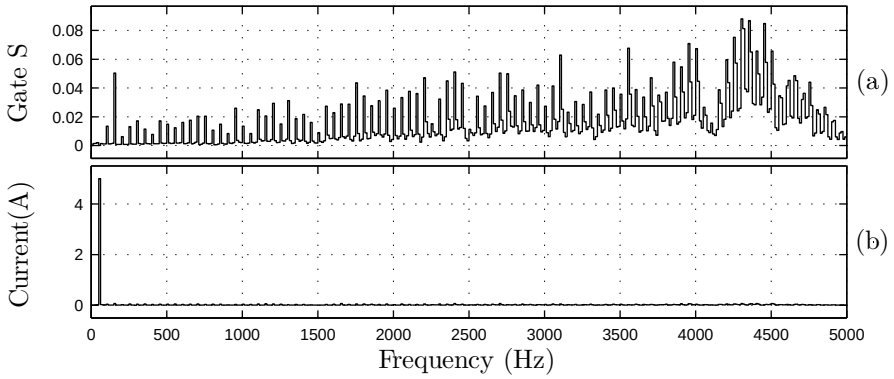

Figure 2.11: Frequency spectrum of the 2-phase 3-level converter with RL load, with no switching frequency control: (a) Switching spectrum and (b) Current spectrum

and spectrum.

Since the problem of switching frequency is of major concern in the research field of FCS-MPC, many alternatives have been presented to solve it. Since it is not possible to address every possible strategy and every variant for any system or set up, a minor set of these solutions is selected for comparison purposes. The main criteria for this selection is the general approach that these techniques apply, being easy to implement in a wide range of converters without major changes in their structure.

2.5.1 Simple Penalization

The easiest and most straightforward way to reduce the switching frequency in FCS-MPC is the incorporation of a new element, J_{sw}, in the cost function that penalizes the act of performing a commutation. As with any element in the cost function, J_{sw} is pondered by the respective weight factor, λ_{sw}, to balance its effects against other control objectives. The equation implemented in the prediction stage of the control is

$$\Delta s_i(t_k) = |s_i(t_k) - s_i(t_{k-1})| \,, \tag{2.85}$$

$$J_{sw} = \lambda_{sw} \sum_{i=1}^{n_s} \Delta s_i(t_k) \,, \tag{2.86}$$

where $s_i(t_k)$, $i \in \{1, ..., n_s\}$, being the i^{th} switching element.

Since what is being penalized is the change of state, the controller is encouraged to keep the state of the semiconductors as they are, leading to an overall reduction of the average switching frequency. Nonetheless, the effective timing at which the switching is performed is still out of the control of the designer, thus producing a seemingly random switching pattern, and the respective frequency spectrum spread over a wide range of frequencies.

The name of Simple Penalization is not a standard in the literature, though no standard name is given to this strategy, but will be used in this document to refer to this strategy. This Simple Penalization has been implemented for multiple system, albeit sometimes with minor variations [41, 42].

The performance of this strategy is exemplified in figures 2.12 and 2.13. For this control method the sampling frequency is increased to 100 kHz, since unlike the case for figure 2.10, the switching frequency is now limited, up to some point, by the controller.

It can be seen here that the spectrum is compacted towards the low frequencies, while reaching a very similar performance in the current control in terms of overall ripple and spectrum. The main difference with the non controlled frequency case is that now the average frequency is near 1100Hz even when the sampling frequency is 10 time faster.

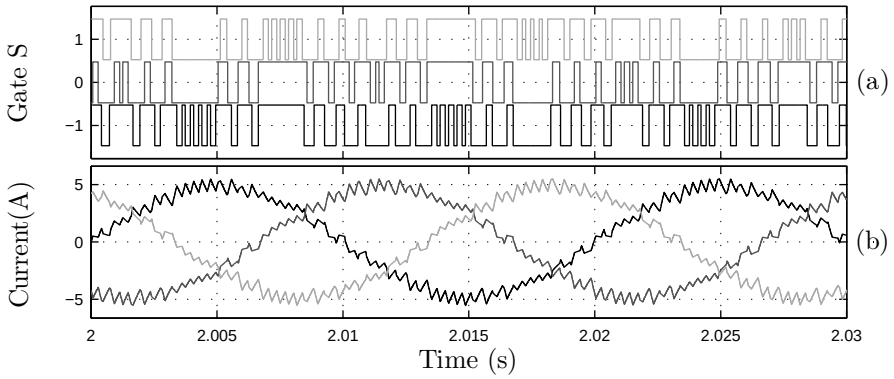

Figure 2.12: Performance 2-phase 3-level converter with RL load, with a Simple Penalization approach: (a) Gate signal and (b) Output current for each phase

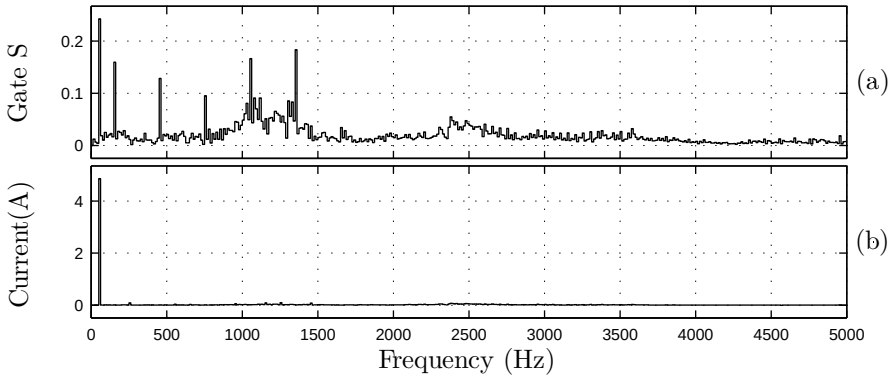

Figure 2.13: Frequency spectrum of the 2-phase 3-level converter with RL load, with a Simple Penalization approach: (a) Switching spectrum and (b) Current spectrum

2.5.2 Sliding Window

The main control objective of Sliding Window strategy is to reach an average switching frequency, $\bar{f}_{sw}$, defined by a reference f_r. This average is measured over a time window of fixed size of n samples, and is updated at every sampling time. To compute this frequency, each switching action in the observed window is added as

$$D_r = \frac{f_r}{f_s} n \ , \ \ n = \frac{T_w}{T_s} \ , \tag{2.87}$$

$$D_i(t_k) = D_i(t_{k-1}) + \Delta s_i(t_k) - \Delta s_i(t_{k-n}) \ , \tag{2.88}$$

$$J_{sw} = \lambda_{sw} \sum_{i=1}^{n_s} \left(D_i(t_k) - D_r \right)^2 \ \ , \tag{2.89}$$

where, f_r and f_s corresponds to the reference and sampling frequency respectively, T_w the length in time of the sliding window and D_r and $D_i(t_k)$ the sum of switching events reference and measurement respectively. The update of the measurement $D_i(t_k)$ is done by adding the new value of $\Delta s_i(t_k)$, defined as in equation (2.85), and subtracting the last value in sampled window, $\Delta s_i(t_{k-n})$. For most operations the size of the observed window, T_w, is the same as one fundamental period of the system. The implementation of this strategy is commonly done through a circular buffer that stores the values of $\Delta s_i(t_k)$. This permits a quick implementation to compute the average frequency. It is important to notice that each semiconductor i has its own measurement $D_i(t_k)$.

The advantages of this method are its low computation requirement, easy implementation and effectiveness in setting an average frequency. It is important to notice that this strategy must be accompanied by a simple penalization of the switching action to operate properly. This requirement comes from the fact that the same average frequency can be achieved with commutations evenly spread over the observed window or concentrated in a short time span. This additional term helps the controller to spread the commutations and achieve a more homogeneous performance.

Figure 2.14 illustrates this strategy's performance for a reference frequency of 1000Hz. The actual average frequency achieved by this strategy is of 1200 for a particular weight factor λ_{sw}. When this weight factor is increased, the average switching frequency is reduced, though unlike with Simple Penalization, the average converges to the desired frequency. It can be seen from figure 2.15 that even the switching spectrum, though slightly focused to the low frequencies, is still spread in a wide band.

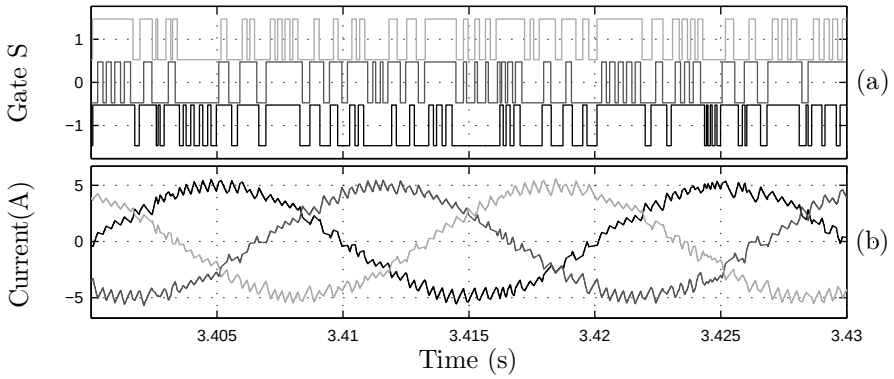

Figure 2.14: Performance 2-phase 3-level converter with RL load, with a Sliding Window approach: (a) Gate signal and (b) Output current for each phase

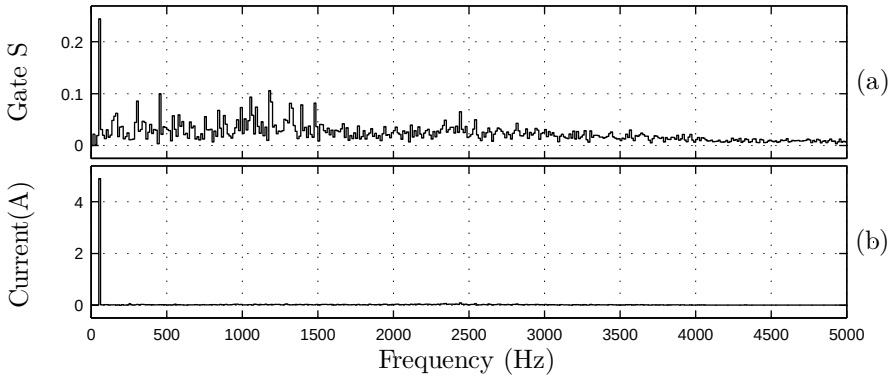

Figure 2.15: Frequency spectrum of the 2-phase 3-level converter with RL load, with a Sliding Window approach: (a) Switching spectrum and (b) Current spectrum

2.5.3 NOTCH Filter

Unlike the previous strategies, that focus on reducing the amount of switching events, this strategy aims to narrow the spectrum of the relevant variables to be around a desired frequency [13]. This is achieved by modifying the cost function of the relevant variable, by passing the error through a NOTCH filter function,

$$e_i = \hat{I}_k - I_r \tag{2.90}$$

$$J_i = \lambda_i F_{notch}\left(e_i, \omega_r\right)^2 \ , \tag{2.91}$$

where I_r and $\hat{I}_k$ correspond to the reference and predicted current respectively, and ω_r is the filtered out frequency .

The NOTCH filter transfer function gives an almost flat output for low and high frequencies but is heavily weakened at the reference frequency ω_r, thus reducing the cost of control actions that produce errors in the band around said reference. This leads to a resonant-like behavior near the desired frequency.

Since MPC is a discrete time control strategy, the implementation of the filter must also be done in discrete time. Considering a Tustin discretization of the transfer function of the NOTCH filter, the discrete filter can be implemented as

$$H(s) = \frac{Y(s)}{X(s)} = \frac{s^2 + \omega_r^2}{s^2 + \xi\omega_r s + \omega_r^2} \quad , \quad s \approx \tfrac{2}{T_s}\tfrac{z-1}{z+1} \tag{2.92}$$

$$H(z) = \frac{Y(z)}{X(z)} \approx \frac{\left(\frac{2}{T_s}\frac{z-1}{z+1}\right)^2 + \omega_r^2}{\left(\frac{2}{T_s}\frac{z-1}{z+1}\right)^2 + \xi\omega_r\frac{2}{T_s}\frac{z-1}{z+1} + \omega_r^2} \quad , \quad m = T_s\omega_r/2 \tag{2.93}$$

$$= \frac{(z-1)^2 + m^2(z+1)^2}{(z-1)^2 + \xi m(z^2-1) + m^2(z+1)^2} \tag{2.94}$$

$$= \frac{z^2(m^2+1) + 2z(m^2-1) + (m^2+1)}{z^2(m^2+\xi m+1) + 2z(m^2-1) + (m^2-\xi m+1)} \tag{2.95}$$

$$, \ m_a = m^2+1 \ , \ m_b = m^2-1 \ , \ m_c = \xi m \tag{2.96}$$

$$= \frac{(z^2+1)m_a + 2zm_b}{z^2(m_a+m_c) + 2zm_b + m_a - m_c}$$

$$\therefore \ y_0 = \frac{m_a\left(x_0+x_2\right) + m_b\left(x_1-y_1\right) - \left(m_a-m_c\right)y_2}{m_a+m_c} \tag{2.97}$$

where $x_i = x(k-i)$, $y_i = y(k-i)$, T_s the sampling time, ξ the inverse of the quality factor of the filter, x the filter input and y the filtered output

With this implementation, the computational burden of the filter is very small, since only one filter is required per controlled current, and each m_x is pre-designed based on the reference frequency.

A big drawback of this strategy is the fact that since the filter is allowing the controller to disregard the current control at a narrow bandwidth, this translate the presence of this frequency in the current. This can be appreciated in figure 2.16(b), where a quite relevant oscillation is present in the current, and over which there is no real control. Nonetheless, thanks to this resonance behavior the switching pattern achieved by the controller becomes very stable, similar to that of a PWM strategy.

The resonance behavior can be further proved by the analysis of the spectrum generated by this controller, in figure 2.17. Here it can be seen a clear peak at the resonant frequency, though it is important to remark that this is not the provided reference, which was defined to be 2000 Hz. In fact, the effective frequency changes with the weight factor associated with the switching penalization, λ_{sw}. For high values of λ_{sw} the system tends resonates at lower frequencies than the defined by the filter.

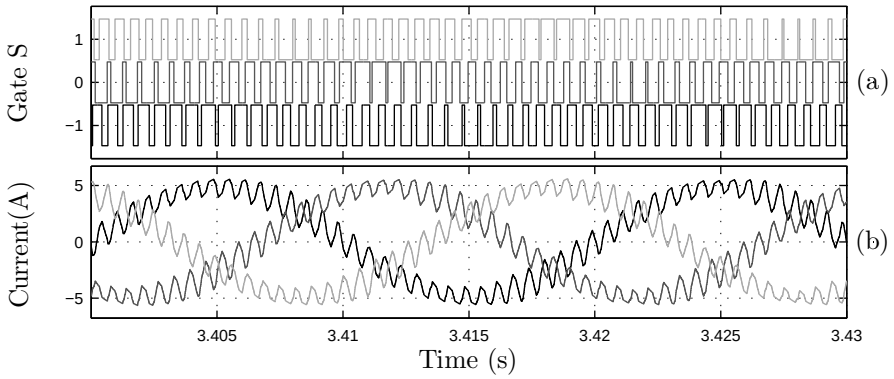

Figure 2.16: Performance 2-phase 3-level converter with RL load, with a NOTCH Filter approach: (a) Gate signal and (b) Output current for each phase

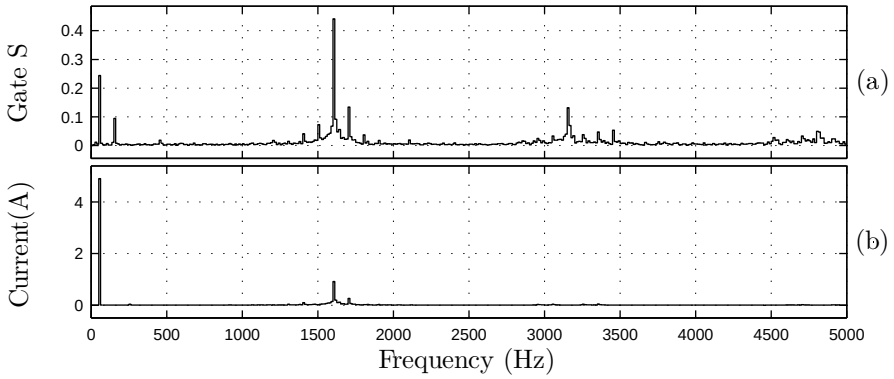

Figure 2.17: Frequency spectrum of the 2-phase 3-level converter with RL load, with a NOTCH Filter approach: (a) Switching spectrum and (b) Current spectrum

Chapter 3

Period Control

So far the presented strategies are, up to some extent, able to reduce or regulate the switching frequency in a power converter. Nonetheless, all these strategies fail to produce a regular switching pattern as the one achieved through PWM control strategies while also achieving a clean control over the other control objectives.

In this chapter a new technique is presented , Period Control based FCS-MPC, to solve the variable average device switching frequency, the spread voltage and current spectra, and uncharacteristic switching pattern. The proposed method is based on an overlap of switching periods (between two up or down edges), which are directly included in the cost function. The addition of this new term in the cost function does not significantly increase the complexity of the predictive model nor the computational burden, as well as being decoupled from other control goals, facilitating the design of the weighting factors. Furthermore, the proposed method is compared to the different techniques reported, through experimental results and analysis applied to a 2-Level 3-Phase voltage source converter connected to a linear load in order to highlight the technique's performance.

The main design objective behind this method is to achieve a similar switching pattern as the one produced by PWM strategies. The goal of mimicking this pattern is to produce a cleaner switching spectrum and decoupling the switching frequency from other control objectives.

The proposed strategy of Period Control gets its name from the approach taken to the control of the switching frequency. Instead of analyzing the effective frequency at which the system switches, this strategy evaluates the time elapsed between commutations, thus measuring the effective switching period.

3.1 Operating Principle

An important characteristic of FCS-MPC is the use of the sampled data values to perform the predictions for the future steps. This means that each variable is measured at the instant it is required, is used for the respective prediction process and is then replace with the next measurement at the next sampling time. In a basic implementation of FCS-MPC no memory is used for storing the state of the system from previous samples. This permits a very fast control action, aiming to fix the state of the controlled system as soon as a deviation is observed. Therefore, it would be desirable to have a similar behavior when measuring the frequency, without memory requirements or delay or damping for the measurement. Nonetheless, there is no real meaning in asking for the instantaneous frequency of a non-continuous signal, as would be the trigger signal of a switch, since this is a variable that concerns with the behavior of a variable in time. Basically, frequency can be defined as the amount of times an event takes place over a time window, thus, it has no meaning as an instant value, since it will always depend on the past data contained in that window or its possible predictions.

An alternative to somewhat solve this time issue is to use the frequency definition as the inverse of a period, i.e. $F = T^{-1}$. This way, the definition of frequency would be the inverse of the time required for an even to repeat itself. Based on this definition, only two consecutive events are required to compute the frequency, thus somewhat reducing the dependence on past data, making the measurement more "instantaneous". Figure 3.1 (a) illustrates how this measurement would be taken by considering the falling edge of a gate signal as the relevant event to consider. Since the relevant event for this measurement is the falling edge, the rising may occur at any time without altering this measurement.

An issue that rises from this measurement strategy can be observed in figure 3.1 (b). In black it is shown how the frequency measurement evolves as time passes without a commutation. It can be seen that every step in in time, the step frequency is smaller than the previous one, showing an ever decreasing and fast changing slope. In most systems controlled by FCS-MPC the slope of the error implemented in the cost function is either constant or varies very slowly with time. Thus, this rapidly changing slope so uncharacteristic of most variables, seems unfit to be used in a cost function. Nonetheless, from the same figure it can be seen that the period measurement grows linearly with each sample taken to reach the next event. This suggest that, instead of using a frequency variable, a better approach would be to measure and control the period of the signal.

The period of the signal, as presented in figure 3.1 is measured from two consecutive falling edge, neglecting the rising edge. If only the falling edge was to be used for the switching control, there is no guarantee that a proper control could be achieved for the rising edges. Since it is required to control both events to properly regulate the commu-

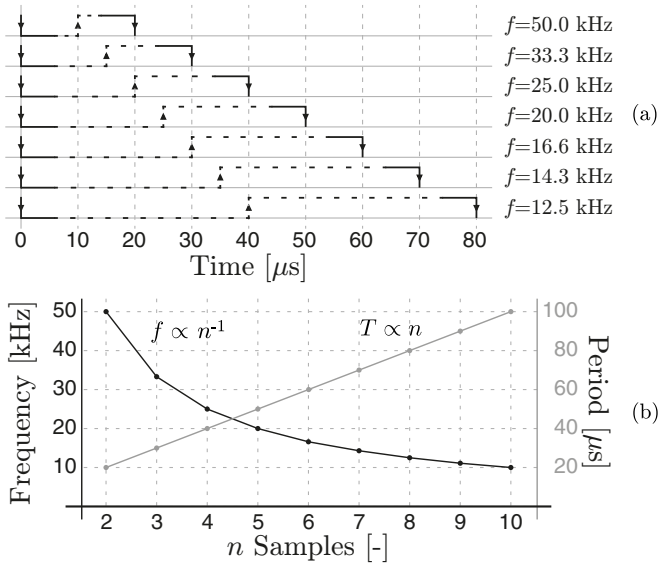

Figure 3.1: Low backtracking strategy (a) Frequency measurement and (b)Frequency and period measurement growth per sample

tations, a measurement from rise to rise is also included for the same signal. Figure 3.2 illustrates this strategy for both measurements, the time between falling edges, T_d, and the time between rising edges, T_u.

A fundamental characteristic of FCS-MPC is the fixed time between two consecutive samples. This means that the period measurements, T_u and T_d, can only achieve a discrete set of values. Taking this into account, and in consideration of computation time, it is better to work with these values not in terms of time, but in terms of the number of steps taken from edge to edge. This conversion allows to work with integer values for T_u and T_d, and simplifies their computation. These values are therefore written as

$$K_u = T_u/T_s \quad , \quad K_d = T_d/T_s \; . \tag{3.1}$$

An interesting property of this measurement is that it is blind to the duty cycle, as illustrated in figure 3.2. This means that for the same switching frequency the resulting periods are always constant, regardless of the relative time at which the rising or falling edges takes place. In most PWM based control strategies the chosen control input is the duty cycle applied to the semiconductors. This leads to the conjecture that with this measurement it might be possible to control the switching frequency without hindering other control objectives, at least in steady state, since the duty cycle is independent of the

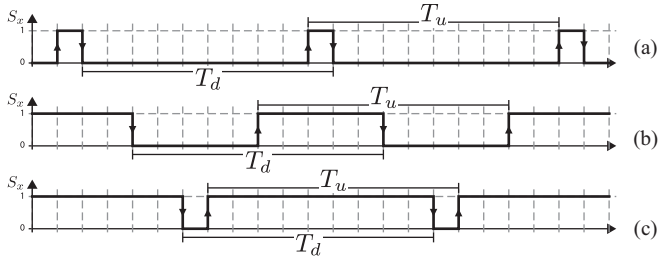

Figure 3.2: Constant measurement of T_u and T_d for duty cycles of (a) 10%, (b) 50% and (c) 90%

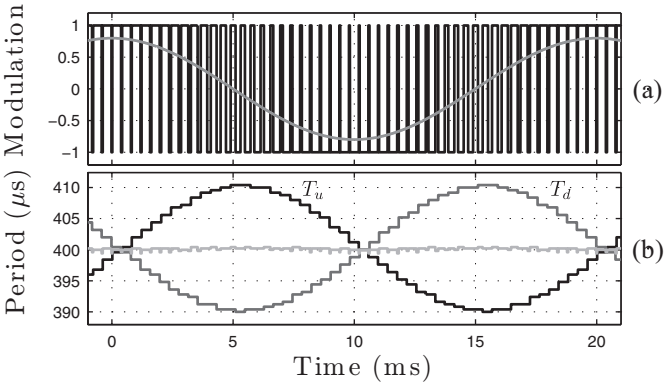

Figure 3.3: Period measurement variation for a PWM signal; (a) PWM and reference, and (b) T_u, T_d and average measurements.

period measurement. It is important to notice that this independence is valid only for a constant duty cycle. If the duty cycle is changed, as would be the case for a sinusoidal output voltage in a VSC, the period measurements would be slightly off of a constant value, as shown in figure 3.3. Here it can be seen that when the duty cycle is close to constant, i.e. at the maximum and minimum of the sinusoidal, the period measurement is very close to, if not exactly the average, for both T_d and T_u. Meanwhile, when the duty cycle changes rapidly, as it is when the sinusoidal is close to zero, the period measurement shows the biggest deviation. It is worth noting that the T_u and T_d show opposite behaviors to the same change in the duty cycle. For a rising duty cycle T_u falls bellow the average while T_d rises above it in a similar fashion; for a falling duty cycle, the situation is reversed. Overall, the average measurement, $T_a = (T_u + T_d)/2$, is roughly the same, regardless of the duty cycle changes.

Table 3.1: Edge detection table

$s_i(t_{k-1})$	$s_i(t_k)$	$E_{i,u}(t_k)$	$E_{i,d}(t_k)$
0	0	0	0
0	1	1	0
1	0	0	1
1	1	0	0

To properly compute the period measurement the edge detection must be properly differentiated between switching events. Since the gate signal can be understood as a boolean variable, the behavior between two samples can be fully mapped, as shown in table 3.1.

Here $E_{i,u}(t_k)$ and $E_{i,d}(t_k)$ are the up and down edge detection of the i^{th} semiconductor. Therefore, the UP and DOWN edge detection for a whole system are respectively computed as

$$\mathbf{E}_u(t_k) = \overline{\mathbf{S}}_{k-1} \wedge \mathbf{S}_k \ , \tag{3.2}$$

$$\mathbf{E}_d(t_k) = \mathbf{S}_{k-1} \wedge \overline{\mathbf{S}}_k \ , \tag{3.3}$$

where $\mathbf{S}_k$ and $\mathbf{S}_{k-1}$ are the state vectors of the n_s semiconductors for the current sampling time and the immediately previous one respectively, with $\overline{\mathbf{S}}$ the negated value of $\mathbf{S}$.

3.2 Two stage algorithm

The main goal of Period Control is to guide the switching pattern to a stable switching period. Due to the nature of the period measurement, the values of K_u and K_d rise steadily when the semiconductors stay constant, but are reset to zero when the respective commutation is performed. These quick changes do not fit in the classical behavior of most common variables of FCS-MPC, such as current or voltage and make the period measurement unsuitable for the optimization stage. The main difference is that the stage of measurement and the stage of prediction can not be implemented following both the same logic. For the implementation of Period Control, two different period measurement algorithms are used. For the computation of both algorithms the negated value of $\mathbf{E}$ is used, which is expressed as

$$\overline{\mathbf{E}}_u = \mathbf{S}_{k-1} \vee \overline{\mathbf{S}}_k \ , \tag{3.4}$$

$$\overline{\mathbf{E}}_d = \overline{\mathbf{S}}_{k-1} \vee \mathbf{S}_k \ . \tag{3.5}$$

The first algorithm used during the delay compensation stage is in charge of keeping track of both period measurements, for each semiconductor, thus being responsible for the gradual rise and abrupt fall of these variables. In this algorithm the values of $\mathbf{K}_u$ and $\mathbf{K}_d$ are increased by $+1$ if no commutation takes place in the respective semiconductor, and resets to 1 when the corresponding up or down commutation occurs. The correct reset value for the period measurements should be 0 when a commutation takes place, but since this process also involves the delay compensation, the measurement is automatically increased by 1. The computed value is also the stored measurement for futures steps, as follows

$$\mathbf{K}_u(t_k) = \mathbf{K}_u(t_{k-1})\overline{\mathbf{E}}_u + 1 \ , \tag{3.6}$$

$$\mathbf{K}_d(t_k) = \mathbf{K}_d(t_{k-1})\overline{\mathbf{E}}_d + 1 \ , \tag{3.7}$$

where $\mathbf{K}_u(t_k)$ and $\mathbf{K}_d(t_k)$ are the period measurement vectors of the n_s semiconductors, between up and down edges respectively. Here it can be seen why the negated value of $\mathbf{E}$ is used, since the reset is required only when a commutation takes place.

The second algorithm, used in the prediction stage, deals with the predicted values of $\mathbf{K}_u$ and $\mathbf{K}_d$ to be used in the cost function. As explained in section 2.4, the mechanism by which the cost function works is by evaluating the differences between all the control alternatives to choose the one that provides the best performance. If the first algorithm were to be used in the prediction stage, it would mean that for a switching semiconductor, the predicted $\mathbf{K}$ value would be reset to 1. This means that a switching semiconductor would always generate the same value in the cost function, regardless of the measured period, which goes against the goal of the algorithm. Therefore, the computation is modified such that, instead of resetting the value of the respective K, it just stays as it is if a commutation takes place, as follows

$$K_{up,j} = K_u(t_k) + \overline{E}_{up,j} \ , \tag{3.8}$$

$$K_{dp,j} = K_d(t_k) + \overline{E}_{dp,j} \ , \tag{3.9}$$

where $K_{xp,j}$ and $E_{xp,j}$ correspond to the respective j^{th} prediction. This logic can be understood as predicting the period measurement for the current cycle, instead of starting a new one, as would do the first algorithm.

Figure 3.4 illustrates how both algorithms are implemented in the control loop, where $a_k = a(t_k)$ for a more compact notation. It can be seen that the state of the system, $\mathbf{x}$, is predicted in the same way for the delay compensation stage as well as for the prediction stage, using the respective function $f(\mathbf{x}, \mathbf{S})$. On the other hand, the period measurement is first updated for the delay compensation, and later predicted for the prediction and optimization.

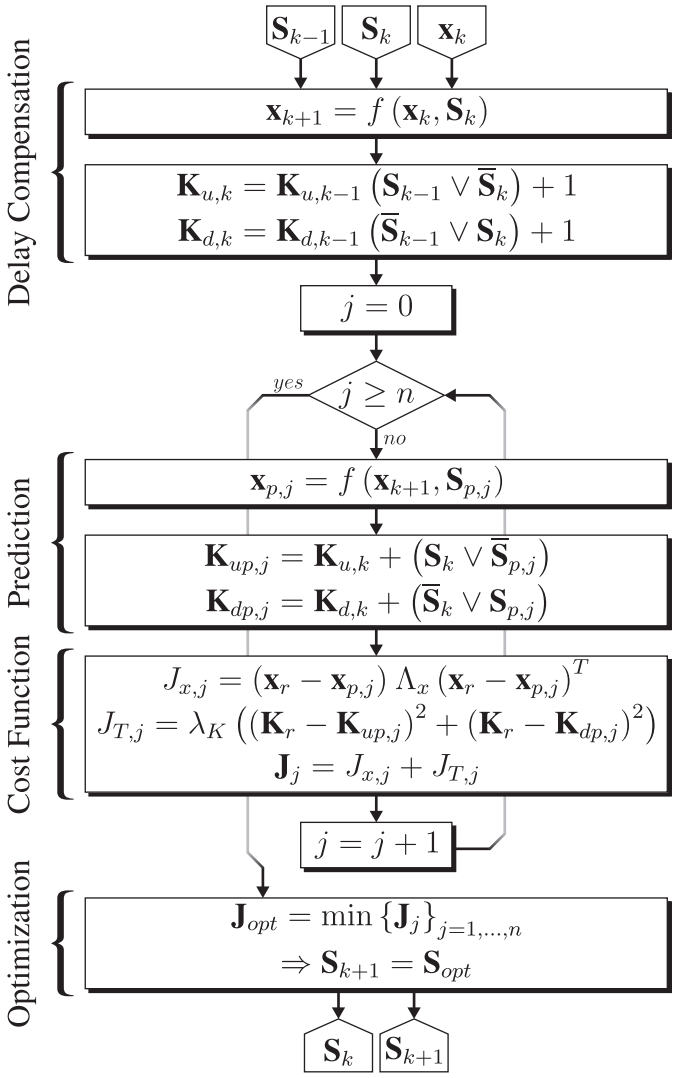

Figure 3.4: Flow diagram of FCS-MPC with Period Control

3.3 Cost Function and Weight Factor Design

A fundamental part of Period Control algorithm is the structure and design of the cost function element J_T, that is responsible of penalizing the Period error. For a small period measurement the cost function should heavily penalize changing the semiconductor states, while for a big period measurement, it should penalize not changing it. With the same logic, for low errors, either positive or negative, the cost function should barely notice any difference between these options, allowing the controller to prioritize other control objectives.

The chosen structure that fit with these requirements is the quadratic error cost, due to its property of penalizing bigger errors with more intensity. Therefore, the new element in the cost function is

$$J_T = \lambda_T \left(T_u - T_r\right)^2 + \lambda_T \left(T_d - T_r\right)^2 \tag{3.10}$$

Using equation (3.1) to express this cost function in terms of sample units

$$\begin{aligned} J_T &= \lambda_T \left(K_u - K_r\right)^2 T_s^2 + \lambda_T \left(K_d - K_r\right)^2 T_s^2 \lambda_T \\ &= \lambda_K \left(K_u - K_r\right)^2 + \lambda_K \left(K_d - K_r\right)^2 \end{aligned} \tag{3.11}$$

Even though K_u and K_d are integers, K_r is not bound to be an integer to properly work in the cost function.

As explained in (2.78), the influence of a control objective in a cost function, when a quadratic form is used, is given by the chosen weight factor and the absolute error of said objective. Another way of seeing this property is that the effective weight of J_T is given by its slope. Figure 3.5 (a) shows the case of a reference $K_r = 20$, where three distinct cases can be appreciated, being these a small period measurement, a near-reference period measurement and a big period measurement. When K, either K_u or K_d, is far lower than the reference, the action of keeping the semiconductor state constant (i.e. increasing K by 1) gives a significantly lower cost than changing it, shown as a big and negative ΔJ_1. This gives the action of not commuting a far greater chance to be chosen by the controller. When K is near the reference, the gap cost ΔJ_2 is much lower, which makes the commutation action almost irrelevant for the final cost. This allows the controller to perform a commutation near the reference if the system does requires so. Finally, when K is bigger than the reference, the action of changing states is better for the cost function, shown as a positive ΔJ_3, suggesting the controller to perform the commutation when a long time has passed since the last one took place.

The value of λ_K, though not being analytically obtained, must contain certain elements to compensate for variations in the control parameters. The first component comes

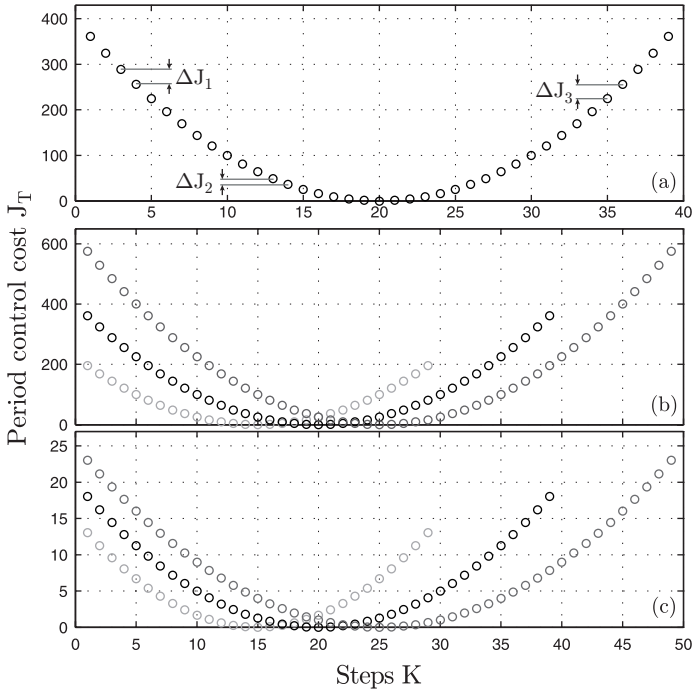

Figure 3.5: Cost J_T vs K for reference $K_r = 20$

from the use of whole integer steps as the computed variable instead of time, as shown in equation (3.11). To properly scale λ_K a factor of T_s^2 must be used.

A different situation rises when the reference is changed. A change in the reference switching frequency leads to a change in the slope of the cost curve, specially noticeable at the extremes, $K = 0$ and $K = 2K_r$, as seen in figure 3.5 (b). Since Period Control moves between high and low errors every time a commutation takes place, a change in the slope of J_T translates into a different effective weight factor when the error is high, that is, just after a commutation takes place. To compensate this change, a factor of $1/K_r$ can be applied to λ_K. With this factor, the slope of J_T at $K = 0$ becomes independent of the reference, which is demonstrated in (3.15) and illustrated in figure 3.5 (c), where each curve present the same slope at $K = 0$.

$$\lambda_K = \lambda_T \frac{T_s^2}{K_r} \tag{3.12}$$

$$J_T = (K - K_r)^2 \lambda_T \frac{T_s^2}{K_r} \tag{3.13}$$

$$\frac{\partial \mathbf{J}_T}{\partial K} = 2\lambda_T T_s^2 \left(\tfrac{K}{K_r} - 1 \right) \tag{3.14}$$

$$= -2\lambda_T T_s^2 \tag{3.15}$$

With these additional changes to λ_K, it is possible to design λ_T for one sampling period and one frequency, and later change them without major impact on the control performance. Though it is not a common practice to change the sampling frequency of a system, it proves to be useful when designing a controller for a different system based on an already functioning one. A similar case can be made for the switching frequency reference, though, as is shown later in this chapter, it can be implemented for the same system to allow corrections in the control performance.

3.4 Period Control Simulation Performance

Period Control is designed to produced a switching pattern similar to what PWM strategies produce. Nonetheless, due to the discrete time nature of FCS-MPC it is not possible to achieve the exact same results that a continuous time strategy would be able to. In this section, a series of simulation are performed to test the limits of this strategy and evaluate its performance.

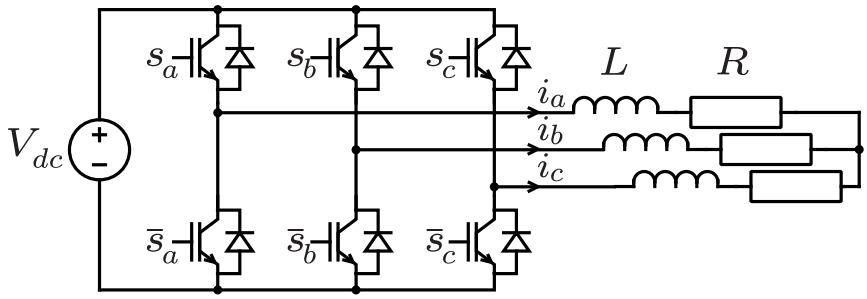

Figure 3.6: 2-level 3-Phase converter with linear load

3.4.1 Voltage Source converter

The chosen system for these simulations is a simple 3-Phase 2-Level converter with an RL-load and a DC Voltage source, as shown in figure 3.6. The goal of choosing such a simple system is to try to evaluate only the performance of Period Control, without the interference of other variables or control objectives. The parameters chosen for these tests are given in table 3.2.

Table 3.2: Simulation parameters

Variable	Parameter	Value
V_{dc}	DC Voltage	200 V
R	Grid Resistance	10 Ω
L	Grid Inductance	10 mH
I_r	Reference Current	5 A
f_s	Sampling Frequency	100 kHz

Since this is a balanced system, the model presented in section 2.3.2 can be used. The main equation for this system is rewritten with complex variables as.

$$L\frac{di}{dt} = -iR + sV_{dc} \tag{3.16}$$

where $i = \frac{2}{3}\left(i_a + ai_b + a^2 i_c\right)$ and $s = \frac{2}{3}\left(s_a + as_b + a^2 s_c\right)$, with $a = \left(-\frac{1}{2} + j\frac{\sqrt{3}}{2}\right)$.

For PWM based strategies to generate a sinusoidal current in this system, a sinusoidal voltage should be modulated by the converter. Equation (3.19) illustrates the voltage re-

quired to be modulated, V_r, for a current magnitude reference, I_r, and a frequency reference, ω_r.

$$i_r = I_r \cos(\omega_r t) \ , \tag{3.17}$$

$$\frac{di_r}{dt} = -\omega_r I_r \sin(\omega_r t) \ ,$$

$$V_r = R i_r + L\frac{di_r}{dt} \ , \tag{3.18}$$

$$= I_r \left(R\cos(\omega_r t) - L\omega_r \sin(\omega_r t)\right) \ ,$$

$$= I_r \sqrt{R^2 + L^2\omega_r^2} cos\left(\omega_r t + atan2\left(L\omega_r, R\right)\right) \ . \tag{3.19}$$

The maximum sinusoidal voltage achievable by this converter is equal to $\frac{V_{dc}}{\sqrt{3}}$. Therefore, the maximum sinusoidal current, for a frequency of $50Hz$, is

$$I_{r,MAX} = \frac{1}{\sqrt{3}} \frac{V_{dc}}{\sqrt{R^2 + L^2\omega_r^2}} \approx 11A. \tag{3.20}$$

3.4.2 PWM-like Performance

A first approach to evaluate Period Control is to give a constant maximum current reference of $\hat{I}_r = 5A$ and frequency reference $\omega_r = 100\pi\frac{rad}{s}$, to evaluate the performance at around half the maximum power. Also for this simulation, the reference for switching frequency is set to $1000Hz$.

As seen in figure 3.7, the voltage generated by the converter shows a strong resemblance with PWM strategies, while the current through this phase is properly controlled. This results provide a great first step to prove that Period Control is capable of achieving a modulated-like performance. Figure 3.8 show the respective current and voltage spectra, where it can be seen that the peaks in frequency are consistent with PWM pulse pattern. Furthermore, figure 3.9 show the magnitude of the relevant frequency peaks generated by bot predictive control and PWM. This curves are obtained by changing the modulation index for a PWM control strategy, and by gradually increasing the current reference for Period Control. It can be seen that, albeit with the presence of noise, the evolution of the harmonic frequency peaks follows very closely the performance of a PWM. These results shows that, for a switching frequency reference of $1000Hz$, Period Control is capable of producing a switching pattern very similar to that achieved with PWM strategies. It is important to notice that, due to the discrete time nature of FCS-MPC, it is not possible to achieve an exact modulation-like performance, since the semiconductor switching can only take place at certain discrete times.

An important advantage of these results over PWM strategies is the resulting voltage THD. As shown in figure 3.10 the resulting voltage THD is consistently smaller with FCS-MPC using Period Control than with PWM, for all modulation indexes.

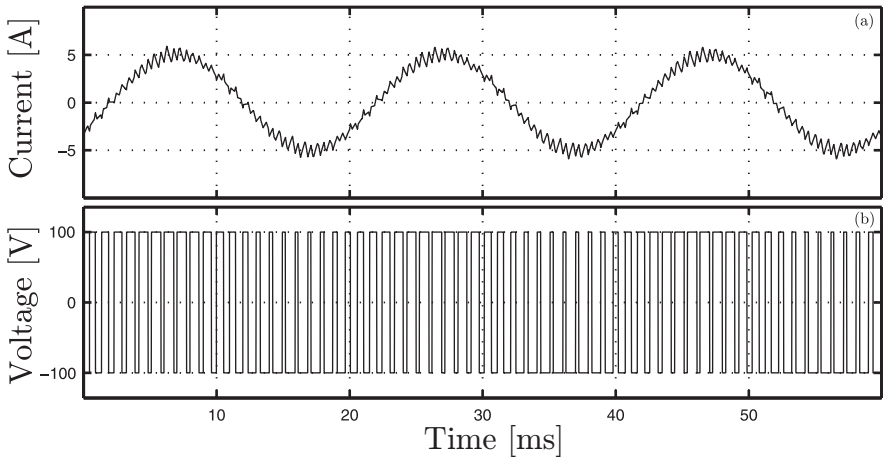

Figure 3.7: Simulation Results for one phase: a) Load current, b) converter Voltage

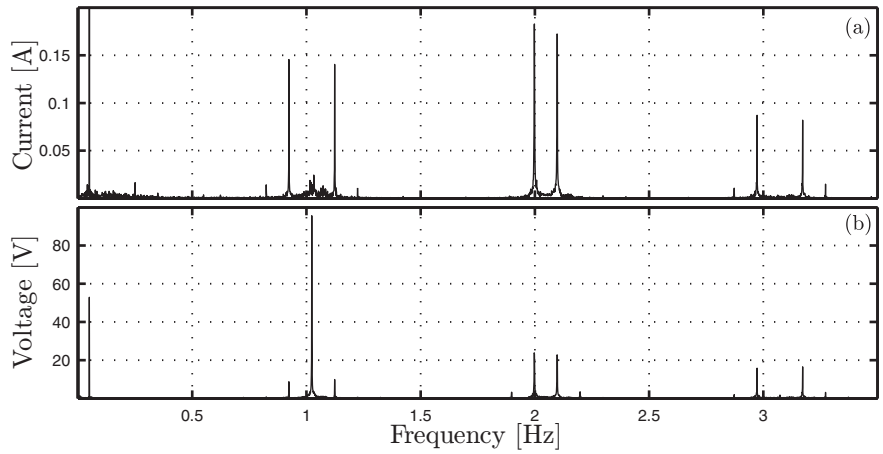

Figure 3.8: Simulated system spectrum: (a) Load current and (b) converter Voltage

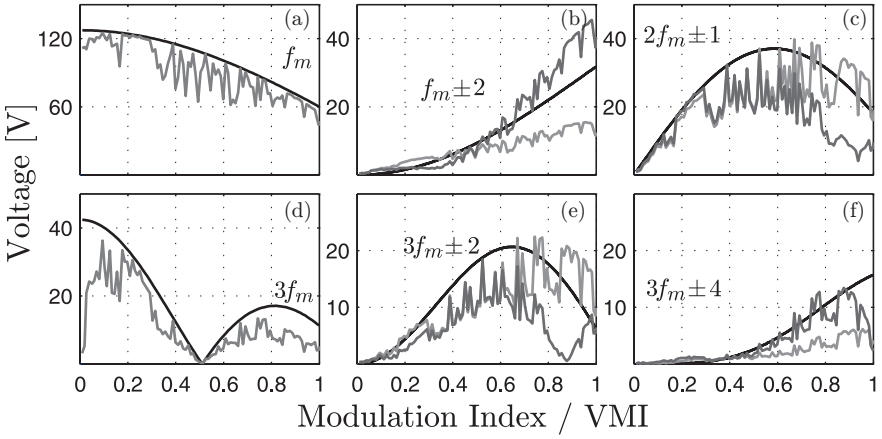

Figure 3.9: Phase voltage side band harmonics amplitude for ideal PWM (blakc) and FCS-MPC (grey hues), for a switching frequency f_m and its respective sidebands

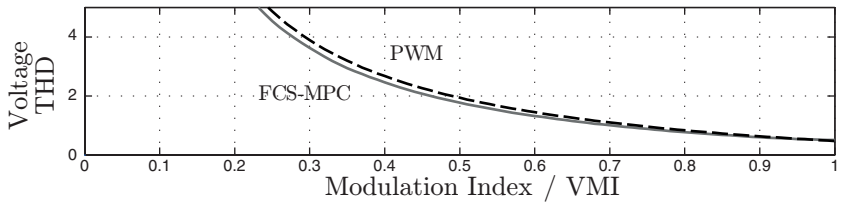

Figure 3.10: Normalized Phase Voltage THD for PWM(dashed) and FCS-MPC(solid)

3.4.3 Dynamic Performance

Predictive control is well known for its fast response to changes in its references. This is achieved by choosing the control action that drives the future state faster in the direction of the reference. By adding a new control element in the cost function, MPC has to balance more control objectives, usually resulting in less control efficiency or speed for the other objectives.

When Period Control is included in the cost function, it imposes a bigger cost on the commutation than on the current control. Thus, the controller is forced to restrain the commutation until the current error becomes too big or the period error becomes low enough. This restrain in the control action is bound to have an effect in the dynamic performance of the controller. This effect is illustrated in figure 3.11, where a current reference step from $1A$ to $5A$ is tested, with and without Period Control. As observed in (a), the controller takes less than a millisecond to reach the desired current values when Period Control is not active. On the other hand, when Period Control is implemented, the controller takes almost $2ms$ to reach the reference.

Though it is not desirable to reduce the response time of MPC, it is not a major drawback, considering that it still provides a fast response, faster than the $20ms$ period of the grid voltage. Figure 3.12 shows the respective gate signal for each leg. It can be seen that the switching frequency control is kept in both steady states and during transition.

3.4.4 Weight Factor Dependence

An important element in the control design of MPC strategies is the choice of the weight factor that accompanies the respective error element in the cost function. As explained in section 3.3, some elements involved in the design of the weight factor λ_T are dependent on the switching frequency reference and sampling frequency. Nonetheless, the final value of λ_K is still left to the user, without a clear design methodology. To properly choose λ_K, a series of test are implemented to evaluate the control performance by sweeping over a wide range of values.

The goal is to analyze the average switching frequency and current tracking error achieved for a set of 4 different switching frequency references, being these 500,1000,1500 and 2000 Hz. Figure 3.13 illustrates these results. Plot (a) presents the average frequency achieved for this range of weights. Here it can be seen that for a small λ_K the final frequency is shifted to high values, an gradually approaches the respective reference for higher weight factor. On the other hand, figures (b) and (c) present how the error in the current tracking grows with λ_K, both in magnitude and in phase. This growth come from the fact that the current control has to compete with the frequency control, thus loosing priority as a control objective. From these it can be seen that for a reference of 500 Hz the

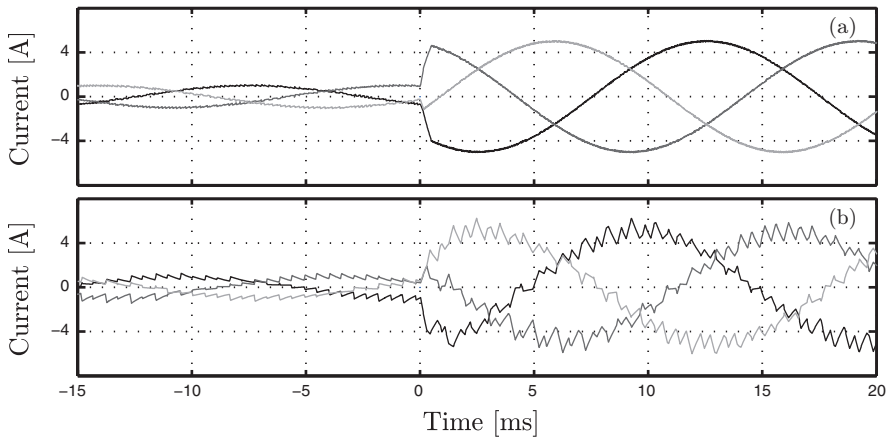

Figure 3.11: Reference step response with a) no control over the commutation vs b) Period Control with $\lambda_K = 20$ and frequency reference of $1kHz$.

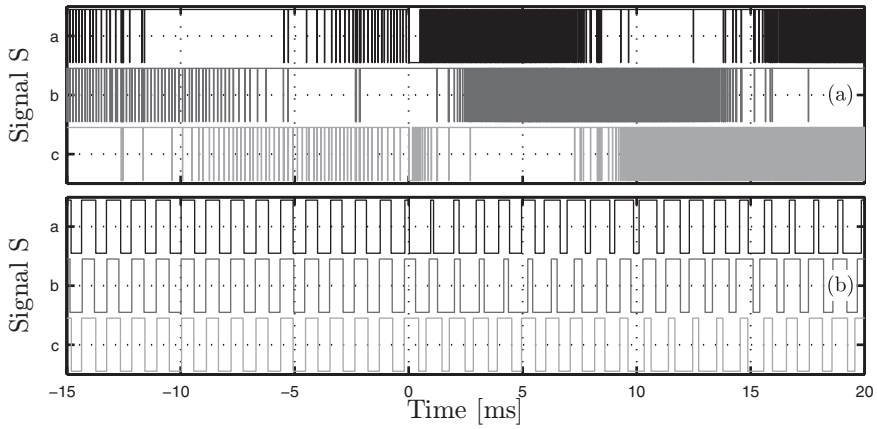

Figure 3.12: Gate signal S for a reference step with a) no control over the commutation vs b) Period Control with $\lambda_K = 20$ and frequency reference of $1kHz$.

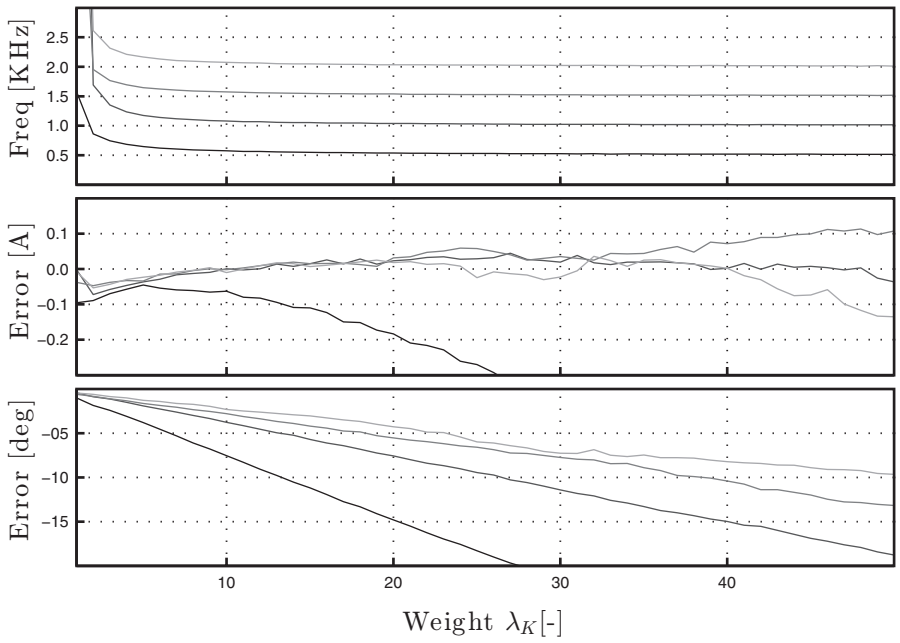

Figure 3.13: Control performance for a range of λ_K: (a) average switching frequency, (b) current magnitude error, (c) current phase error

current tracking error grows very rapidly, much more than the other reference frequencies. Though not studied in detail in this work, this rapid growth may come from the inability of the system to properly operate at such low frequencies, thus forcing the system to quickly fail in the current control to favor the switching frequency. For the other references, the error in magnitude is quite constant along the studied range, starting to spread when a value of λ_K around 20 is used, and diverges when reaching a value over 35, though always under an error of 3% of the reference, or 0.15 A. Meanwhile, the phase error behaves linearly with the weight factor, increasing with the highest slope for a reference of 500 Hz, and the lowest for 2000 Hz. From These results it can be seen that a good performance is achieved for frequency references of 1000 Hz and above, and a weight factor λ_K of around 10 to 20. Therefore, the following simulation and experimental results are taken with a $\lambda_K = 20$.

3.5 Special Considerations on Period Control Implementation

The design of Period Control as presented so far has been focused of the control of a single semiconductor as independent from the others. This means that each semiconductor is free to changes its state without consideration of the others. This causes no issue in the control of a simple system such as the 2-level 3-phase voltage source converter, used so far as an example. Nonetheless, there are some systems where the state of a semiconductor or its switching pattern should be, if not bounded, at least aware of how the others semiconductors are behaving. For these system, special considerations must be taken to allow a proper period control without hindering other control objectives nor forcing an unfeasible state on the system.

In this section two particularly relevant cases are studied. The first case is a mains connected NPC converter, and the second is an interleaved boost converter. Its relevant to note that these are not the only converters that might require special treatment, but are considered here due to their importance in renewable energy conversion systems.

3.5.1 NPC Period Control

As discussed in previous chapters, NPC converters are among the most widely used configurations in the industry, which makes them relevant for study and consideration. For the analysis of this topology, the system presented in figure 3.14 is studied and simulated. Table 3.3 presents all the possible states this converter can take, along with the generated voltage in $\alpha\beta$ coordinates. The discrete model of this system is quite similar to the 3-phase

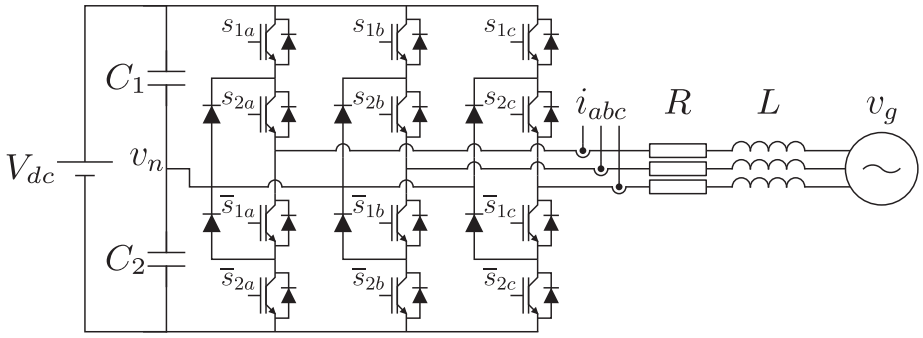

Figure 3.14: NPC basic structure for a grid connected system

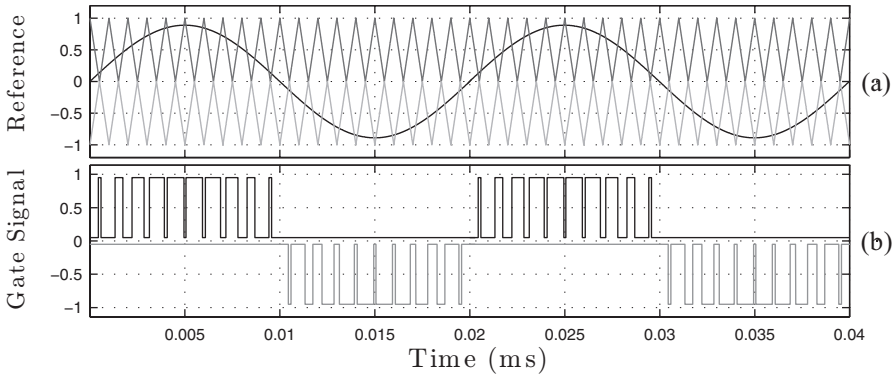

Figure 3.15: PWM NPC control; (a) reference and carriers, and (b) gate signal

converter with capacitive dc-link and grid connection, presented in figure 2.7. The only difference is that the possible voltages generated by the converter are much more varied.

As a first approach the implementation of Period Control for this system would consists on the use of period measurements for each pair of opposing semiconductors. This way there would be a measurement for up and down periods for each of the semiconductors in the first and second rows, $S_{x,y}$ $x \in \{1,2\}$ $y \in \{a,b,c\}$. As the third and fourth row have the negated value of the first and second respectively, no period counters are implemented for them. These periods would be used directly in the control strategy to fix the switching frequency.

The main problem that rises with this implementation of Period Control is the fact that for a normal operation, as shown in figure 3.15, the semiconductors should only switch for half the period of the reference signal, remaining constant during the other half. As it

Table 3.3: NPC 3-Phase Converter States

Voltage Vector	Switching State						Voltage $\alpha\beta$	
	s_{1a}	s_{2a}	s_{1b}	s_{2b}	s_{1c}	s_{2c}	v_α	v_β
v_0	0	0	0	0	0	0		
v_7	0	1	0	1	0	1	0	0
v_{26}	1	1	1	1	1	1		
v_1	0	1	0	0	0	0	$\frac{2}{6}v_{dc}$	0
v_8	1	1	0	1	0	1		
v_2	0	1	0	1	0	0	$\frac{1}{6}v_{dc}$	$\frac{1}{2\sqrt{3}}v_{dc}$
v_9	1	1	1	1	0	1		
v_3	0	0	0	1	0	0	$-\frac{1}{6}v_{dc}$	$\frac{1}{2\sqrt{3}}v_{dc}$
v_{10}	0	1	1	1	0	1		
v_4	0	0	0	1	0	1	$-\frac{2}{6}v_{dc}$	0
v_{11}	0	1	1	1	1	1		
v_5	0	0	0	0	0	1	$-\frac{1}{6}v_{dc}$	$-\frac{1}{2\sqrt{3}}v_{dc}$
v_{12}	0	1	0	1	1	1		
v_6	0	1	0	0	0	1	$\frac{1}{6}v_{dc}$	$-\frac{1}{2\sqrt{3}}v_{dc}$
v_{13}	1	1	0	1	1	1		
v_{14}	1	1	0	0	0	0	$\frac{4}{6}v_{dc}$	0
v_{15}	1	1	0	1	0	0	$\frac{3}{6}v_{dc}$	$\frac{1}{2\sqrt{3}}v_{dc}$
v_{16}	1	1	1	1	0	0	$\frac{2}{6}v_{dc}$	$\frac{2}{2\sqrt{3}}v_{dc}$
v_{17}	0	1	1	1	0	0	0	$\frac{2}{2\sqrt{3}}v_{dc}$
v_{18}	0	0	1	1	0	0	$-\frac{2}{6}v_{dc}$	$\frac{2}{2\sqrt{3}}v_{dc}$
v_{19}	0	0	1	1	0	1	$-\frac{3}{6}v_{dc}$	$\frac{1}{2\sqrt{3}}v_{dc}$
v_{20}	0	0	1	1	1	1	$-\frac{4}{6}v_{dc}$	0
v_{21}	0	0	0	1	1	1	$-\frac{3}{6}v_{dc}$	$-\frac{1}{2\sqrt{3}}v_{dc}$
v_{22}	0	0	0	0	1	1	$-\frac{2}{6}v_{dc}$	$-\frac{2}{2\sqrt{3}}v_{dc}$
v_{23}	0	1	0	0	1	1	0	$-\frac{2}{2\sqrt{3}}v_{dc}$
v_{24}	1	1	0	0	1	1	$\frac{2}{6}v_{dc}$	$-\frac{2}{2\sqrt{3}}v_{dc}$
v_{25}	1	1	0	0	0	1	$\frac{3}{6}v_{dc}$	$-\frac{1}{2\sqrt{3}}v_{dc}$

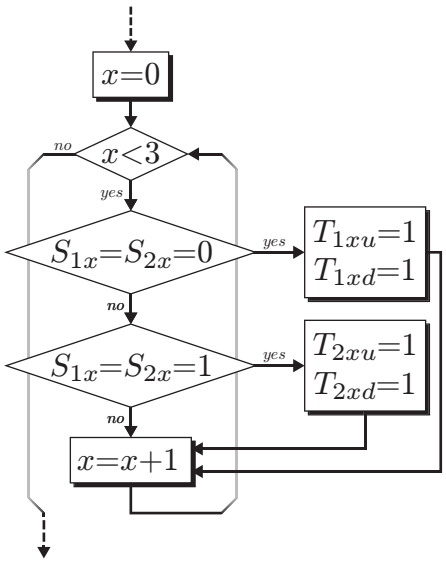

Figure 3.16: Period Control measurement changes

is defined so far Period Control penalizes both short and long switching periods, reducing the penalization near the reference. If Period Control is implemented as it is, the controller would try to force a commutation of the semiconductors during the time it should remain steady, forcing unexpected control actions and hindering the control performance.

A first approach to solve this issue would be to simply forbid certain states for either positive of negative references, avoiding this problem completely . Nonetheless, the prohibition of states in a controller reduces the control flexibility by limiting the available actuation range. This is not a desirable characteristic, due to the need to answer to unexpected situations, caused by either noise, disturbances, malfunctions, reference changes, etc. Therefore, a better solution is to heavily penalize the undesired states, while still allowing their application if and extreme cases would occur.

The solution given to this problem is to implement the same period counters as explained previously, but changing the events that resets them. So far, with the basic implementation, each period counter is reset when the respective event occurs. The intended change is to add a new reset event to the period counters, being this the detection of maximum or minimum voltage on the converter. This means that if a phase is switching on the positives voltages, the lower semiconductors are penalized as if recently switched, and vices versa. Thus, if a phase is connected to $+V_{dc}$, the period measurement for the second row semiconductor on said phase is reset. On the contrary, if said phase is connected to 0, the the measurement for the first row semiconductor is reset. This way, using figure 3.14

as reference, the period counter for the semiconductors in the first row are reset to 1 when the respective semiconductor in the second row, S_2x, becomes inactive. In the same way, the period counter for the semiconductors in the second row are reset when the respective S_1x, is active. A flow diagram for this changes is presented in figure 3.16 With these resets the cost function still takes into consideration the commutation of all semiconductors, but always penalizes with greater emphasis the inactive semiconductors as if a commutation just took place.

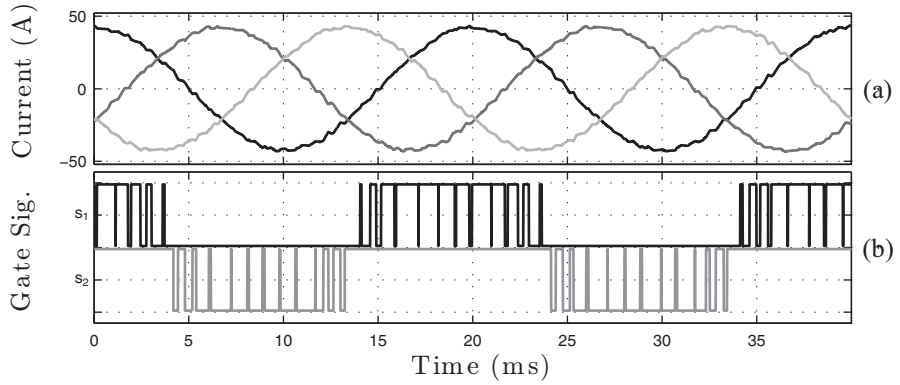

Figure 3.17: NPC with Period Control; (a) Output Current and (b) Gate signal for phase A

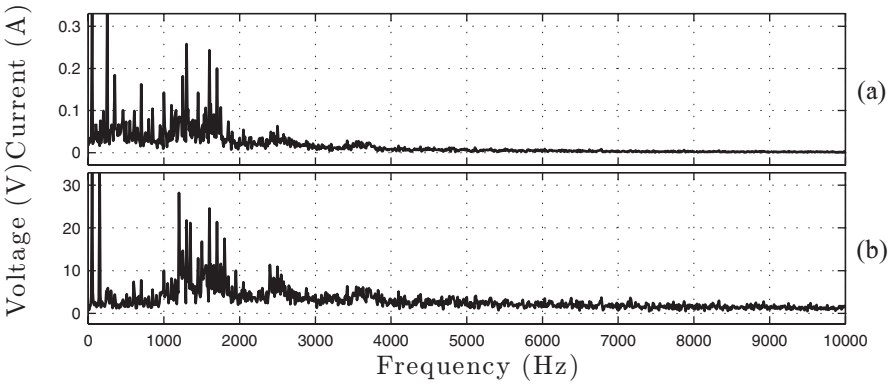

Figure 3.18: Spectral analysis; (a) Current spectrum and (b) NPC Voltage spectrum

The NPC system of figure 3.14 is simulated to validate the proposed strategy. To simplify the control and reach a better analysis of the proposed changes, the capacitors C_1 and C_2 are replaced by constant dc voltage sources of $\frac{1}{2}V_{dc}$. The parameters used for this simulation are listed in table 3.4

Table 3.4: Simulation parameters

Variable	Parameter	Value
V_{dc}	DC Voltage	600 V
R	Grid Resistance	$0\ \Omega$
L	Grid Inductance	10 mH
V_g	Grid Voltage	$220\sqrt{2}$ V
F_g	Grid Frequency	50 Hz
I_r	Reference Current	$30\sqrt{2}$ A
f_s	Sampling Frequency	100 kHz

Figure 3.17 shows the resulting current for a switching frequency reference of 1000 Hz, as well as the gate signal controlling the semiconductors of phase A (black current). On the same line, the spectrum of both output current and converter voltage are plotted in figure 3.18.

It is shown that the final switching pattern maintains a stable performance, with an almost constant switching period, which translates into a stable switching frequency. From the voltage spectrum, in figure 3.18(b) it can be seen that a third harmonic of high amplitude is present. This is similar to what a Min-Max injection strategy would achieved, though no input is given to the controller to reach this behavior. As expected due to 3-phase cancellation, this third harmonic is not present in the current. A fifth harmonic seems to be of relevance in the current due to the scale of the plot, but the value of this peak is of $.24$ A, that compared to the 42.3 A of the fundamental of 50 Hz is negligible.

With this good performance to backup the strategy modifications, the same simulations are performed with different weight factors, in order to evaluate the sensitivity of the controller to this parameter. Figure 3.19 shows the spectra of both the output current and the NPC output voltage, with a gradually increased weight factor, with higher weight factor at the top and close to zero at the bottom. It can be appreciated that for a higher weight factors the resulting spectrum becomes more prominent in narrow bands, and these bands aim to the reference frequency of 1000 Hz. Also, as expected with lower frequency commutations, the control over the current is less effective, allowing the presence of low frequency harmonics and increasing the overall current tracking error. This error can also be observed in figure 3.20, where it is shown the error in the current tracking, both in magnitude and phase. As expected based on the results obtained for a 2-level converter, the current tracking is worst when the weight factor applied to the period control element is higher. For the error in magnitude, it seems to show a more erratic increment than the 2-level converter, though an increment nonetheless. On the other hand, the phase error seems

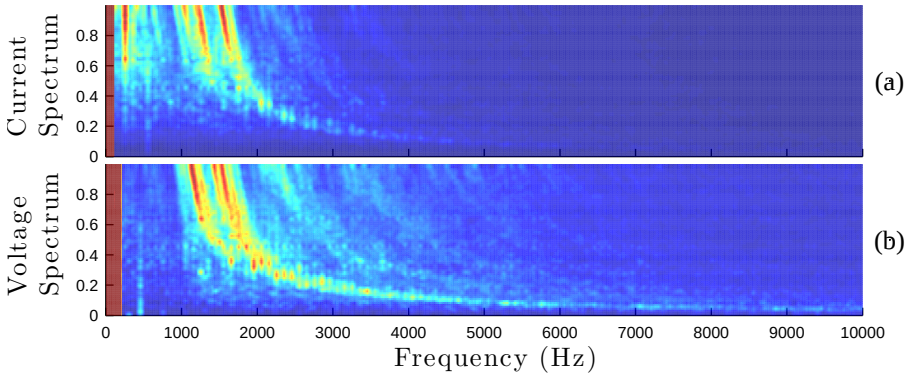

Figure 3.19: NPC spectra for increasing Period weight factor; (a) Current spectrum and (b) Voltage spectrum

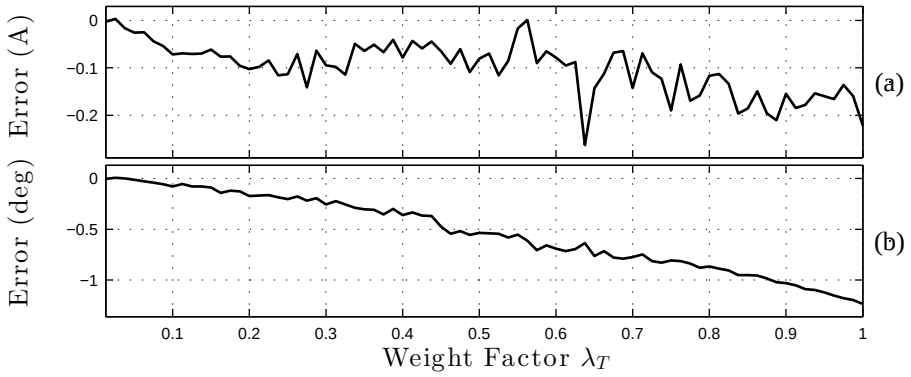

Figure 3.20: NPC current tracking error; (a) Current error magnitude and (b) phase

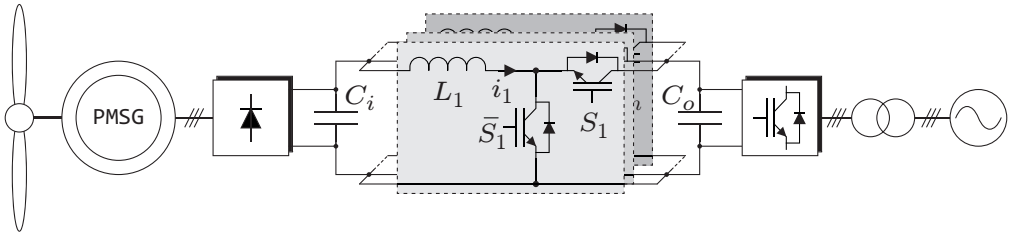

Figure 3.21: Interleaved Converter for WEC system

to present a similar linear behavior as the one obtained previously, thus being candidate for the same correction strategy presented early in this section.

The main issue with the achieved performance comes from the deviation from the desired frequency near the transition between high an low voltage. The main reason for this deviation is due to the change rate of the demanded voltage, which forces a drastic change in the ideal period counts, as explained in section 3.1.

Overall, the performance achieved with the implementation of Period Control on the NPC converter is satisfactory in the objective of reducing the switching frequency and focusing the spectra in a narrower band. Nonetheless, the desired performance of a PWM-like switching pattern is not achieved with the proposed modifications. This is most likely due to the high change in the required duty cycle for each leg of the converter, particularly at the transitions between positive and negative output voltage.

3.5.2 Interleaved Boost Converter

Another common converter topology, that has already been mentioned in previous chapters is the interleaved boost converter. The main advantage of this converter is that it permits the distribution of the power management among multiple identical converter, while also allowing to reduce the ripple caused by commutations on the total current. Figure 3.21 illustrates this system for a wind energy conversion system, though the same system can be devised for a PV system, though in a different power scale. Here the input, composed by the rectifier and backwards, can be simplified as a current source. On the other side, the output , composed by the output capacitor and forward can be simplified as a voltage source, since for most applications the output converter is the one in charge of keeping this voltage as constant. The model of this system is therefore the same as presented in section 2.3.1. Table 3.5 shows the parameters used for the simulation of this system.

For the first objective, of power distribution, with classic controllers, each module is

Table 3.5: Interleaved Converter Simulation parameters

Variable	Parameter	Value
V_o	DC Voltage	600 V
L_x	x^{th}Module Inductance	150 mH
C_i	Input Capacitor	10 mF
I_i	Input Current	30 A
f_s	Sampling Frequency	100 kHz
F_{sw}	Switching Frequency	1000 Hz
V_i^*	Input Voltage Reference	300 V
W_i	Current Weight Factor	10^0
W_v	Voltage Weight Factor	10^3
W_s	Switching Weight Factor	10^{-2}
n	# of Interleaved Modules	3

given a reference that is a fraction of the whole current,while managing the same input ad output voltages. When implementing predictive control in this system the first objective of power distribution is not difficult to achieve the same goal with a similar strategy.

When addressing the challenge of reduced ripple with the same switching frequency some issues rises. The ripple reduction is achieved in classic control strategies by shifting the carrier signals of each module by a fraction of the switching period. Therefore, from the perspective of the input capacitor, the interleaved converter is switching n times faster than a single module. Here is where Period Control becomes insufficient. One of the characteristics of Period Control is that it considers each semiconductor as independent of each the other. This means that, for its implementation in the interleaved boost, where each module is mostly independent of each other, the controller has no way to establish a connection between them in order to achieve a shifted carrier like behavior. This is illustrated in figure 3.22, where it can be seen that a constant switching frequency is achieved, as well as a proper control over the currents through each module. Nonetheless, the total current ripple is quite high, and in a similar magnitude as that of each module.

To address this issue, a new control element is included in the cost function. This new element is structured as a limit, as presented in section 2.4.4, and is responsible of restricting the total current. When properly chosen, this limits forces each module to shift their performance in time in order to comply with the restrictions. In the presented simulation, the limit is set as a band around the total current of magnitude equal to $1/3$ of the ripple at each module. Along with this limit, a second restriction is set on each

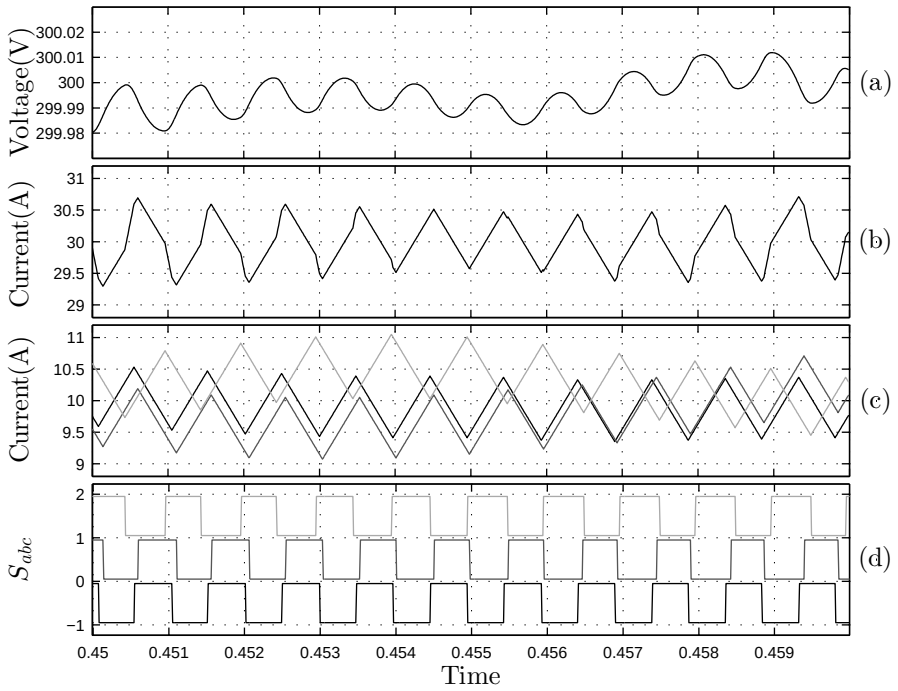

Figure 3.22: Interleaved converter simulation, without ripple correction: (a) Input capacitor voltage, (b) Total current, (c) Module currents and (d) Gate signals

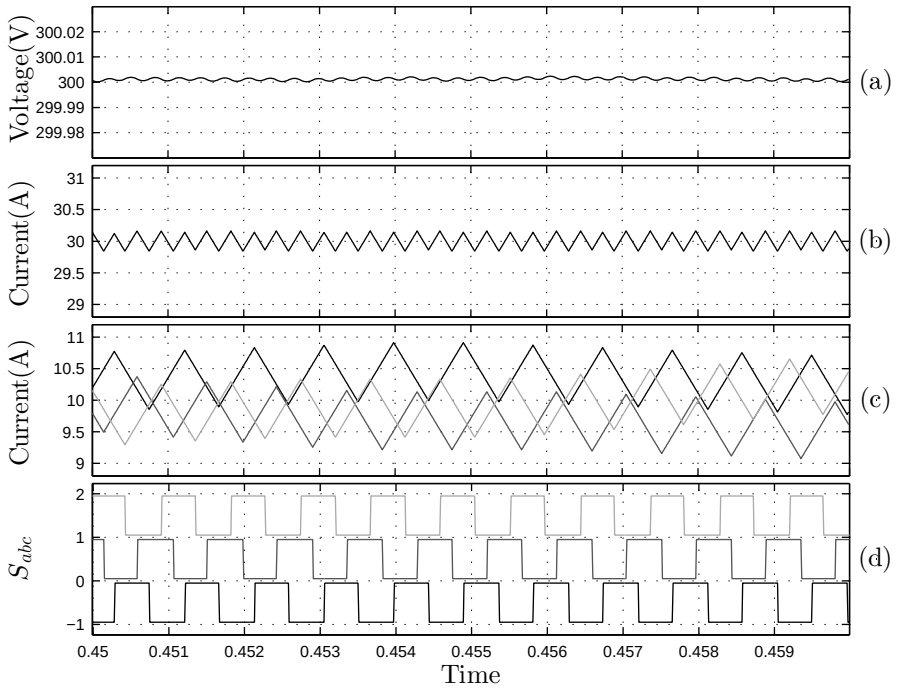

Figure 3.23: Interleaved converter simulation, with ripple correction: (a) Input capacitor voltage, (b) Total current, (c) Module currents and (d) Gate signals

module to bound the currents in a band of 4 times the expected ripple, to allow some room for balance between each module. The weight applied to these restrictions is 100 time the weight of the current.

As can be appreciated, the balance between each module remains inside the established boundaries, while the frequency control is achieved without obstruction. Along with these, the total current shows a significant improvement in its ripple, which is the expected performance of this converter. Though this is caused by the time shifting in the switching patterns, this shifting is caused strictly as a response to comply with the new operation boundaries, and is not established as a control parameter. Along with the ripple reduction, comes a much more stable capacitor voltage, thanks to the better tracking of the reference currents.

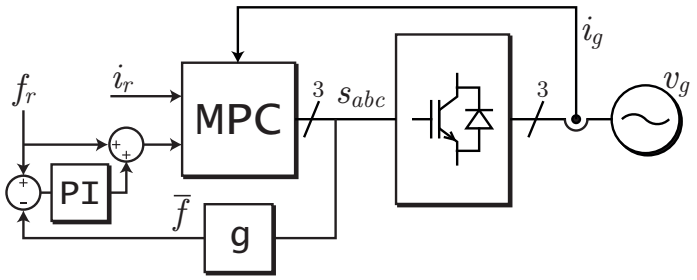

Figure 3.24: Modified control loop for fixed frequency

3.6 Modified Reference for Improved Control

As seen from simulations, and corroborated by the experimental results, Period Control is capable of achieving a stable switching pattern similar to that of a PWM strategy. Nonetheless, from the same results it can be seen that two major issues arise from this strategy. The first issue comes from the phase error in the current tracking. This error can also be seen as a delay in the current tracking, since the effective current is always behind the reference. The second issue comes from the compliance of a constant and well define switching frequency. For every frequency reference given to the controller the final result is a slight deviation towards the high frequencies, that changes according to the weight factor λ_K. Both issues demand for a change in the control structure to properly correct the final results.

The issue of frequency tracking is addressed in a fairly simple way, adding almost no computational demand, though

3.6.1 Frequency Fixing

As seen by all the results shown in figure 3.13, the final switching frequency achieved by Period Control is always higher than the given reference, and approaches it in what seems to be an asymptotic curve. It is also important to highlight that this behavior is true for any reference frequency. This means that a specific switching frequency can be achieved by either changing the weight factor or by changing the reference given to controller. This permits the design of a feedback loop that fixes the frequency reference given to MPC in such a way that the switching frequency actually matches the desired reference. Figure 3.24 illustrates the new control loop required for this to be implemented. Here the block g corresponds to the operation to get the average switching frequency. The measurement of the average frequency is done through a sliding window, just as the strategy

of the same name does, where all the switching events are added and then divided by the window size. This average value is then compared with the reference frequency, to get the frequency tracking error. Later, this error is given as an input to a PI controller, that gives as output a deviation value to fix the frequency error.

3.6.2 Phase Correction

An important characteristic of the current phase error caused by Period Control is the fact that it grows linearly with the weight factor, and is inversely proportional to the reference frequency. This characteristic, though only proper of the system analyzed in this work, can be extrapolated to design a correction index of the current reference. This means that the reference provided to the controller would be ahead in phase from the actual reference, in order to compensate for the controllers delay. Since this delay is proportional both to the weight factor λ_k and inversely proportional to the reference switching frequency, it is possible to design this correction factor as a constant times a function of both variables. The implemented delay compensation can thus be computed as

$$\theta_+ = M_\theta \frac{\lambda_K}{f_r}, \tag{3.21}$$

where M_θ is obtained from the phase error curves on figure 3.13. Since this strategy makes no effort in measuring the control delay in real time, since this would be additional computation in a very time restricted operation, the correction is left as an open control loop. Nonetheless, since the phase behavior is fairly stable and linear, it is not hard to design a test algorithm to get these curves and compute the value of M_θ for different systems.

For a more complex system, or when more complex or numerous variables are being controlled by MPC, there is no guarantee of reaching a similar behavior as obtained here. Therefore, the proper study of the control delay should be done, and a more suitable correction should be implemented for these systems.

3.6.3 Period Reference VMI Change Correction

As explained in section 3.1, a PWM based control strategy that generates a sinusoidal reference for the modulation will generate a period measurement that slightly differs from the switching frequency. In a similar fashion, Period Control reaches a virtual modulation index (VMI) that follows a similar behavior. This deviation is ingrained in the functioning principle of PWM, but creates no problem on the controller since it is not a relevant parameter for the control structure. This is not the case for Period Control for FCS-MPC, where the period measurement is essential to the proper regulation of the switching frequency,

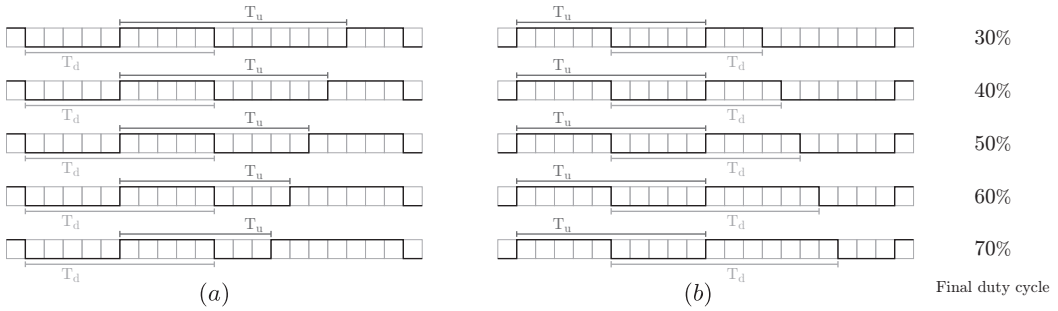

Figure 3.25: Correction alternatives for duty cycle changes, starting at 50%: (a) Up period change and (b) Down period change

but is twisted when the VMI changes in time. Therefore, the issues that this deviation may produce on Period Control and a solution to overcome them must be studied.

As a first approach to this issue, the way this deviation affects the period measurement is illustrated in figure 3.25. Here, when the controller requires a change in the duty cycle of the generated signal, it has two means to do so. The first option is to change the Up period, increasing it for a lower duty cycle, or reducing it for a higher one. The second alternative is to change the Down period, having the opposite effect as previously. Either way, the controller would have to fail in the compliance of the control period in order to achieve the required change in duty cycle. Figure 3.26 illustrates how the period measurement deviates from the average for a PWM strategy with varying modulation index amplitude, M, and switching frequency, f_{sw}. Here the deviation is expressed as a percentage from the average period. It is not hard to notice that for higher values of M the deviation increases, and when carefully measured, as shown in figure 3.27(a), it can be seen that it does so in a linear way. A similar phenomenon takes place when the switching frequency is changed, figure 3.27(b), where for lower switching frequencies it can also be appreciated an increased deviation. In this case the deviation is also proportional to the change, thought not to frequency but to its inverse, that is, the switching period.

When the modulation is sinusoidal it can be seen that the period deviation is zero, for both Up and Down measurements, when the sinusoidal reaches its peaks, and is maximum when it is zero. Based on this, it can be concluded that the deviation is also proportional to the rate of change of the modulation, that is, its derivative. Based on this data it can be concluded that for a sinusoidal modulation, the amplitude of the period deviation, δ_T, is proportional to the modulation index its derivative and the switching period, that is,

$$\delta_T = K\dot{m}\frac{M}{f_{sw}}\,, \tag{3.22}$$

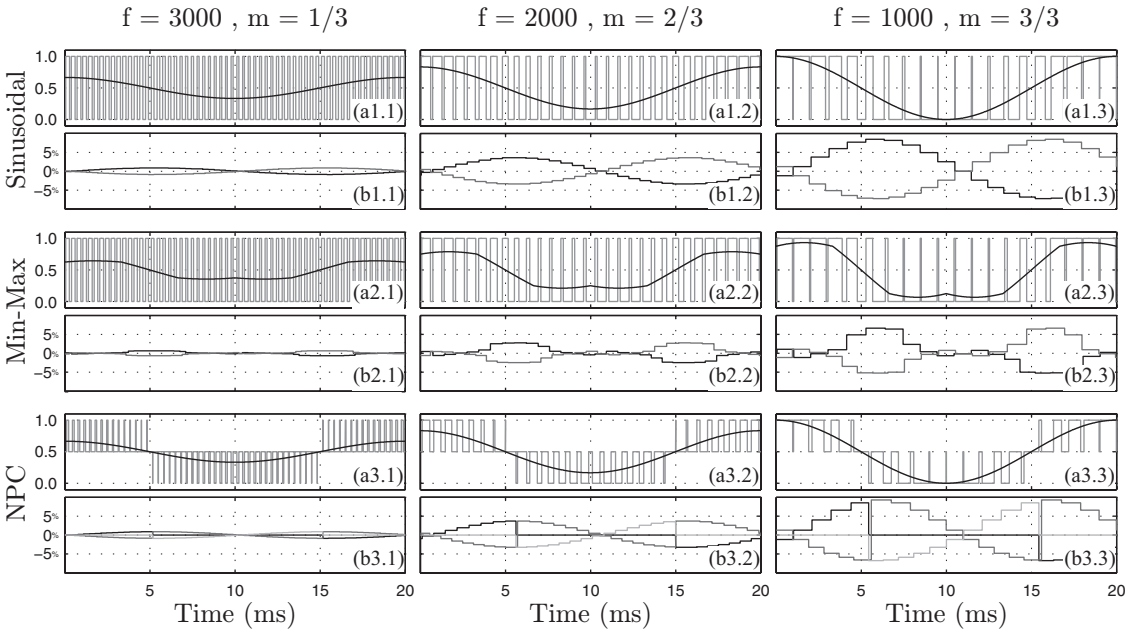

Figure 3.26: Period measurement variation for a PWM signal: (a) Modulation index (black) and Modulated signals (grey) and (b) Period deviation as percentage of the average for Up and Down period measurements (black and grey respectively).

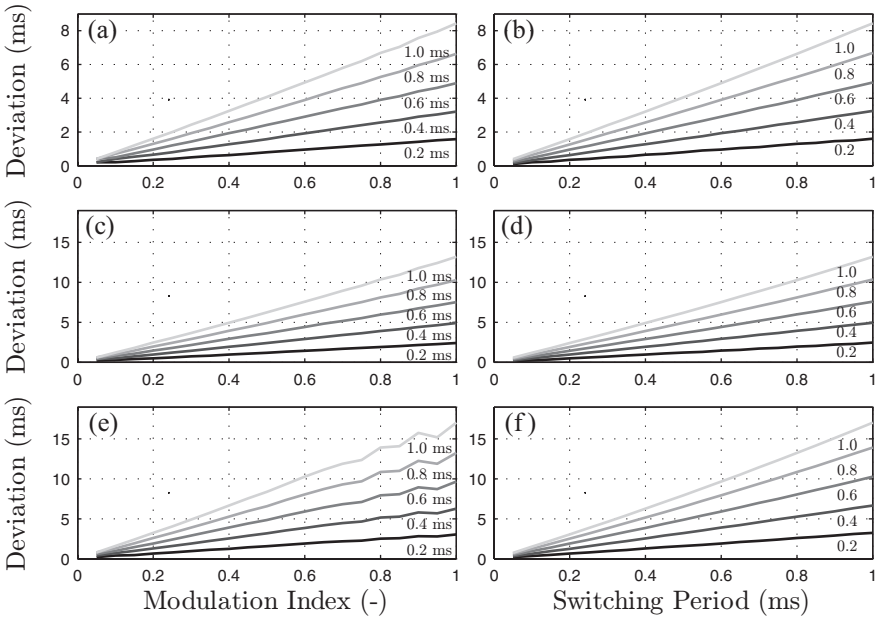

Figure 3.27: Period measurement deviation evolution for changes in (a,c,e) Modulation Index, and (b,d,f) Switching Period, for (a,b) 2-level converter, (c,d) 2-level converter with Min-Max injection, and (e,f) an NPC converter

where K is a constant computed from the deviation measurements.

The same analysis can be done for the same converter but when the implemented modulation is not purely sinusoidal, but includes a third harmonic injection in the form of Min-Max. The resulting period deviation is illustrated in figure 3.27(c,d). Unlike with a sinusoidal modulation, the measured period does not follow a clean shape with this modulation, but it is proportional to its derivative, thus holding the same conclusion. Also, as shown in figures 3.27(a,b) the amplitude remains proportional to both modulation index and switching period.

Something similar happens with an NPC converter, as shown in figures 3.26(a3.1-3) and 3.26(b3.1-3). Nonetheless, since there are more semiconductors in this converter, and the are period where these remain static, minor changes has to be done to the measurement. For each phase, the measurement is done normally for the switching pair of semiconductor, but the opposing pair has its measurement fixed to the average. With this in mind it can be seen that the measurements of all the semiconductors are complementary, continuing the curve formed by their counterpart.

As explained before, the existence of a deviation between the desired period, which

would produce a PWM-like commutation in FCS-MPC, and the given reference to the controller, which is based only on the average switching period, may cause a deviation of the controller from the desire behavior. To overcome this issue, it is proposed to include this deviation as an additional reference correction factor, δ_{Tr}, for the period reference, in order to allow a better transition between duty cycles, as follows

$$T_r = \bar{T}_r + \delta_{Tr} \ , \tag{3.23}$$

where $\bar{T}_r$ corresponds to the average period reference given by the user. Since δ_{Tr} is proportional to the derivative of the intended modulation index, each phase requires its own separate deviation factor. The same occurs with Up and Down period references, which require opposite deviations.

Even though δ_{Tr} has an amplitude as described so far, the actual value to be implemented as a reference correction is dynamic, and changes according to the fundamental frequency of the system. As can be seen in figure 3.27, the actual period measurement is not in line with the derivative of the modulation index, but its shifted in time. This delay comes from the fact that the measurement takes place only when a period finishes. Thus, the delay magnitude is equal to the switching period. Since the main goal for this strategy is to mimic PWM, this delay should be included in the correction factor.

Thus, the final structure of this correction factor is

$$\delta_{Tr}(t) = K\dot{m}\frac{M}{f_{sw}}\sin\left(2\pi f_r t + \theta_0 - \theta_d\right) \tag{3.24}$$

$$\theta_d = \pi\frac{f_r}{f_{sw}} \tag{3.25}$$

where f_r is the reference frequency, θ_0 the phase shift required from the system and θ_d the delay for a proper period measurement.

As an example of this principle in action, the 2-level 3-phase converter used previously is simulated with this changed references and the achieved performance is evaluated in terms of the average frequency achieved and the error in current, both in magnitude and phase.

As can be seen in figure 3.28, the final error in magnitude, remains almost the same for both converters regardless of the presence of the correction factor. Nonetheless, the error phase is improved by the use of this factor, by shifting the resulting current closer to the reference. This suggests that the current control has to compete in less degree with Period Control, thus improving the overall performance. To further emphasize this improvement, figures 3.29 and 3.30 illustrate the current spectra achieved for each converter, for the last values of λ_T. Here it can be seen that the current spectrum for each test is almost the same per converter. Therefore, the achieved switching pattern is maintained while also

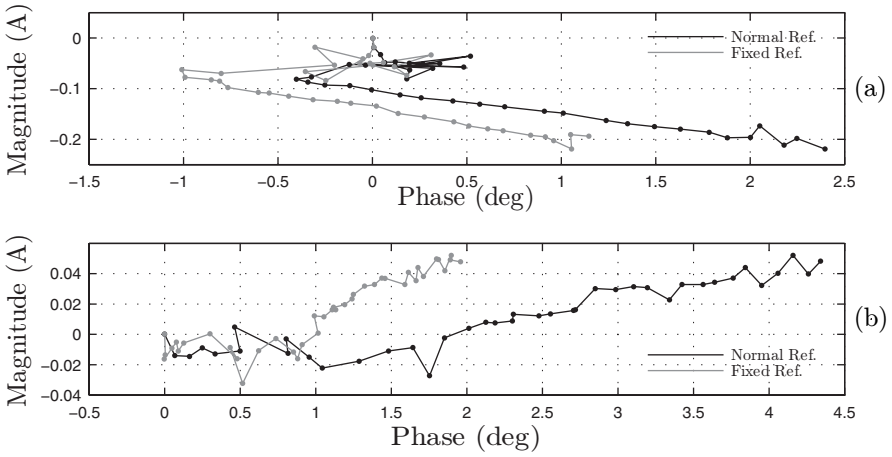

Figure 3.28: Current tracking error for multiple λ_T, (a) for a 2-level converter and (b) an NPC converter

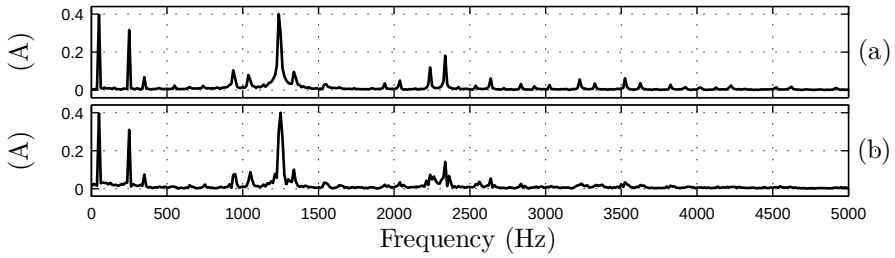

Figure 3.29: Current spectra for a 2-level converter, (a) without $\delta_{Tr}(t)$ and (b) with $\delta_{Tr}(t)$

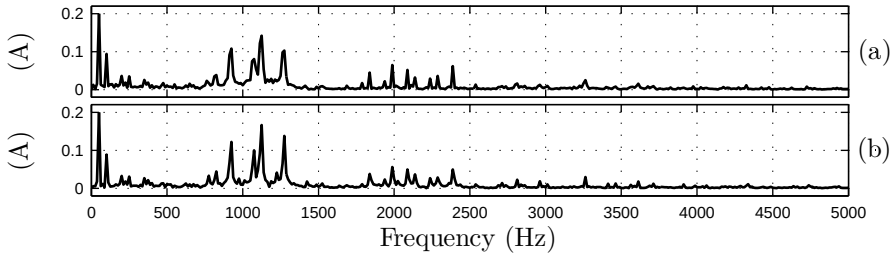

Figure 3.30: Current spectra for an NPC converter, (a) without $\delta_{Tr}(t)$ and (b) with $\delta_{Tr}(t)$

achieving a better current performance, thus validating the use of the correction factor $\delta_T(t)$.

Chapter 4

Experimental Results

The proposed strategy of Period Control presents interesting results in a simulated environment. Since in this setup there is no measurement noise, parameter deviations nor computation delay, there is no guarantee that it might work in a real environment. The following experimental setup is put together, using the same topology as presented for the simulations to validate proposed strategy.

4.1 Setup

The experimental setup used for these tests is shown in figure 4.1(a). The 3-Phase 2-Level converter is built from three identical systems shown in 4.1(b). Each of these circuit boards corresponds to one leg of the converter. The main DC power source, a Keysight N5772A, is set for dc voltage of 200 V, and a maximum current of 2.5 A. The gate drive dc source, of 12 V, is used as a dedicated source for the converter control circuit. The dSPACE 1103 is the main processing unit of the system, where all the programs to run predictive control are implemented. The gate signal digital board is in charge of allowing the communication between the dSPACE and each of the converters boards.

4.2 Steady state Performance

The first simulation to be tested is the steady state performance, illustrated in simulations in figure 3.7. The same current reference of $5A$, and switching frequency reference of $1000Hz$ is used for this tests, as well as a weight factor λ_K of 20.

As shown in figure 4.2 the experimental performance is almost identical to 3.7. A slight increase in the current ripple can be observed, but the control is kept in line, as

(a) (b)

Figure 4.1: Experimental Setup (a) Front photo and (b) converter phase

expected. This extra ripple can also be appreciated in 4.3, where the harmonic content for the current is slightly higher. Nonetheless, the spectrum of both current and voltage is kept focused on narrow peaks, which proves that a regular switching pattern is achieved. The most likely explanation for the deviation of the experimental results from simulations is the parameter error of the load elements. Also, unmodeled behavior of the semiconductors, or measurement noise may induce variations between simulation and experimental results.

4.3 Dynamic Performance

In a similar fashion as presented in figure 3.11, a dynamic test is performed to confirm the time response of the controller under reference changes. The following experimental results, presented in figure 4.4, shows the dynamic performance obtained by the experimental setup. Like in the simulations, the current reference is a step from $1A$ to $5A$.

It can be seen that, just as obtained in the simulations, the response time of the controller is kept very fast without hindering the switching control. It is important to notice that the control structure and the cost function are completely identical during steady state as during the transient. No modification is applied to the controller to achieve a proper response, which provides evidence of the robustness of the controller in this system.

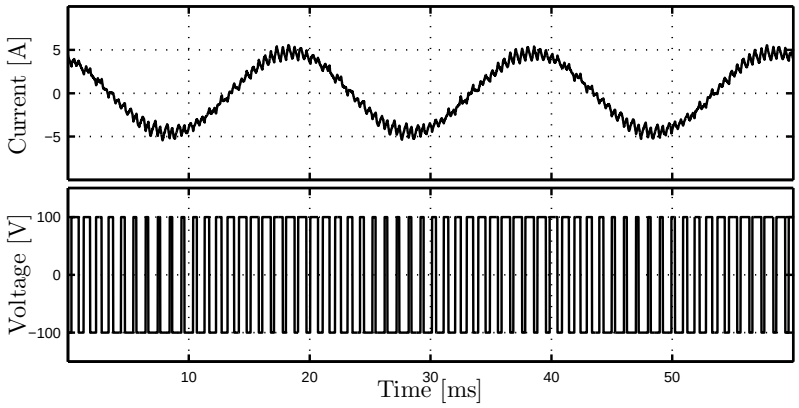

Figure 4.2: Experimental steady state results through a phase: a) Current and b) Voltage

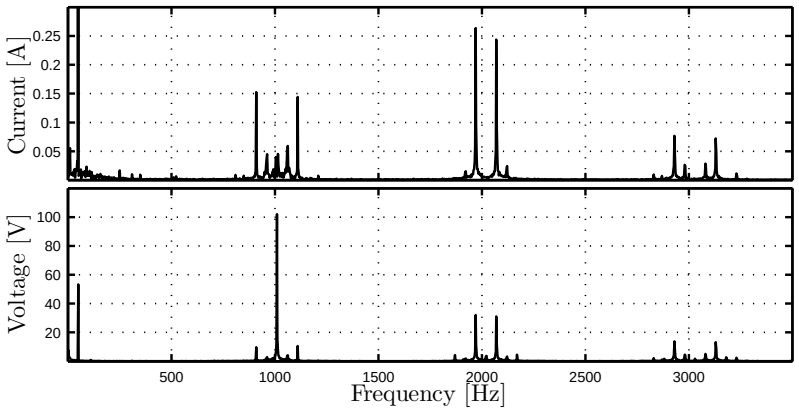

Figure 4.3: Experimental steady state results through a phase: a) Current and b)Voltage

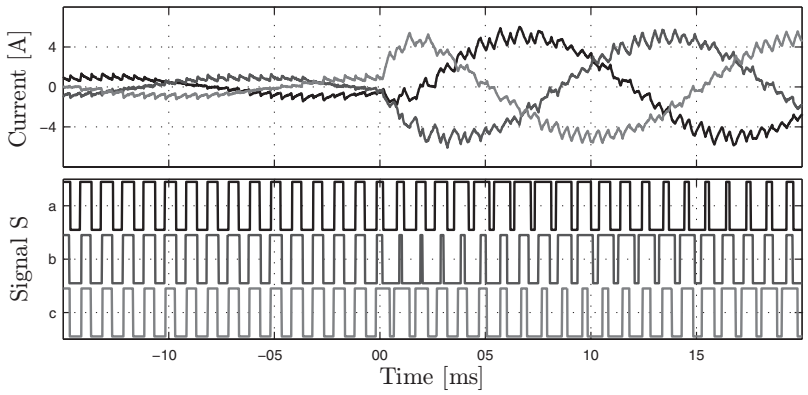

Figure 4.4: Experimental dynamic performance: a) Output current and b) Gate signal

4.4 Strategies Comparison

In section 2.5, the reported strategies were introduced to establish the state of the art in this topic. In this section, a series of steady state tests are performed in order to evaluate and compare the performance of these different strategies under various criteria. The experimental results obtained in these experiments and the respective data analysis is presented in figures 4.5 and 4.6. The implemented strategies are, from left to right, Simple Penalization (1), Sliding Window (2), NOTCH Filter (3) and the proposed Period Control (4).

As a first approach to the comparison, the different strategies are implemented for a switching frequency reference of 1000 Hz, with a current reference for all the tests of 5 and 50Hz. The output current generated by each strategy and the gate signal generated by the controller are illustrated in table 4.5 (a)-(b). The performance observed for Period control is the very similar as shown previously through simulations, with the respective modulation-like performance. Meanwhile, the other strategies, though effective in reducing the switching frequency, present either grater current ripples or higher irregularities in the frequency control. Both Simple Penalization and Sliding Window present effective control of the current, but the switching frequency, though reduced, suggests no steady switching frequency. In the case of NOTCH Filter the controlled current presents a strong resonant behavior, while the switching patter of the converter seems to be very stable.

The results presented in table 4.5 (c)-(f) show the current spectra reached in steady state for different switching frequency references, being these 500, 1000, 1500 and 2000 Hz respectively. In the case of Simple Penalization, the only plotted spectra is for an average switching frequency around 1000 Hz, since no actual reference is implementable for

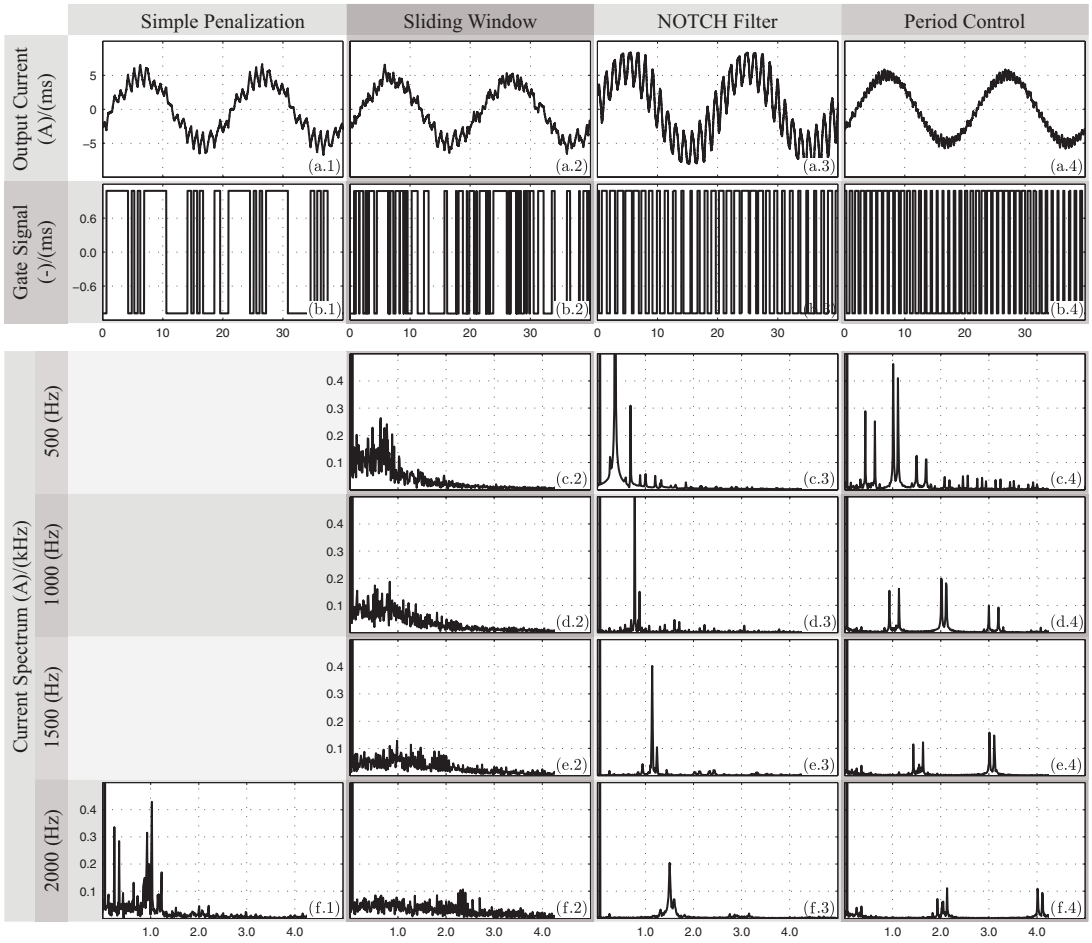

Figure 4.5: Experimental results for a 2-level 3-phase converter with RL load with switching frequency control: Current, Gate Signal and Current Spectrum

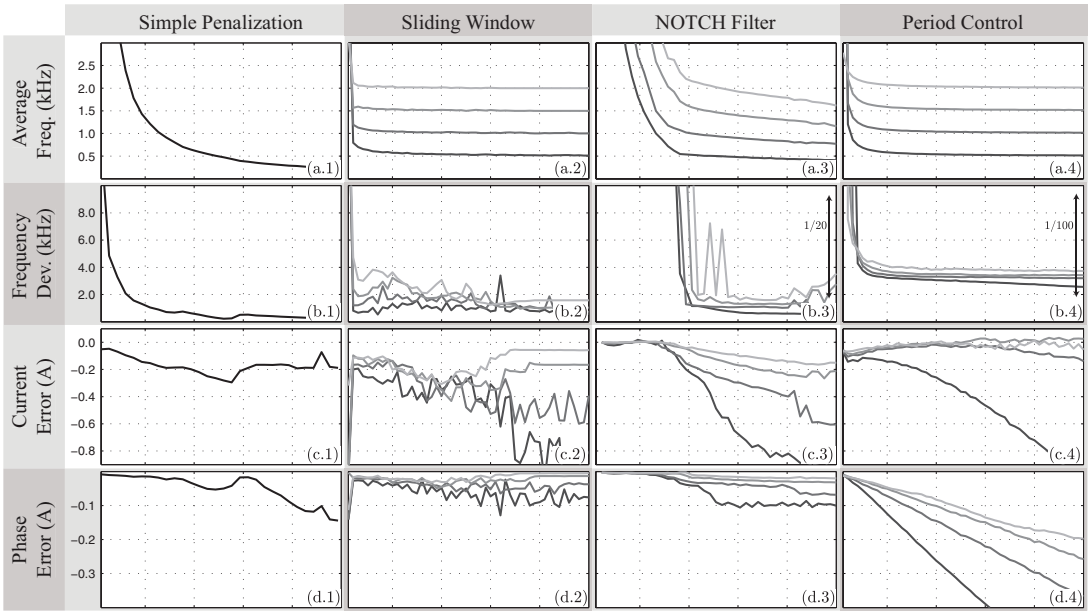

Figure 4.6: Experimental results for a 2-level 3-phase converter with RL load with switching frequency control: Average Frequency, Frequency Deviation, Current Error in Magnitude and Current Error in Phase

this strategy. From these plots it can be observed that in the case of Simple Penalization the current spectrum shows a peak near the average frequency, but also show comparable values at seemingly random frequencies. Since Simple Penalization makes no attempt to reach a specific switching frequency, is not unexpected to have this behavior, and the actual average frequency is achieved by changing the associated weight factor, and not by a reference. In the case of Sliding Window, independent of the switching frequency reference, the spectrum is spread along a wide frequency band, though in a more compact bandwidth for lower frequencies. The strategy of NOTCH Filter, among the studied strategies, provides the cleanest spectrum in terms of noise reduction. Nonetheless, it does not provides a precise tracking of the reference frequency, shifting to the low frequencies. Finally, Period Control produces a very stable switching pattern, with a clean spectrum, presenting peaks only at the desired frequencies and its harmonics, as would be expected from a modulated strategy. Period Control produces the closest frequency tracking, when evaluating the generated spectrum, though always at slightly shifted towards the higher frequencies.

For a clearer comparison between these strategies, a set of criteria are evaluated, as

measurement of their performance. These different criteria are compared for all four strategies and for different switching frequency references, plotted in 4.6 with darker grey hues for lower references.

4.4.1 Average Switching Frequency

The first criterion to be tested is the effective average frequency achieved by each strategy in steady state operation. The average switching frequency is computed as the half number of switching events divided by the time, since an Up and Down switching complete one cycle. These results are illustrated in table 4.6(a) as plots of the average switching frequency vs the frequency weight factor λ_k.

In the case of Simple penalization, the average frequency achieved is in inverse relation with the weight factor applied to the frequency element. Thus, for a low penalization over the act of commutation, the controller chooses to switch almost freely, and this freedom is reduced for increasing weight factors. The final average frequency achieved by this strategy is highly dependent on the parameters of the systems, as well as the different references given to the controller. This render this strategy as highly dependent on the state of the system, requiring an accurate knowledge to achieve a specific average frequency.

The second strategy, Sliding Window, shows a very good performance in reaching the desired average switching frequency, as shown in 4.6$(a.2)$, approaching the reference from the top. This performance is as expected, since the whole structure of this control strategy is aimed to reach this average. Nonetheless, this clean performance in average frequency does not match with the achieved spectrum, thus showing that both analysis are not necessarily interconnected. A favorable trait of this strategy is that the approach to the reference frequency is asymptotic, which means that the controller is less sensitive to the weight factor for high values.

In the case of NOTCH filter, the average frequency is very poor for low weight factors, but when this is increased it eventually locks in place, stabilizing near the reference. Nonetheless, the achieved average frequency is smaller than designed, contrary to what happens with sliding window, and drifts away for higher values. This makes this strategy effective in controlling the switching frequency, though at the expense of being sensitive to the weight factor.

Finally, Period Control shows a performance similar to Sliding Window, approaching the reference average frequency in a continuous way. Unlike Sliding Window, Period Control does reach a spectrum concentration near the reference frequency, and is also slightly shifted to the high frequencies, matching the average frequency plots. The asymptotic performance is also present for this strategy.

4.4.2 Switching Frequency Standard Deviation

With the average switching frequency it is possible to observe the general tendency of the strategies to reach a switching frequency slower than if no control was applied. Nonetheless, even when the average is low, there is no guarantee that this average is properly distributed in time. This means that the switching events might be concentrated in some small windows of time, and very sparse on others. This leads to a high stress in the semiconductors at some times, and lack of usage on others, making an uneven use of the devices. Thus it is desirable to have low variability from the average frequency. To analyze this variable, the standard deviation of the frequency is evaluated. The standard deviation is computed as

$$\sigma_x = \sqrt{\frac{\Sigma_{i_1}^{N}(x_i - \bar{x})^2}{N}}, \tag{4.1}$$

where $X = \{x_1, ..., x_N\}$, and $\bar{x}$ is the average value of X, To compute the instantaneous frequency, the Up and Down period period measurement are used. These periods are the same used for Period Control. The use of these periods instead of the time between two consecutive commutations is to avoid false high values of frequency when the required duty cycle is near 0 or 1, since at these points two consecutive commutations would be very close.

The resulting deviations as function of the weight factor λ_k are illustrated in table 4.6(b). For the case of Simple Penalization, shown in $4.6(b.1)$, the deviation goes in line with the average frequency, following the logic of less commutations when the weight increases.

For the case of Sliding Window the deviation is as big as the reference frequency, though bounded to a certain degree. By increasing the weight factor, the deviation is reduced, albeit slightly, but it is still on the order of a few kHz.

For NOTCH Filter the deviation is quite significant for low weight values, but when the controller properly locks the frequency, the deviation attenuates significantly. Notice that for 4.6(b.3) the plot is scaled by 20, meaning that it ranges from 0Hz to 500Hz, instead of several kHz.

Finally, the standard deviation achieved with Period Control is presented in $4.6(b.4)$. It is important to notice that this plot is scaled by 100, meaning that these values range between 0 and 100 Hz, instead of 10 kHz. Period Control provides the most stable switching frequency of all the presented strategies by a considerable margin.

4.4.3 Current Error

The next comparison criterion is the induced error over the main control objective that is the output current of the converter. Since in the cost function all control objectives must compete to be fixed, the addition of a new objectives is bound to increase the error in the previous ones. Figure 4.6$(c - d)$ show the induced error due to each frequency control strategy in amplitude and phase respectively.

For the case of Simple Penalization, no major error is induced in amplitude, nor phase, though both increase when the respective weight factor is increased. This increment does not seems to obey any pattern.

In the case of Sliding Window, the final error in phase is quite regular and very close to zero. Nonetheless, the error in amplitude shows a wide range of variability, changing erratically for different weight factors. As with the Simple Penalization, the current control is hindered when the switching frequency is forced to be reduced too much. Nonetheless, this strategy provides a much wider range of weight factors for which a good current tracking is achieved with a good average switching frequency.

The best current tracking is achieved with the use of NOTCH filter prior to the lock, where both magnitude and current are kept tightly controlled. Since this situation can be equated to having no frequency control, it is not of much value. On the other hand, for higher weight factor values the magnitude seems to drift away proportionally to the weight factor, and inversely proportional to the switching frequency.

Finally, Period Control shows one of the best performances in terms of magnitude error, staying around the reference for a wide range of weight factors and frequencies. A notorious deviation is shown for a frequency reference of 500 Hz, which may have the same origin as with the previous strategies, where a low switching frequency cant be maintained for this system. On the topic of phase error, this shows to increase steadily with the weight factor, for all frequency references, as obtained in simulation. Here, for high switching frequencies the phase error increases with lower slope, while for lower frequencies, it increases in what seems to be a linear relation, and inversely proportional to the reference frequency. Thus, the phase delay changes twice as fast for 500 Hz reference when compared with 1000 Hz reference.

4.4.4 Computation Demand

The final comparison between strategies is the computation demand that each imposes over the control platform. Since Predictive Control, and in particular FCS-MPC, is highly demanding in computing resource, any changes in the control structure must be done so in a way that the computation demand does not increase drastically. As presented previously, the additional computation done for the purpose of implementing Period Control can be

Table 4.1: Computation Times

Strategy	Average Time
Simple Penalization	6.4 μs
Sliding Window	7.1 μs
NOTCH FILTER	7.4 μs
Period Control	6.6 μs

reduced by the use of Integer operations and simple boolean logic, which suggest a minor increase in the amount of operations that the control platform must execute.

The control platform used for this comparison is a dSPACE 1103, and the computation demand is evaluated as the average time required to finish all the operations required for one control cycle over 1 second. The results of these averages are presented in table 4.1. As can be seen form this table, the least demanding strategy is Simple Penalization, which is not a surprise thanks to the simplicity of its operations. Sliding Window presents a higher computation time, most likely caused by the need of a circular buffer and the computation of the averages in real time, which must be computed for each semiconductor. The highest computation time is for the NOTCH Filter strategy, that must compute the filter output at each prediction, which is not light in the required operations. A remarkable result here is the computation time achieved by Period Control, which is just slightly higher than Simple Penalization, while achieving a much better performance.

Chapter 5

Variable Weight Switching Frequency

As it is well known, one of the main motivations to reduce and control the switching frequency of a power conversion system is to reduce the power losses due to commutations. The origin of these losses resides on the dynamics of the semiconductors when transiting from a blocking state to a conducting state and vice versa. These losses are particularly relevant in medium and high power systems, where a small percentage in power losses is still a significant amount of heat generated by the semiconductors. The switching losses are directly linked to the voltage being blocked by the semiconductors and the current passing through them. A strategy that takes into account these switching losses is studied in this chapter, evaluating its performance for different variations.

5.1 Single Phase Variable Weight

An approach to reduce the issue of switching losses with FCS-MPC is analyzed in [43] for a single phase system. The system in question is an H-Bridge NPC (H-NPC) connecting a PV array directly to a single phase grid, as shown in figure 5.1. For the control of this system a new element is included in the cost function that aims to penalize the control actions that changes the state of the semiconductors. The structure of this new element is such that a high penalization is given to the commutations is higher for high current values, thus avoiding switching during these periods. The idea behind this strategy is to penalize the switching action when it would cause the biggest losses, while also relaxing this penalization when the losses would be low.

The control structure used for this system is that of a cascade control as shown in figure 5.2. Here the inner loop is in charge of the capacitor balance and output current, and it consists of a FCS-MPC control structure. The next loop is responsible for the voltage control, which give as output the current reference for the inner loop, and constructed

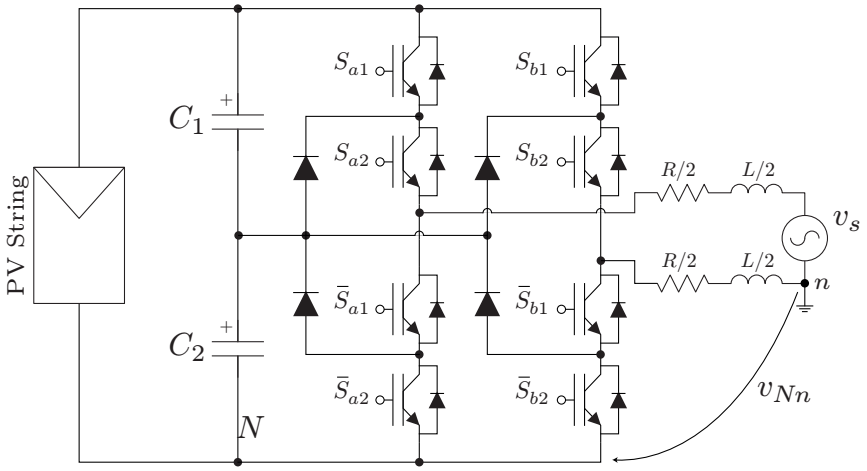

Figure 5.1: Single phase H-NPC converter for a PV string connection

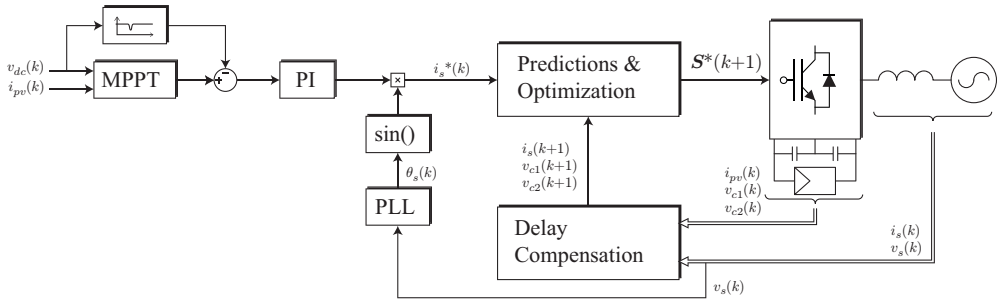

Figure 5.2: Control diagram for the single phase H-NPC

by a PI controller. The most exterior loop deals with the MPPT of the PV string, which provides the reference for voltage in the capacitors, and is based on a Perturb and Observe MPPT algorithm.

The main focus of this control is in the elements involved in the cost function used for the FCS-MPC at the inner most control loop. The basis structure of this cost function is the quadratic error, which is used for all control objectives. The main control objective is the output current tracking, whose reference is designed to allow 0 reactive power to the grid. This variable is treated through its quadratic error without modifications to the quadratic structure. In a similar fashion, the capacitor unbalance control is set such that the difference between them is equal to a reference of 0V.

To address the issue of commutation frequency, the selected strategy is the computation

of an average frequency using Sliding Window. One of the main reasons why this is used is because it permits the controller to reduce and redistribute the switching events, which comes in handy when aiming to reduce the commutations for high values of current. The solution given here for the redistribution is the use of a varying weight factor that heavily penalizes commutations when they are undesired.

The implementation of sliding window does not allow by itself to control when a switching event takes place. Therefore, an additional cost element is included in the cost function. The implementation of this cost element is done through a simple penalization of the switching action, as presented in section 2.5.1. The weight factor in charge of penalizing this element is modified in such a way that changes in time in relation with the current, as follows

$$\Delta S_p = |S_{k,p} - S_k| \ , \tag{5.1}$$

$$J_{sw} = C\lambda_{sw} \sum_{i=1}^{n_s} \Delta s_i(t_k) \ , \tag{5.2}$$

$$\lambda_{sw} = \begin{cases} |i_s/I_s| & if \quad |i_s/I_s| \geq I_{lim} \\ 0 & if \quad |i_s/I_s| < I_{lim} \end{cases} \ , \tag{5.3}$$

where S_k is the current state of the semiconductors, $S_{k,p}$ is the predicted state for prediction p, and i_s, I_s and I_{lim} are the current measured at time k, the current amplitude and the current limit respectively. The constant C is just a very high value in comparison with other control objectives to effectively penalize the switching action over the the rest. The profile generated by these equations is shown in figure 5.3. With this cost element, the system avoids switching when the current is high, and permits a normal operation when it is low.

As can be seen in figure 5.4 this strategy is effective in reducing the switching frequency when the respective current presents high values, thus reducing the switching losses. Nonetheless, this comes at the price of increasing the current ripple, and therefore distortion, as seen in figure 5.5. Also, the system is not capable of completely blocking the commutations due to the fact that this is a single phase system, an no other option is there to control output.

This results shows this variable weight factor structure as a promising one for others systems. In particular for 3-phase systems, where redundancies in switching states are not uncommon, it is possible to reach a proper actuation even when one of the semiconductors is blocked. It is also favorable to analyze a 3-phase system due to the natural cancellation of third harmonics for the output signals.

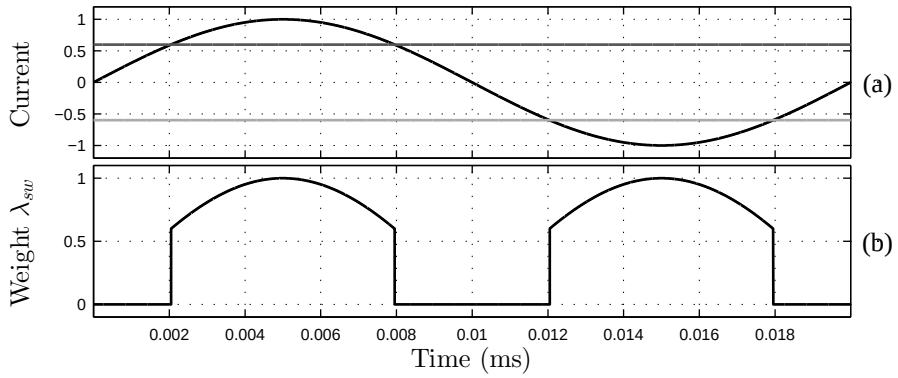

Figure 5.3: Weight factor as function of the current: (a) Current i_s and its limits, and (b) weight factor λ_{sw}

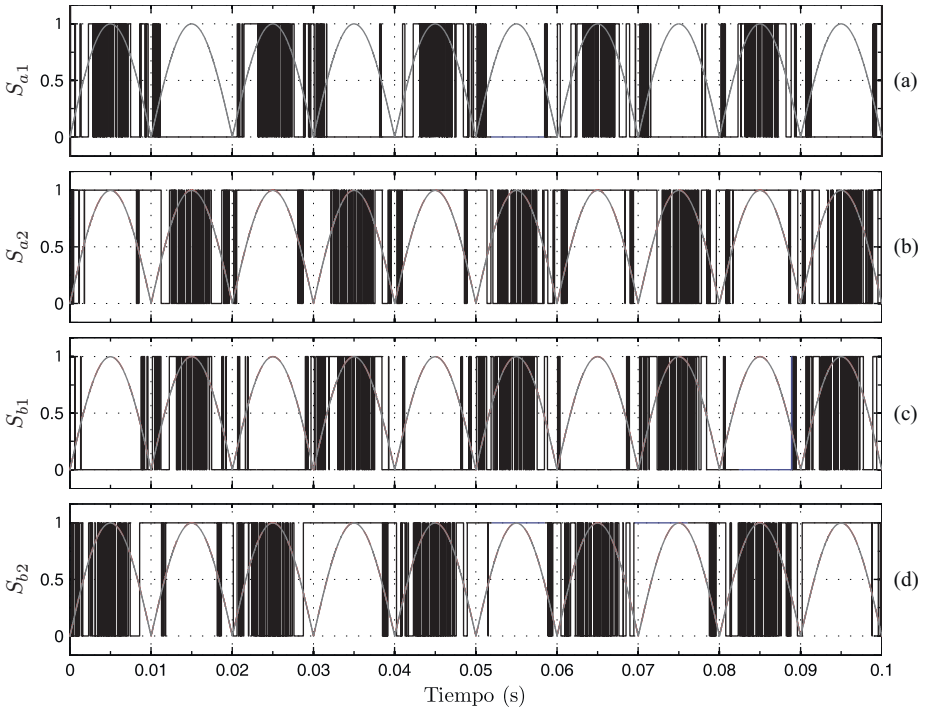

Figure 5.4: Gate signals for each semiconductor pair and absolute value of the reference

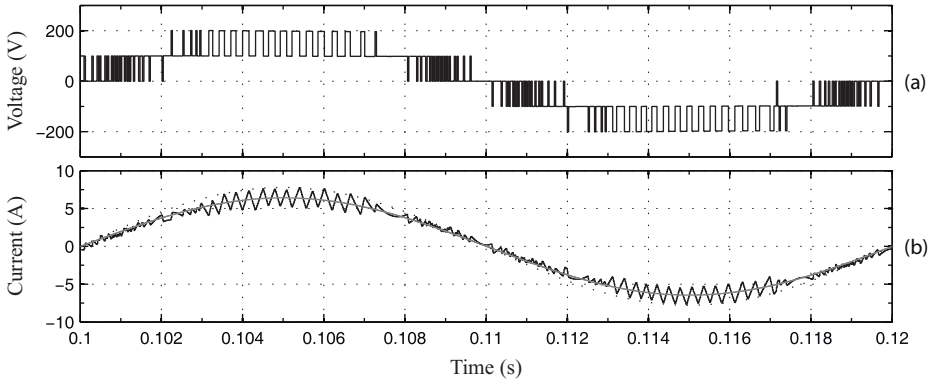

Figure 5.5: Output voltage and current of the converter and the respective current reference

5.2 Switching Losses

A first step to reduce the switching losses in a power conversion system is to understand its origins. An ideal semiconductor or switching device is capable of fully blocking the current flow passing through it or permitting its flow without obstruction as commanded, while also instantly changing states. Nonetheless, in reality these devices have many limitations, such as switching delays, resonances, blocking voltage limits, flowing current limits, unmodeled dynamics, etc. These limitations cause the devices to drift from their ideal performance, causing power losses, voltage drops or ringing, among others.

The main sources of power losses in a semiconductor are the conduction losses and switching losses. The conduction losses are mainly caused by the internal resistance of the device and the voltage drop of the semiconductor, thus being mostly unavoidable through control techniques alone. Addressing this issue requires changes in the structure of the converter to reduce its effects. On the other hand, the switching losses are caused by the dynamic behavior of the switching device. Since the switching event is not instantaneous, the voltage and current of the device change gradually, causing a rise in the power consumed. These losses are in direct proportion to the current passing through the semiconductor, but is also dependent on the voltage being blocked and the amount of commutations that takes place.

An example of a commutation event, albeit simplified, is illustrated in figure 5.6. Here it can be seen that the time taken to reduce the flowing current from the active state to zero is not instantaneous. In a similar fashion, the blocked voltage increases gradually until reaching the full blocking voltage. A real commutation event is not as simple as illustrated here, and other dynamics are present, such as delays, overshoots and undershoots

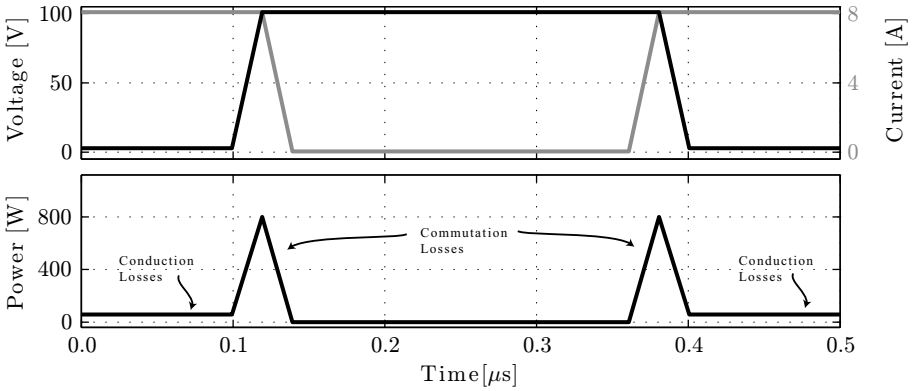

Figure 5.6: Semiconductor transition dynamic

or ringing among others. It is also common to have differences between an opening and closing commutations, and even changes in time, due to temperature, stress, electromagnetic noise or any disturbance. Nonetheless, this simplification illustrates the source of the power losses in these devices in enough detail to be considered by a fast sampling control strategy as is MPC.

Unlike the conduction losses, that require physical changes in the converter to improve the performance, the switching losses are caused by the controller decisions, by selecting the time and condition at which the commutation should take place. This suggests the possibility of reducing the switching losses by improving the control techniques, thus making better choices in this regard.

For analysis and simulation purposes, the losses due to switching events are computed as

$$E_{sw}(I_{on}, V_{off}) = \tau I_{on} V_{off}/2 \,, \tag{5.4}$$

where I_{on} and V_{off} are the current flowing through the device while active, and the respective blocking voltage when inactive respectively, and τ is the time of activation or deactivation of the semiconductor, taken as symmetrical to simplify the analysis. This equation comes from integrating the inverse parabola in the power curve, caused by the ideal ramp-like behavior presented in 5.6.

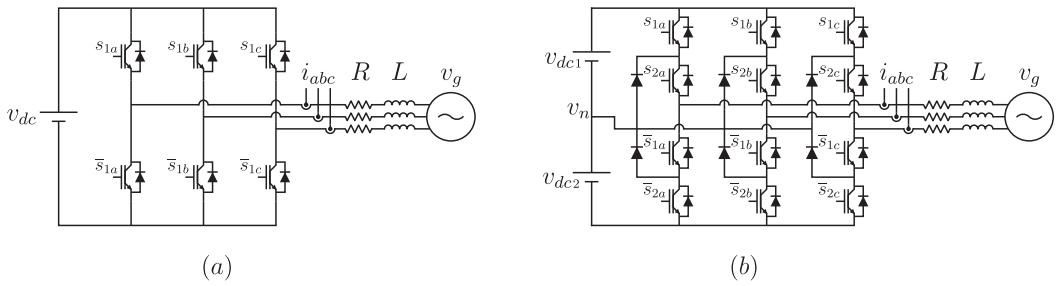

Figure 5.7: Studied systems for Current Aligned Switching, (a) 2-Level 3-Phase converter and (b) NPC converter.

5.2.1 Switching Power Losses vs. Harmonic Distortion for 3-phase systems

For simulation purposes, the studied systems in this chapter are the 2-level three phase converter and an NPC converter, presented in figure 5.7.

As a starting point in this study it is important to understand what is the base to which everything is to be compared against, in order to properly asses the achieved performances. The main performance criteria in this study is the Switching Power Losses (SPL) vs. Total Harmonic Distortion (THD).

The THD of a signal is the measurement of the harmonic content present in it, and works as an indication of how far this signal is from a pure sinusoidal. This value is computed as the ratio of the sum of the power contribution of all harmonic components against the power of the fundamental frequency. For the following analysis, the signal to be studied is the output current of the converter, thus

$$THD = \frac{\sqrt{(\sum_h I_h^2) - I_1^2}}{I_1} \,, \tag{5.5}$$

where I_n is the n^{th} harmonic of I, considering a fundamental of 50 Hz.

Meanwhile, the switching power losses (SPL) as explained previously, correspond to the power dissipated y the semiconductors during the switching operation. These (SPL) are computed as the energy lost by the converter for each switching event, based on equation (5.4), divided by the time elapsed for an sampling window. For the purpose of these analysis, the sampling window is of 100ms, which corresponds, for a fundamental frequency of 50Hz, to 5 complete cycles. This is to reduce the effect that noise may induce

in the computations. Finally, the switching power losses are computed as

$$SPL = \frac{\frac{\tau}{2}\sum_{t=0}^{T} I(t)V(t)}{T} \tag{5.6}$$

The goal of analyzing these variables at the same time is to evaluate how much effort, represented as switching losses, requires a control strategy to achieve a clean output signal, measured by the THD.

5.2.2 System Parameter Design

To evaluate the converters and the relevant control strategies, a 20kW system is designed, as illustrated in figure 5.7. The parameters for this systems are $V_{dc} = 600$V, $\hat{V}_g = 220\sqrt{2}$V with a frequency $2\pi\omega_g = 50$Hz, and a reference current $\hat{I}_r = 20\sqrt{2}$ in phase with the grid voltage. The inductance and resistor values are chosen in such way that the nominal output current corresponds to 90% of the maximum for the system. For a purely inductive load, the value of L should be

$$L_0 = \frac{\sqrt{\left(V_{dc}/\sqrt{3}\right)^2 - \hat{V}_g^2}}{\omega_g \hat{I}_r/0.9} = 0.010285... \approx 0.01(mH)\ , \tag{5.7}$$

For this case of purely inductive load, the modulation index, for a modulated control strategy, required in steady state is

$$m = \frac{\sqrt{\hat{V}_g^2 + \hat{I}_r^2\omega^2 L_0^2}}{V_{dc}/2} \approx 1.128 \tag{5.8}$$

5.2.3 Performance Benchmark

The three control strategies to be analyzed are PI control with modulation, FCS-MPC with Simple Penalization and FCS-MPC with Period Control.

The first strategy of PI control is implemented in dq coordinates, aligned with the grid voltage, thus having 2 PI controllers to address the error in both i_d and i_q. The design of the PI controllers is not of relevance here, since the analyzed data corresponds only to the steady state of the system, for which the tracking error is near zero. The output of each PI corresponds to the required voltage to be generated by the converter, in dq, which is transformed into abc coordinates, modified by Min-Max injection, and modulated by a triangular carrier signal. The frequency of this carrier signal is the relevant variable to be changed in this control strategy, thus reaching different steady states performances. For

high frequency carriers it is expected to have low THD with high SPL, while the opposite should occur for low frequency carriers.

For the cases of FCS-MPC with either Simple Penalization or Period Control, the relevant variable to be changed is the weight factor associated with the switching penalization, λ_{sw} and λ_T respectively. In a similar fashion as with a PWM strategy, when a low penalization is given to the switching events, a low THD should be achieved, due to the low restrictions in the control actions, which should also yield high SPL. It should be emphasized that the actual weight factors used for both strategies do not need to have the same nor similar values to reach similar performances.

Figure 5.8 illustrates the obtained results for a purely inductive load for the three control strategies. Both FCS-MPC strategies show a high SPL along a low THD when the implemented weight factor associated with the switching penalization is near zero, while for high values the SPL are much smaller at the cost of a higher THD. In order to compare these results in a more tractable way, each set of points is approximated by a best fitting curve. The computation of this curves is better explained in section 6.1. For this analysis, the independent variables are constructed as the inverse of the THD, and the dependent variable as SPL, i.e.

$$X = \begin{bmatrix} x_1 & x_2 & ... & x_n \end{bmatrix}^T , \tag{5.9}$$

$$Y = \begin{bmatrix} y_1 & y_2 & ... & y_n \end{bmatrix}^T , \tag{5.10}$$

$$x_i = 1/THD_i \ \forall \, i \in \{1, ..., n\} \ , \tag{5.11}$$

$$y_i = SPL_i \ \forall \, i \in \{1, ..., n\} \, . \tag{5.12}$$

These best fitting curves are plotted along each set of points in figure 5.8. With these curves it is possible to subtract to each pondering profile the result of no profile, thus allowing a better comparison between these curves, as shown in figure 5.9.

An important conclusion of these results is that FCS-MPC with Simple Penalization always reaches a better performance than a modulated PI controller. The same is true for FCS-MPC with Period Control, though unlike Simple Penalization, for higher weight factors, the performance becomes closer to a PWM control strategy, which is expected due to the design of Period Control. This is easier to appreciate in figure 5.9, where each strategy is plotted for a THD of 0.5%, 2% and 3.5%. Here it can be seen how, for the same current THD, MPC with Simple Penalization performs the least amount of commutations, while PWM PI is forced to switch at every cycle of the carrier. Meanwhile, Period Control shows an in between performance, being very close to the reference switching frequency of 1kHz, but not being completely capable of maintaining this frequency when the required voltage changes quickly. This permits a lower THD performance than PWM, while also being able to improve the SPL for the same reference.

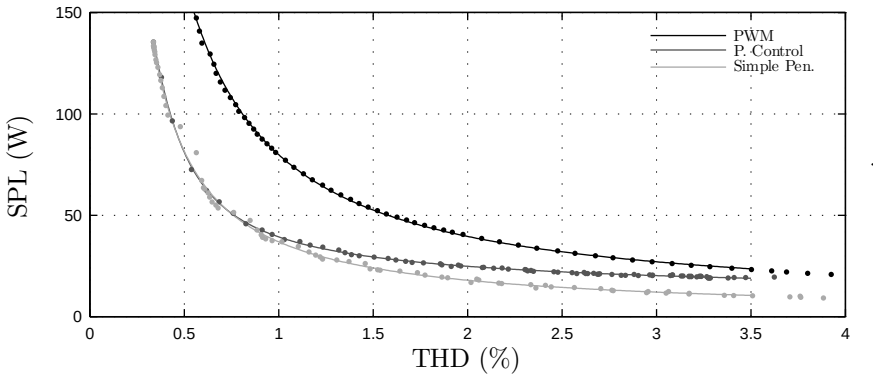

Figure 5.8: Performance curves for a 2-level 3-phase converter with purely inductive load

A similar Performance can be observed for a 3-phase NPC converter, as shown in figures 5.10 and 5.11. It can be seen that the range of THD and SPL is smaller due to the higher efficiency and better waveforms achieved by the NPC. Regardless of this, the tendency of relative performance among the three control strategies remains the same.

5.2.4 Load Dependence

So far the test has been performed for a purely inductive load, which is a favorable system for FCS-MPC due to the filtering nature of the inductance. To evaluate the effects a resistive load would cause on the control strategies, the value of the resistor R is fixed, between 0Ω and 0.7Ω, and the inductance L is changed accordingly in order to reach the same current amplitude of $30\sqrt{2}$ A with the same modulation index, or VMI, as with L_0, as shown in (5.8). This is achieved by choosing L as (the development of equation is explained in section 6.1)

$$L = \frac{\sqrt{\hat{I}_r^2\left(\omega^2 L_0^2 - R^2\right) - 2\hat{V}_g\hat{I}_r R}}{\omega\hat{I}_r} \tag{5.13}$$

As shown in figure 5.12, the relative performances for different loads are the same, showing a clear advantage of Simple Penalization MPC over PWM.

5.2.5 Discontinuous Modulation

Even though FCS-MPC with simple penalization shows the best performance in terms of THD and SPL, there are techniques to improve the performance of PWM by the injec-

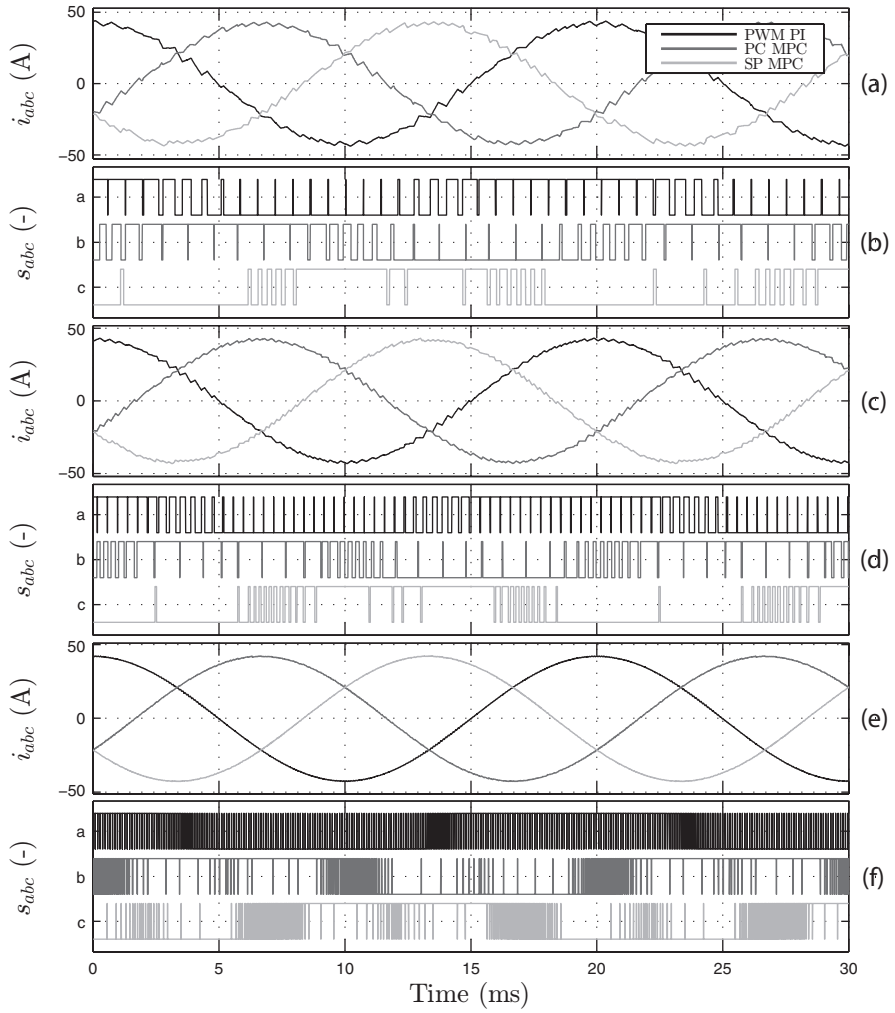

Figure 5.9: Current and output signal of a 2-level 3-phase converter with purely inductive load, for (a)-(b) THD $\approx 3.5\%$, (c)-(d) THD $\approx 2.0\%$ and (e)-(f) THD $\approx 0.5\%$

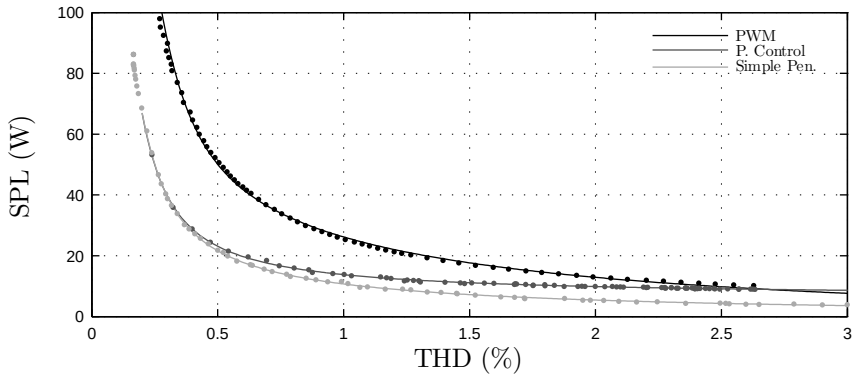

Figure 5.10: Performance curves for an 3-phase NPC converter with purely inductive load

tion of a discontinuous signal of frequency 3 times the fundamental [44](Discontinuous Sinusoidal Space Vector Modulation, SSVM), as shown in figure 5.13. This modulation technique is designed with the objective of minimizing the commutations by blocking one of the phases, delegating the control action to the other two. The blocked phase modulation index is set to one, while the others are shifted appropriately to compensate. The blocked phase can be chosen based on the modulation index, the grid current or another arbitrary reference. When the modulation index is used, the resulting discontinuous third harmonic and the modified modulation are as illustrated in figure 5.13(b), where the phase with the biggest index is blocked. When aligned with the grid current or another variable not in phase with the modulation, the injected signal becomes asymmetric, as shown in 5.13(d), though still setting one of the phases to one and shifting the others.

The performance achieved in terms of SPL vs THD for these strategies is presented in figure 5.14, where a self aligned signal and a current aligned signal are tested. Here is also illustrated the performance of PWM with Min-Max injection (as in the previous simulations) and the performance of FCS-MPC with simple penalization. As shown by these results, the use of D3HI has an major effect in the performance of PWM strategies, achieving an significant reduction in SPL. It is also shown that the alignment with the grid current improves the performance, though in less degree, since this blocks the phase with the biggest current. Nonetheless all this, the use of FCS-MPC with simple penalization over the switching does provide a better performance than any of the PWM strategies.

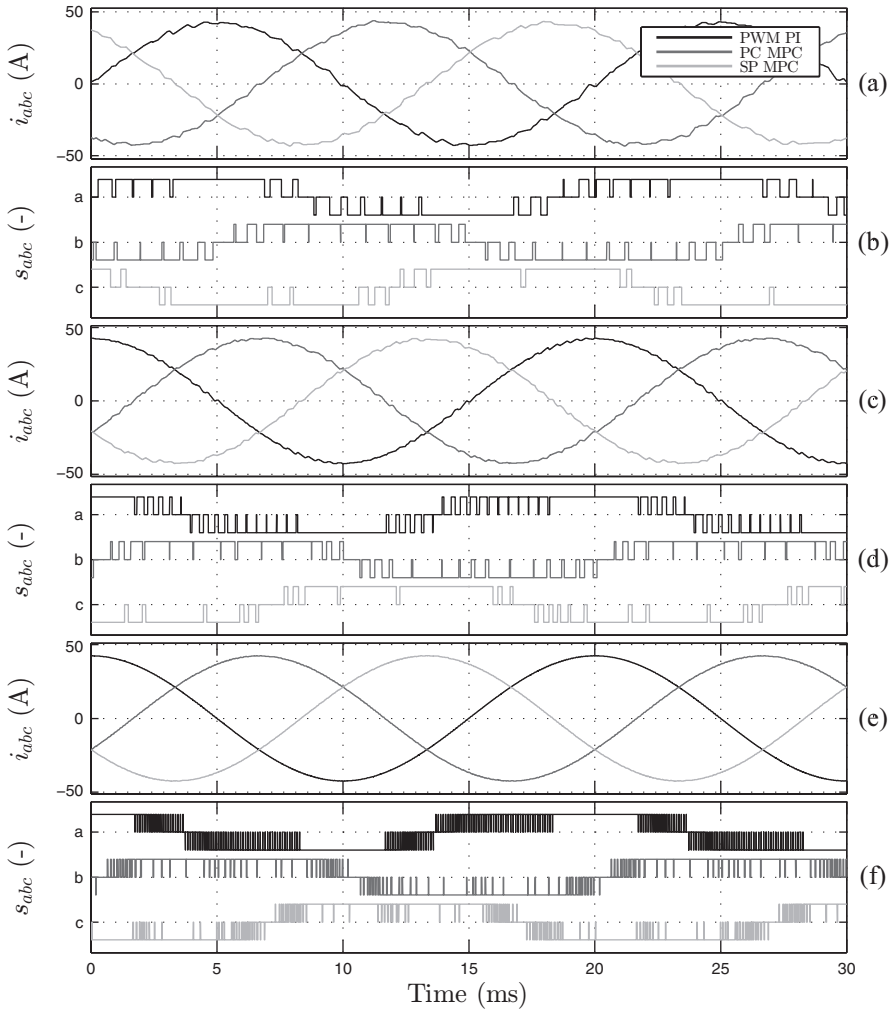

Figure 5.11: Current and output signal of a 3-phase NPC converter with purely inductive load, for (a)-(b) THD$\approx 2.5\%$, (c)-(d) THD$\approx 1.5\%$ and (e)-(f) THD$\approx 0.5\%$

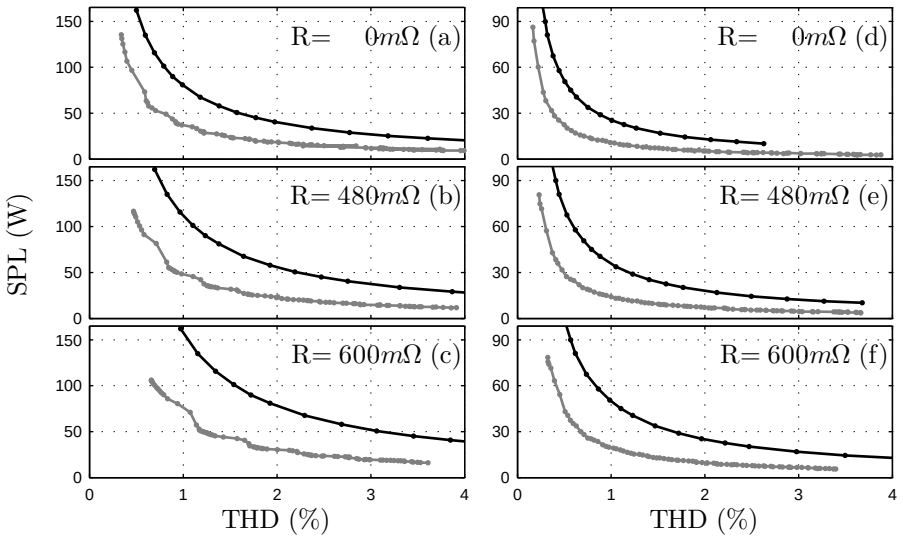

Figure 5.12: Performance curves of the (a)-(c) 2-level 3-phase converter and the (d)-(f) NPC converter for different loads

5.3 Three Phase Current-Aligned Weight

The aim of this work is to expand the ideas presented in [43], about penalizing the switching with a current alignment, to a three-phase system and evaluate its performance. Unlike the alignment profile presented in [43], that drastically changes the weight factor associated with the switching penalization, the new proposal also includes new profiles that aim to smooth the transition between high and low weight factors. Therefore, along with the two topologies, different alignment profiles are evaluated, implementing the cost function element

$$J_{sw}(t) = \lambda_{sw} \sum_{x \in \{a,b,c\}} P_x(t) \Delta S_{p,x} \ , \tag{5.14}$$

where $P_x(t)$ corresponds to the value of the pondering profile at time t for phase $x \in \{a, b, c\}$, $\Delta S_{p,x}$ is the switching detection for phase x, and λ_{sw} is a constant weighting factor used as base.

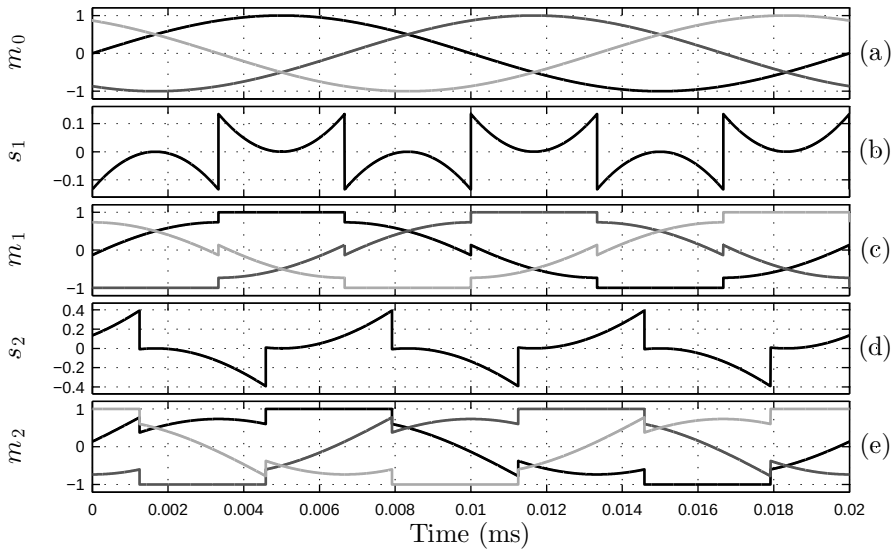

Figure 5.13: Discontinuous S-SVM; (a) Original modulation, (b) Injected discontinuous self-aligned signal and (c) the respective modified modulation, (d) Injected discontinuous current-aligned signal and (e) the respective modified modulation

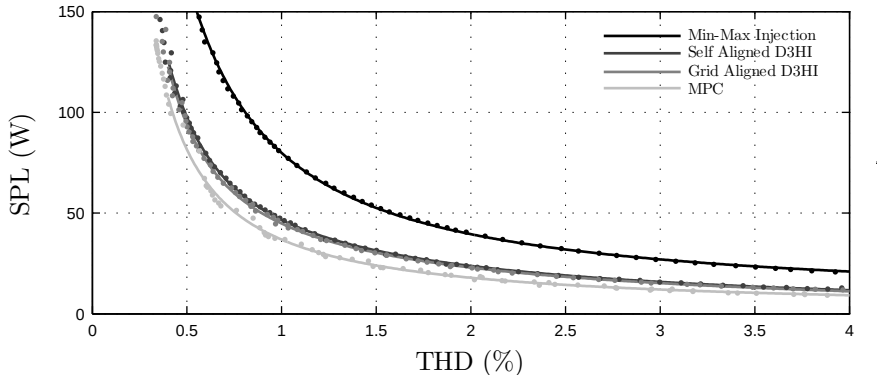

Figure 5.14: Discontinuous 3^{rd} harmonic injection performance

5.3.1 Pondering Profiles

The strategy used in [43] makes use of a varying weight factor to allow more or less commutations in line with the current. This weight factor is proportional to the current when said current is above a defined limit, thus penalizing high current switching, and is set to zero when it is bellow this level, releasing the switching control. Though effective in penalizing the switching for high currents, it provides no guarantee of being actually better than other profiles, or simply no profile, in terms of power losses. This is due to the fact that for low levels there is no control over the commutations, thus neglecting the switching losses during this period. The behavior of a two-level converter using this profile is illustrated in figure 5.15. Here it can be seen that for low current values the switching control is completely neglected, resulting in a very smooth current and a high amount of non zero current commutations. This leads to high switching losses, though less than without control whatsoever, while also reducing the current quality in the peaks.

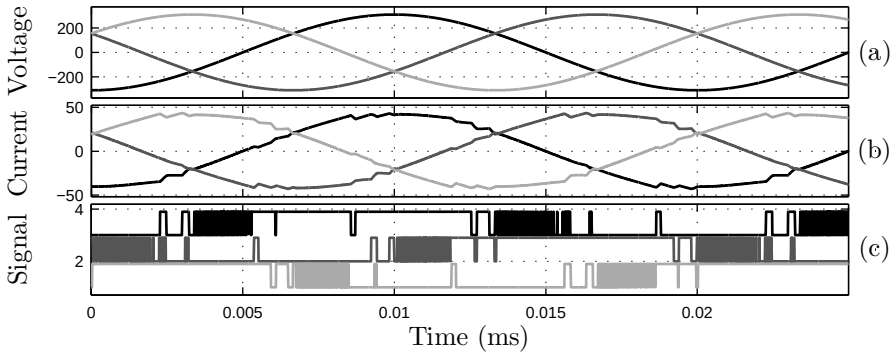

Figure 5.15: Switching weight alignment with the current, Square profile: (a) Grid voltage, (b) Grid Current and (c) Gate signals

To address this issue, different pondering profiles are proposed for evaluation. These profiles aim to soften the transitions between high and low effective weight factors, thus expecting to get a smoother performance. Figure 5.16(a) illustrates the normalized sinusoidal phase current to which the respective profile would be aligned to. The first pondering profile, 5.16(b), follows the same design criteria illustrated in [43], with an on-off behavior of the switching penalization, allowing a free switching for low currents. The second one, 5.16(c), aims to soften the transition between active and inactive with medium step. In the same line of thought, 5.16(d) transits from full weight to zero in a straight line, from which is expected a much smoother performance. The fourth and fifth profiles, 5.16(e) and (f), aim to transit between weights through different paths, being these the rec-

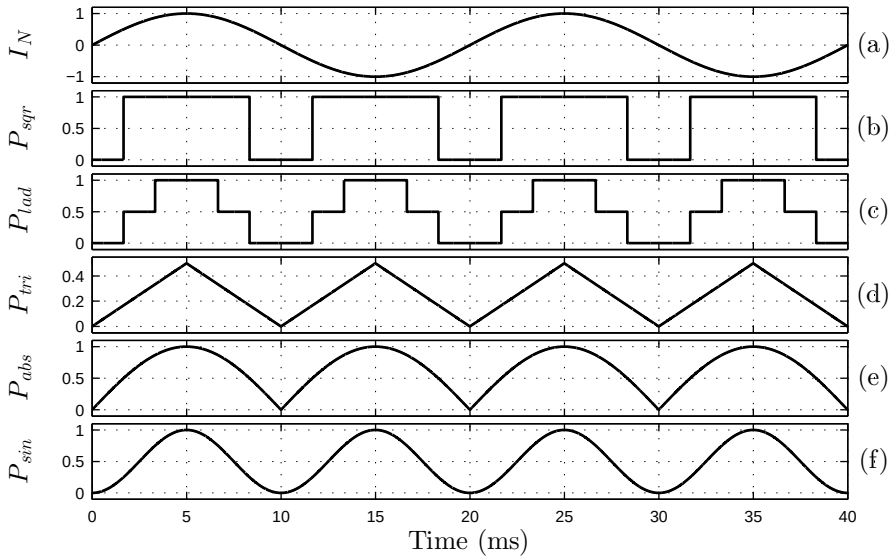

Figure 5.16: (a)Normalized phase current and (b)-(e) Pondering profiles aligned to said current

tified current and its squared value respectively, in order to evaluate the difference between these paths. Each of the pondering profiles is computed as follows,

$$P_{sqr}(t) = \begin{cases} 1 & if \ \ |i_r(t)|/\hat{I} > \frac{1}{2} \\ 0 & if \ \ |i_r(t)|/\hat{I} < \frac{1}{2} \end{cases} \tag{5.15}$$

$$P_{lad}(t) = \begin{cases} 1 & if \quad \frac{\sqrt{3}}{2} < |i_r(t)|/\hat{I} \\ \frac{1}{2} & if \quad \frac{1}{2} < |i_r(t)|/\hat{I} < \frac{\sqrt{3}}{2} \\ 0 & if \qquad |i_r(t)|/\hat{I} < \frac{1}{2} \end{cases} \tag{5.16}$$

$$P_{tri}(t) = \begin{cases} 2 + \frac{2\theta_r(t)}{\pi} & if \quad -1 < \frac{\theta_r(t)}{\pi} < -\frac{1}{2} \\ -\frac{2\theta_r(t)}{\pi} & if \quad -\frac{1}{2} < \frac{\theta_r(t)}{\pi} < 0 \\ +\frac{2\theta_r(t)}{\pi} & if \quad 0 < \frac{\theta_r(t)}{\pi} < \frac{1}{2} \\ 2 - \frac{2\theta_r(t)}{\pi} & if \quad \frac{1}{2} < \frac{\theta_r(t)}{\pi} < 1 \end{cases} \tag{5.17}$$

$$P_{abs}(t) = |i_r(t)|/\hat{I} \tag{5.18}$$

$$P_{sin}(t) = \left(|i_r(t)|/\hat{I}\right)^2 \tag{5.19}$$

where i_r is the respective current reference for each phase, $\theta_r \in]-\pi, \pi]$ the corresponding phase angle, $\hat{I}$ the reference amplitude

Table 5.1: Simulation parameters

Variable	Parameter	Value
V_{dc}	DC Voltage	600 V
L	Grid Inductance	10 mH
V_g	Grid Voltage	$220\sqrt{2}$ V
F_g	Grid Frequency	50 Hz
I_r	Reference Current	$30\sqrt{2}$ A
f_s	Sampling Frequency	100 kHz
P_N	Nominal Power	20 kW

As described so far, each of the pondering profiles is capable of reaching zero at some point in a fundamental cycle. Reaching zero in the weight factor means that the switching is neglected during that period of time, albeit short for the three last profiles. This could lead to undesired commutations and unnecessary losses. To address this issue, the actual value of the profile implemented in the cost function is lifted by a shift factor $\beta \in]0, 1]$, leading to

$$\mathbf{P} = P_n(1 - \beta) + \beta \tag{5.20}$$

where P_n is either of the proposed pondering profiles.

5.3.2 Simulation Performance

To evaluate the performance of the proposed pondering profiles the two presented three-phase systems are simulated under the same conditions. The parameters for these simulations are listed in table 5.1.

Both systems are simulated for each pondering profile, leaving the base switching weight factor, λ_{sw}, as a tuning parameter. For the purpose of all simulations the profile alignment is locked to the reference current instead of the measured one, since this should yield a more stable performance.

2-Level 3-Phase converter

As a first approach to the evaluation of each pondering profile, the 2-level 3-phase converter is tested. Figure 5.17 shows the outcome of each pondering profiles with a shift factor $\beta = 0.2$. The base weight factor, λ_{sw} is tuned independently for each profile in order for each to present a THD around 3%. A constant weight factor, not pondered by profile,

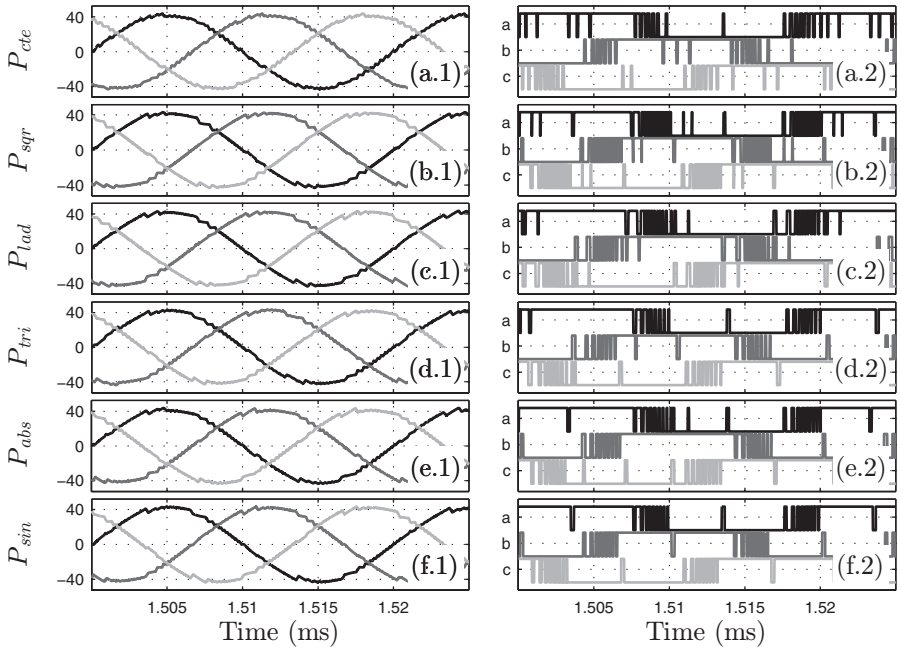

Figure 5.17: 3% THD performance for each pondering profile for $\beta = 2$: (x.1) Output current and (x.2) Gate signals

is also included in the analysis as reference, to evaluate if there is actually an improvement with the proposed changes.

From these simulations it can be seen that the performance achieved for the current tracking for each profile is actually very similar. A better tracking performance seems to be achieved for low current levels for all profiles other than constant, whereas for high currents it can be appreciated a slight increase in the ripple. Whilst the currents are very similar, the switching pattern differences for each profile are more noticeable. Though it is possible to recognize some differences among pondering profiles, it is not enough to properly asses their performance in a meaningful manner.

By testing each pondering profile for multiple base weight factors, an SPL vs THD plot can be constructed, in a similar fashion as presented section 5.2.3. These results are shown in figure 5.18, along the PWM performance as reference. Since all the curve obtained from MPC are very close to each other it is difficult to see how they behave in relation to each other. To address this issue, the Flat Profile performance curve is subtracted from the other MPC curves, thus getting a better look at how the behave in relation to the base. To do this, each curve has to be approximated by a best fitting curve, process that is explained

in 6.1. The result of this approximation is presented in solid line in figure 5.18, and the subtractions in figure 5.19. Here it can be seen that the originally proposed profile, in cyan, provides worst results than if no profile is used, in blue, since for the same THD the switching losses are actually worse than before. On the same line, but with slightly better performance than the base, is the ladder profile, that also provides worst results than when no profile is used. On the other hand, the triangular and rectified profiles present almost identical performances, providing less power losses than no profile for the same harmonic distortion. A similar result can be observed for the P_{sin} profile, though slightly shifted up, thus reaching a performance almost identical to the base line. Overall, these results confirm that, for the 2-level 3-phase converter, the use of a pondering profile aligned with the current does change, albeit slightly, the overall performance of the controller. The three last pondering profiles do improve the performance of the system, which is the main objective to be achieved in this study.

5.3.3 Shift Factor

An element not evaluated so far is the effect that a change in the shift factor β has in the overall performance of the controller. The previous results where obtained for a $\beta = 0.2$. Nonetheless, different performances can be achieved for each profile when this factor is modified.

Figure 5.20 show the computed performance for different values of β for the P_{sqr} profile. Here it can be seen that for a properly chosen value of β, the Step profile can actually improve the performance of FCS-MPC. As can be observed, for values of β greater than 0.5 the performance is improved, showing the best results near $\beta = .6$. For the purpose of this analysis, the best result is considered to be the one that provides the lowest SPL in widest range of THD. It is also included in this criteria the demand that the pondering profiles SPL remains bellow the SPL achieved by a flat profile in all the studied range.

In a similar fashion, it is possible to search for the best shift factor β for each pondering profile in order to reach the best performance. Figure 5.21 shows the performance of each pondering profile, each for the best values of β. It can be seen that, aside from the P_{sqr} profile, all curves reach a very similar performance, and all improving in terms of power losses in comparison to a constant weight factor. The values of β for these results are, in order off appearance, 0.5, 0.3, 0.2, 0.3 and 0.3.

From these results it can be concluded that the use pondering profiles to change the weight factor associated with the switching penalization does improve the control performance of FCS-MPC. The main reason to use different pondering profiles, instead of just using the step profile originally proposed, is to allow a smoother transition between high and low penalization of the switching. This concept showed to be effective in improving

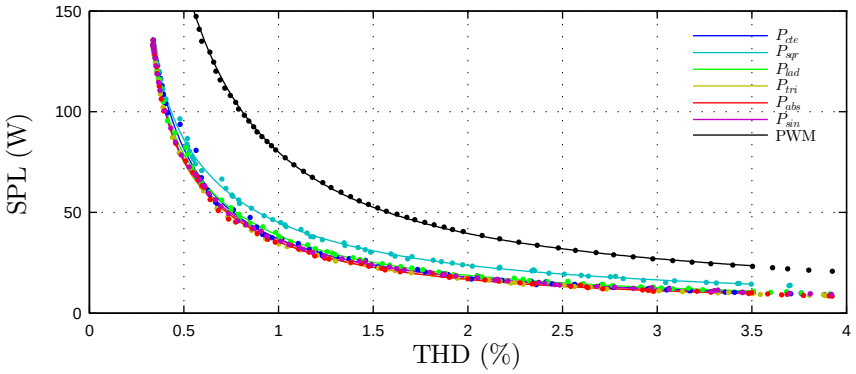

Figure 5.18: Simulation performance of the 2-level converter, for each pondering profile with multiple base weight factors λ_{sw}: $(\cdot\cdot)$ Simulated data and $(-)$ Best fitting curves

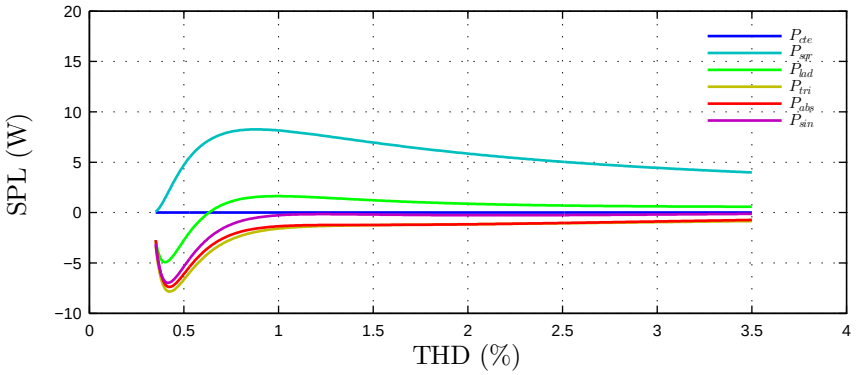

Figure 5.19: Switching losses of the 2-level converter, for each pondering profile compared to a constant pondering profile

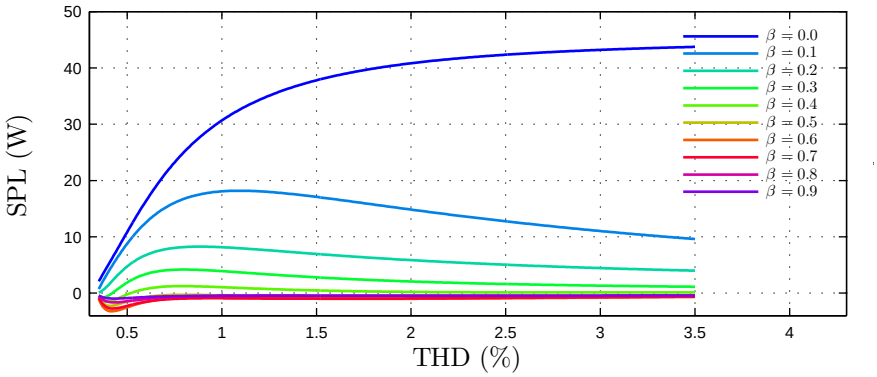

Figure 5.20: Switching losses for the step profile compared to a constant pondering profile, for different values of β

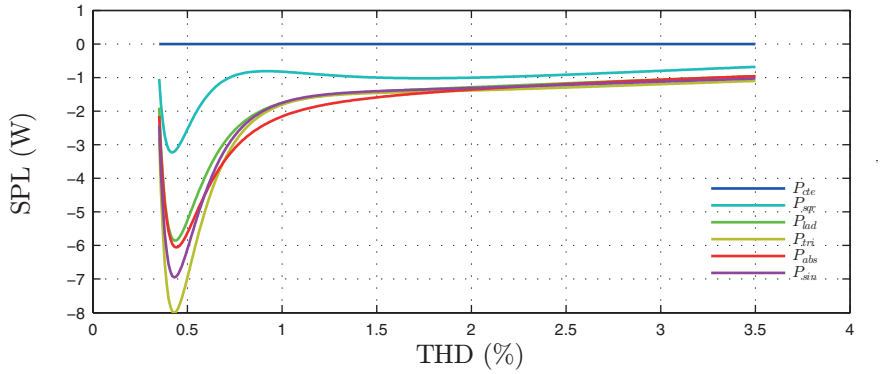

Figure 5.21: Simulation performance of a 2-level converter for each profile compared to the constant pondering profile, tuned for the best values β

the loss reduction, since softer curve do perform better. This is further reinforced by the fact that a properly chosen shift factor β also improves the performance, since this factor softens the effects of each profiles.

The base weight factor over which each profile was tested, though similar in magnitude and range, is not identical, and there seems to be no correlation between one another to suggest a predictable behavior when changed. The same analysis applies to the best shift factor β, that is independent for each profile.

3-Phase NPC Converter

So far the use of pondering profiles to modify the weight factor associated with the switching cost have shown to be effective in improving the control performance for the 2-level 3-phase converter. The goal now is to verify if this improvement can be expanded to a different system without major changes in the strategy, and if it this improvement is of similar magnitude.

As done with the previous system, the NPC is simulated with the same load and grid, as well as the same DC source and current references. Each of the pondering profiles is tested for a wide range of weight factors, though adjusted to move in a THD range up to 4%. In a similar fashion as before, figure 5.22 shows the resulting waveforms generated by the use of each profile with a shift factor $\beta = 0.2$, reaching for a THD value of 2%. As with the 2-level converter, the resulting current for each profile is very similar, but still showing a better tracking behavior for small current values. The main difference between the performance shown here and the one achieved by the 2-level converter is the lower THD and SPL range. These differences can be attributed to the higher amount of voltage levels available to the NPC converter and the smaller voltage blocked by each semiconductor, thus reaching a much more efficient performance.

Aggregating these results for multiple weight factors λ_{sw} in the SPL vs THD plot, and computing the best fitting curve for each, figure 5.23 is constructed. Here is also presented the switching losses vs THD caused by a PI control strategy for a range of switching frequencies.

As happened with the 2-level converter, all the profiles achieved a better performance than a PWM control by virtue of generating less switching losses for the same harmonic distortion. Yet again, the Step profile is the one that produces the worst result in terms of switching losses, followed by the Ladder profile, and then the others, that generate similar performances.

By changing the shift factor β it is possible to improve the performance of each profile, reaching the best possible outcomes. These results are presented in figure 5.25, where the values of β are, in order of appearance, 0.5, 0.5, 0.2, 0.3 and 0.2.

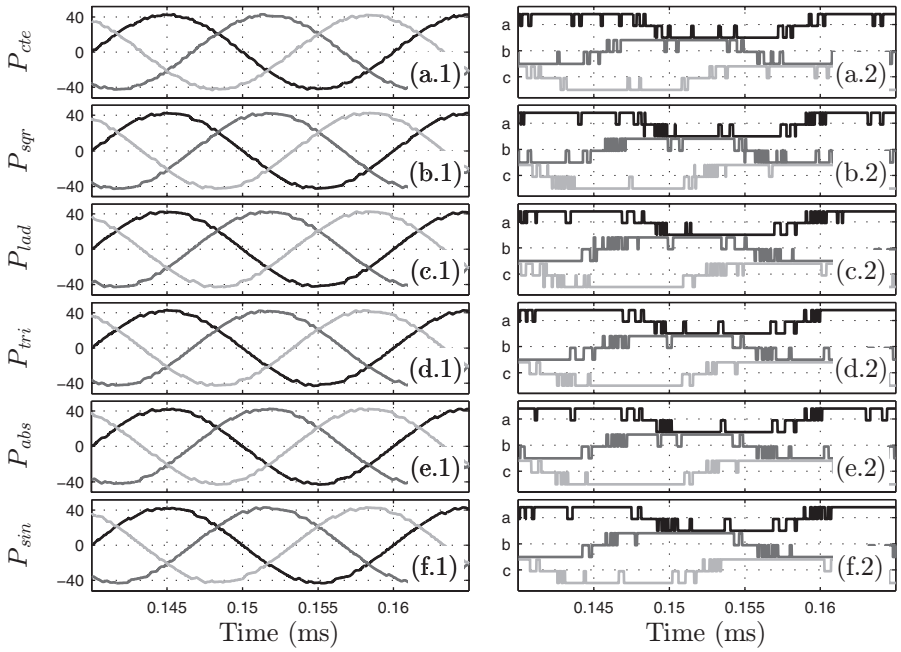

Figure 5.22: 2% THD performance for each pondering profile for $\beta = 2$: (x.1) Output current and (x.2) Gate signals

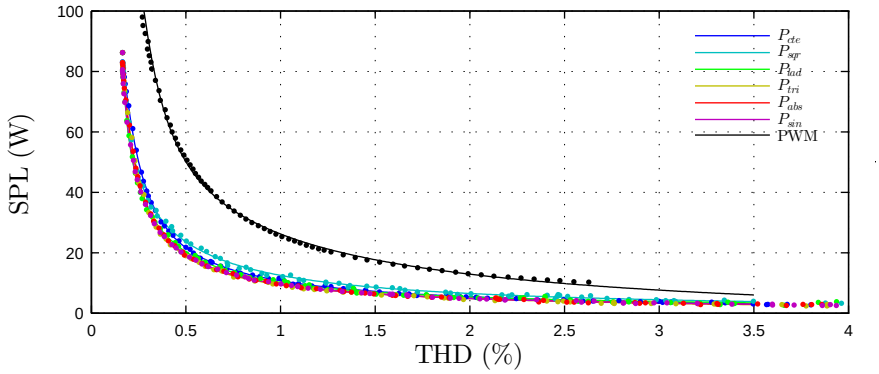

Figure 5.23: Simulation performance for each pondering profile with multiple base weight factors λ_{sw}: $(\cdot\cdot)$ Simulated data and $(-)$ Best fitting curves

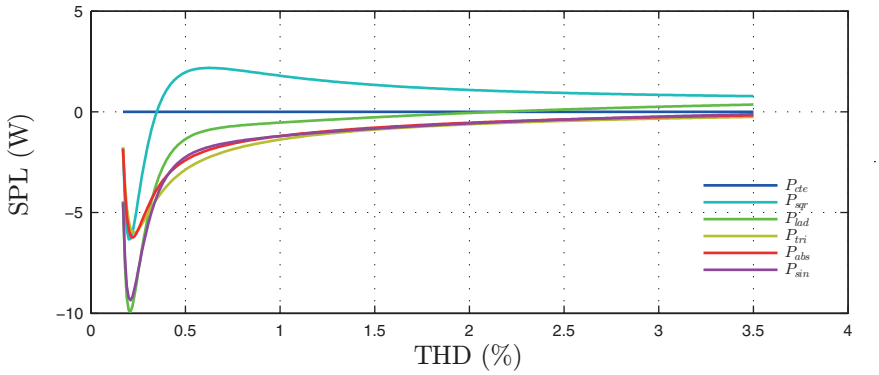

Figure 5.24: Switching losses for each pondering profile compared to a constant pondering profile

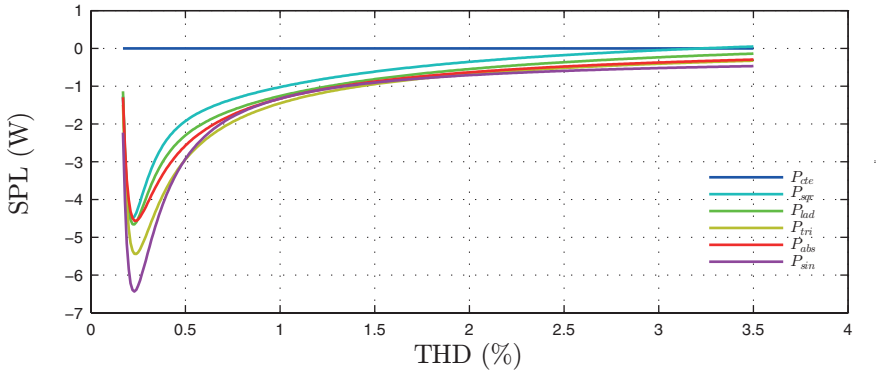

Figure 5.25: Simulation performance of an NPC converter for each profile compared to the constant pondering profile, tuned for the best values β

From these results it can be seen that with a proper selection of the shift factor β it is possible to improve the performances of many of the profiles. Nonetheless, even with the best β, the Step profile still reaches a worst performance than a constant weight factor, albeit only for high THD values.

Overall, the improvement achieved by using pondering profiles on the control of the NPC seems to yield good results, though not as consistent as the ones obtained for the 2-level converter, where all the profiles are capable of reaching a better performance in all the studied range. This reduced improvement may be caused by the fact that the system is already more efficient due to the increase number of levels involved in the control, thus making it harder to reach better performances. It is important to notice that the reduce improvement is seen only for higher THD values, while for low THDs the performance is similar in each converter.

5.4 Current Aligned Period Control

The use of pondering profiles to change the weight factor associated with the switching penalization has shown to be effective in improving the control performance for FCS-MPC. The studied controller so far makes use of a Simple Penalization strategy to punish the switching action on the cost function. The choice of this strategy is based on its simple design, implying a reduced amount of variables involved in the final control design. This allows to verify the importance of the design elements in this control strategy, being these the chosen profile P_x, the base weight factor λ_{sw} and the shift factor β

Section 2.5 presents some alternatives to control the switching frequency, among which

Simple Penalization is the easiest to understand and implement. In the following chapter it is presented Period Control as an alternative to control the switching frequency, showing favorable results in terms of spectrum and compliance with the frequency reference. Based on these favorable characteristics, it becomes interesting to study the effects that the pondering profiles might have over its performance. Therefore, Period Control is implemented in both the 2-level converter as well as the NPC converter, and its weight factor is dynamically changed in line with the output current.

In a similar fashion as with the simple penalization tests, the base weight factor λ_{sw} is changed along a wide range of values, and the respective steady state for each is evaluated for its harmonic distortion and switching losses. The results of these test for a flat profile where presented previously in figures 5.8 and 5.10, for the 2-level and NPC converters.

Since the used of the shifting factor β has already been shown effective in improving the controller performance, figure 5.26 shows the SPL vs THD results of each profile tuned to the best outcome for a 2-level converter. Figure 5.27 presents the same results subtracting the constant value profile. As can be seen here, though an improvement can be appreciated when compared with a constant profile, the results are much more modest than those obtained with simple penalization, while also reaching a final performance that is definitely worse than with simple penalization in terms of SPL and THD, as can be seen when compared with figure 5.18 This is due to the main trait of Period Control, that is, to reach a similar performance as can be achieved with a PWM strategy.

This behavior can also be appreciated in the NPC converter, as shown in figures 5.28 and 5.29. For this converter, the performance of NPC with Period Control still reaches the same performance of PWM for high values of the base weight factor λ_{sw}, regardless of the use of pondering profiles to improve it. Nonetheless, an improvement can be appreciated, albeit small when compared with Simple Penalization.

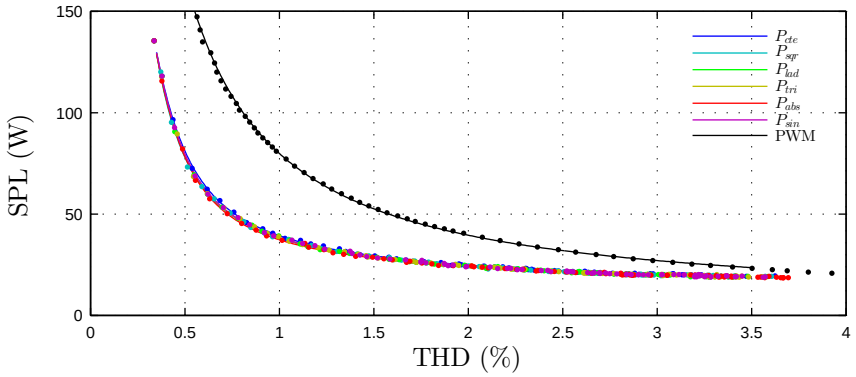

Figure 5.26: Simulation performance of a 2-level 3-phase converter with Period Control strategy, for each profile tuned for the best values β

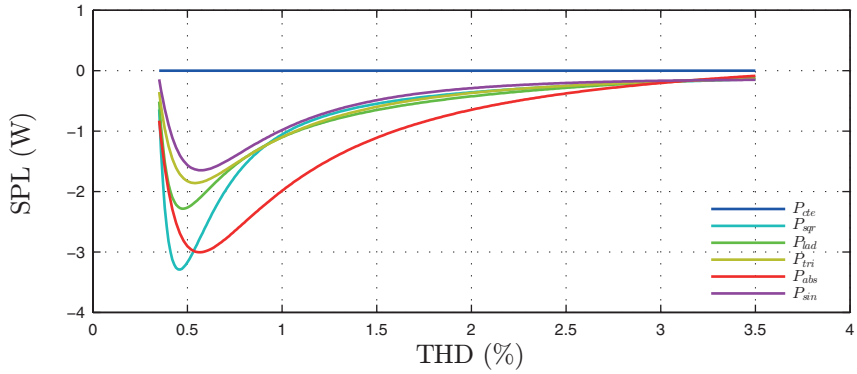

Figure 5.27: Simulation performance of a 2-level 3-phase converter with Period Control strategy, for each profile compared to the constant pondering profile, tuned for the best values β

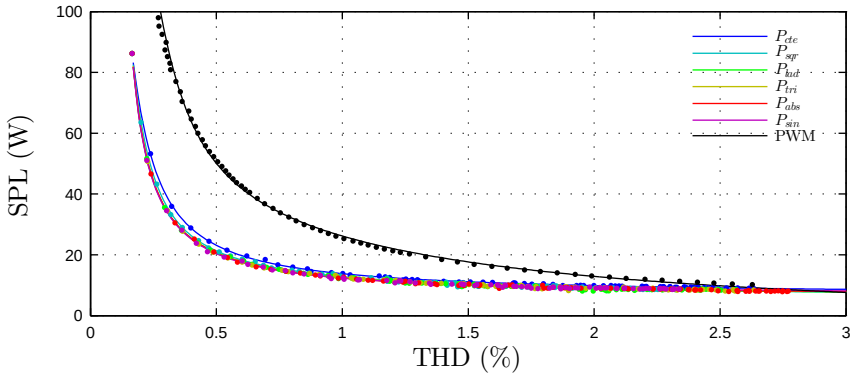

Figure 5.28: Simulation performance of an NPC converter with Period Control strategy, for each profile tuned for the best values β

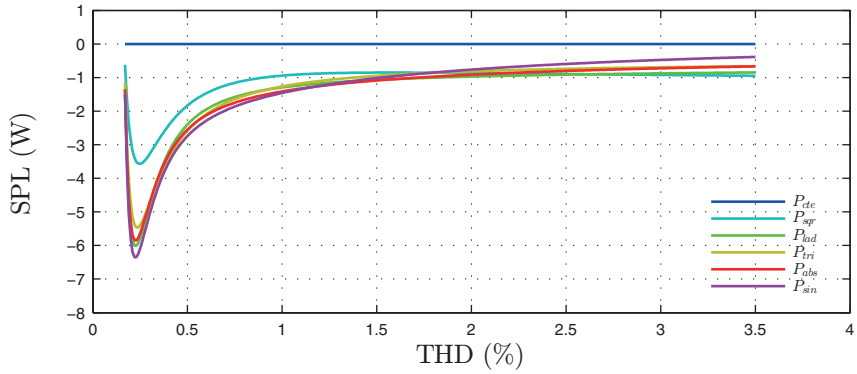

Figure 5.29: Simulation performance of an NPC converter with Period Control strategy, for each profile compared to the constant pondering profile, tuned for the best values β

Chapter 6

Conclusions

The main objective to the work presented in this document was to address the problem of variable switching frequency for FCS-MPC, due to the limitation this impose in its implementation in renewable energy conversion systems. The goal of addressing the switching frequency is to reduce the switching losses, which is a major issue in high power applications, and improve the power quality provided to the grid. For this, two solutions has been presented. The first solution, Period Control, achieves the proper control of the switching frequency through the design of a measurement that is included in the cost function as new control objective. The second solution embraces the variable frequency quality of FCS-MPC, by designing a variable weight factor associated with the switching frequency, to allow a better distribution of the switching events for 3-phase systems in order to reduce the switching losses.

On regard of Period Control, the main objective of this strategy was not only to achieve a lower switching frequency, but to do so in a similar way as modulated strategies operate. This is achieved through the design of a new variable in charge of measuring the switching period, as well as a two step prediction strategy that treats differently the delay compensation and the prediction stage. The use of Period Control as switching frequency controller has shown to be effective in reaching a switching performance very similar to that of a PWM strategy. Even more, this similarity is proved to be present even in the harmonics generated by the controller, which confirms that the achieved performance is in fact strongly related to a PWM strategy.

Not only it is proven that Period Control mimics a PWM strategy, but also that is can be implemented in any kind of converter, as long as the operation of each semiconductor is free from restriction. This is due to the structure of the period measurement, that focus

on each semiconductor independently. Regardless of this limitation, it is fairly straightforward to implement this strategy in an interleaved converter or an NPC converter, albeit with minor changes to control structure. It is also proven that a wide range of switching frequencies are achievable by this strategy. This provides Period Control with an additional control variable that most controller do not posses, that is the possibility of changing the switching frequency online.

On the design of the strategy it also established the necessary precautions for the weight factor design to allow a seamless transition between systems, either for different switching frequency references or sampling frequency. With these precautions it is possible to design a weight factor for a particular control system, and be fairly confident that it should operate properly if these parameters are changed.

Along all these favorable traits, Period Control can be implemented in a FCS-MPC controller with barely any drawback other than an easy to fix phase delay. This strategy is fairly easy to program, requiring very few modifications to an already functioning controller. Since the period measurement have dynamics similar to other control objectives, the inclusion of this element in a cost function should not cause major disturbances, other than reducing the switching frequency and the corresponding consequences. Also, if a system is already impervious to the switching frequency used for its control, the addition of this control element should behave as a decoupled variable, which further reinforce the idea of little disturbance in other control objectives.

An important analysis reported in this document is the comparison of Period Control against other previously reported strategies that share similar objectives and structure. Against these strategies Period Control showed significant advantages, though not coming ahead in every aspect, but presenting a better overall performance. In terms computation time, it falls short only to Simple Penalization, which is by default the least demanding switching regulation strategy. In terms of reaching a reference average switching frequency, Sliding Window proved to be a fair contender, approaching both asymptotically to the objective frequency. In terms of clean spectrum, NOTCH filter was capable of reaching a cleaner performance, though Period Control was capable or producing a very clean spectrum.

Among all these strategies, only Period Control showed the capability of consistently reaching a performance similar to PWM techniques. It generates the most stable switching frequency among these strategies, guaranteeing a very predictable steady state switching pattern. It also provided the best control over the current amplitude, while causing a very linear phase shift that is easily corrected.

On the topic of variable weight factor, a strategy to better select the switching events has been designed. This strategy has been proved to be effective in reducing the switching power losses when compared against a raw simple penalization strategy, which in turn is better than PWM strategies. The core idea behind this strategy is to reduce the switching events of a semiconductor when the current flowing through it is high. Multiple alternatives to change the weight factor has been tested, in the form of pondering profiles, arriving to the conclusion that as long as the parameters are well selected each of these profiles is capable of improving the performance. The critical parameter to make a these profiles feasible is the shift factor β.

An attempt has been made to fuse both Period Control and Variable Weight Factor strategies, but without significant results. The main reason for this is that Period Control aims for a switching pattern similar to a PWM. Therefore, the expected performance of Period Control, in terms of switching losses, goes in the same direction as PWM, which conflicts with the Variable Weight Factor goal.

Since so far it has not been achieved a proper integration between the proposed strategies, the question rises about which one would be most effective for a renewable energy conversion system as presented before.

Period Control allows a clean power quality by virtue of reaching a stable switching frequency. This makes it easier to comply with the grid code, and assures a consistent performance. Nonetheless, by stabilizing the frequency, the efficiency of the converter approaches more to a PWM strategy, which has been shown to be less efficient than predictive control with simple penalization. If for the particular system in which these strategies would be tested Variable Weight Factor is capable of complying with the grid code, then this would always be the go to alternative due to the reduced power losses. This could be achieved by moving the base weight factor of Simple Penalization, reaching a better harmonic distortion, accompanied by a lower switching losses that Period Control.

An important matter in this analysis is that Period Control is not bound to work only in renewable energy systems. The strategy has been designed with the objective of controlling the switching frequency regardless of the system that is being controlled. In this matter Period Control has shown to be really effective. It is an easy to implement strategy that can be seemingly included in any FCS-MPC algorithm with minor disturbance to other control objectives. It is easy to compute, which makes it a feasible option for multiple control platforms, and requires very little effort to scale it to more complex systems.

Overall, Period Control solves, at least for the systems presented in this document, one

of the main counterarguments for FCS-MPC, that is the irregular switching frequency.

6.1 Future Work

During the research process that lead to the contributions presented in this document many ideas and project have come to the table that, due to time constrains or other limitations, has not been completed or studied appropriately. The following is a brief list of some of these topics.

- Implementation of Period Control in a wider variety of converters. One of the strongest claims during this work is that it is possible to implement Period Control in multiple systems, without major changes to the base structure and without detriment to other control objectives. Though tested during the development phases of this strategy, these application has not been properly documented nor analyzed in due detail.
- Combine both contributions of Variable Weight Factor and Period Control into one improved strategy. Even though the results of the attempt of merging both contributions are unsatisfactory, not all alternatives to fuse both strategies has been implemented or tested thoroughly, and are interesting topics for future research.
- Experimental implementation of the Variable Weight Factor strategy in order to properly validate the improvements proposed by this strategy.

Bibliography

[1] REN21, *Renewables 2018 Global Status Report*, 2018.

[2] H. Abu-Rub, M. Malinowski, and K. Al-Haddad, *Power Electronics for Renewable Energy Systems, Transportation and Industrial Applications*. John Wiley & Sons Ltd, 2012.

[3] A. Molina, M. Falvey, and R. Rondanelli, "A solar radiation database for chile," *Scientific Reports*, vol. 54, no. 6, pp. 2045–2322, Nov 2017.

[4] M. de Energía Gobierno de Chile and GIZ, *Energías Renovables en Chile: Potencial eólico, solar e hidroeléctrico de arica a chiloé*, 2014.

[5] C. A. Rojas, M. Aguirre, S. Kouro, T. Geyer, and E. Gutierrez, "Leakage current mitigation in photovoltaic string inverter using predictive control with fixed average switching frequency," *IEEE Transactions on Industrial Electronics*, vol. 64, no. 12, pp. 9344–9354, Dec 2017.

[6] D. Lopez, H. Renaudineau, F. Flores-Bahamonde, and S. Kouro, "Evaluation of photovoltaic microinverter configurations based on different converter stages and step-up voltage ratios," in *2017 19th European Conference on Power Electronics and Applications (EPE'17 ECCE Europe)*, Sept 2017, pp. P.1–P.8.

[7] S. Kouro, M. A. Perez, J. Rodriguez, A. M. Llor, and H. A. Young, "Model predictive control: Mpc's role in the evolution of power electronics," *IEEE Industrial Electronics Magazine*, vol. 9, no. 4, pp. 8–21, Dec 2015.

[8] S. Kouro, P. Cortes, R. Vargas, U. Ammann, and J. Rodriguez, "Model predictive control – a simple and powerful method to control power converters," *IEEE Transactions on Industrial Electronics*, vol. 56, no. 6, pp. 1826–1838, June 2009.

[9] J. Holtz, "Pulsewidth modulation for electronic power conversion," *Proceedings of the IEEE*, vol. 82, no. 8, pp. 1194–1214, Aug 1994.

[10] J. Holtz and X. Qi, "Optimal control of medium-voltage drives; an overview," *IEEE Transactions on Industrial Electronics*, vol. 60, no. 12, pp. 5472–5481, Dec 2013.

[11] L. Gil-Antonio, M. B. Saldivar-Marquez, and O. Portillo-Rodriguez, "Maximum power point tracking techniques in photovoltaic systems: A brief review," in *2016 13th International Conference on Power Electronics (CIEP)*, June 2016, pp. 317–322.

[12] R. Kennel and A. Linder, "Predictive control of inverter supplied electrical drives," in *2000 IEEE 31st Annual Power Electronics Specialists Conference. Conference Proceedings (Cat. No.00CH37018)*, vol. 2, 2000, pp. 761–766 vol.2.

[13] P. Cortes, M. P. Kazmierkowski, R. M. Kennel, D. E. Quevedo, and J. Rodriguez, "Predictive control in power electronics and drives," *IEEE Transactions on Industrial Electronics*, vol. 55, no. 12, pp. 4312–4324, Dec 2008.

[14] J. Holtz and S. Stadtfeld, "A predictive controller for the stator current vector of ac machines fed from a switched voltage source," in *Proc. IPEC, Tokyo, Japan*, 1983, pp. 1665–1675.

[15] S. Vazquez, J. Rodriguez, M. Rivera, L. G. Franquelo, and M. Norambuena, "Model predictive control for power converters and drives: Advances and trends," *IEEE Transactions on Industrial Electronics*, vol. 64, no. 2, pp. 935–947, Feb 2017.

[16] J. D. Barros and J. F. Silva, "Multilevel optimal predictive dynamic voltage restorer," *IEEE Transactions on Industrial Electronics*, vol. 57, no. 8, pp. 2747–2760, Aug 2010.

[17] P. Acuña, L. Morán, M. Rivera, R. Aguilera, R. Burgos, and V. G. Agelidis, "A single-objective predictive control method for a multivariable single-phase three-level npc converter-based active power filter," *IEEE Transactions on Industrial Electronics*, vol. 62, no. 7, pp. 4598–4607, July 2015.

[18] J. D. Barros and J. F. Silva, "Optimal predictive control of three-phase npc multilevel converter for power quality applications," *IEEE Transactions on Industrial Electronics*, vol. 55, no. 10, pp. 3670–3681, Oct 2008.

[19] R. Vargas, U. Ammann, B. Hudoffsky, J. Rodriguez, and P. Wheeler, "Predictive torque control of an induction machine fed by a matrix converter with reactive input power control," *IEEE Transactions on Power Electronics*, vol. 25, no. 6, pp. 1426–1438, June 2010.

[20] H. Miranda, P. Cortes, J. I. Yuz, and J. Rodriguez, "Predictive torque control of induction machines based on state-space models," *IEEE Transactions on Industrial Electronics*, vol. 56, no. 6, pp. 1916–1924, June 2009.

[21] T. Geyer, G. Papafotiou, and M. Morari, "Model predictive direct torque control part i: Concept, algorithm, and analysis," *IEEE Transactions on Industrial Electronics*, vol. 56, no. 6, pp. 1894–1905, June 2009.

[22] C. A. Silva and J. I. Yuz, "On sampled-data models for model predictive control," pp. 2966–2971, Nov 2010.

[23] C. A. Rojas, J. I. Yuz, M. Aguirre, and J. Rodriguez, "A comparison of discrete-time models for model predictive control of induction motor drives," in *2015 IEEE International Conference on Industrial Technology (ICIT)*, March 2015, pp. 568–573.

[24] R. Vargas, J. Rodriguez, U. Ammann, and P. W. Wheeler, "Predictive current control of an induction machine fed by a matrix converter with reactive power control," *IEEE Transactions on Industrial Electronics*, vol. 55, no. 12, pp. 4362–4371, Dec 2008.

[25] J. L. Elizondo, A. Olloqui, M. Rivera, M. E. Macias, O. Probst, O. M. Micheloud, and J. Rodriguez, "Model-based predictive rotor current control for grid synchronization of a dfig driven by an indirect matrix converter," *IEEE Journal of Emerging and Selected Topics in Power Electronics*, vol. 2, no. 4, pp. 715–726, Dec 2014.

[26] M. A. Perez, J. Rodriguez, E. J. Fuentes, and F. Kammerer, "Predictive control of ac-ac modular multilevel converters," *IEEE Transactions on Industrial Electronics*, vol. 59, no. 7, pp. 2832–2839, July 2012.

[27] R. P. Aguilera, P. Lezana, and D. E. Quevedo, "Finite-control-set model predictive control with improved steady-state performance," *IEEE Transactions on Industrial Informatics*, vol. 9, no. 2, pp. 658–667, May 2013.

[28] M. A. Perez, P. Cortes, and J. Rodriguez, "Predictive control algorithm technique for multilevel asymmetric cascaded h-bridge inverters," *IEEE Transactions on Industrial Electronics*, vol. 55, no. 12, pp. 4354–4361, Dec 2008.

[29] R. Kennel, A. Linder, and M. Linke, "Generalized predictive control (gpc)-ready for use in drive applications?" in *2001 IEEE 32nd Annual Power Electronics Specialists Conference (IEEE Cat. No.01CH37230)*, vol. 4, 2001, pp. 1839–1844 vol. 4.

[30] C. F. Garcia, C. A. Silva, J. R. Rodriguez, P. Zanchetta, and S. A. Odhano, "Modulated model predictive control with optimized overmodulation," *IEEE Journal of Emerging and Selected Topics in Power Electronics*, pp. 1–1, 2018.

[31] Z. Gong, X. Wu, P. Dai, and R. Zhu, "Modulated model predictive control for mmc-based active front-end rectifiers under unbalanced grid conditions," *IEEE Transactions on Industrial Electronics*, pp. 1–1, 2018.

[32] S. Vazquez, A. Marquez, R. Aguilera, D. Quevedo, J. I. Leon, and L. G. Franquelo, "Predictive optimal switching sequence direct power control for grid-connected power converters," *IEEE Transactions on Industrial Electronics*, vol. 62, no. 4, pp. 2010–2020, April 2015.

[33] S. A. Larrinaga, M. A. R. Vidal, E. Oyarbide, and J. R. T. Apraiz, "Predictive control strategy for dc/ac converters based on direct power control," *IEEE Transactions on Industrial Electronics*, vol. 54, no. 3, pp. 1261–1271, June 2007.

[34] P. Cortes, J. Rodriguez, C. Silva, and A. Flores, "Delay compensation in model predictive current control of a three-phase inverter," *IEEE Transactions on Industrial Electronics*, vol. 59, no. 2, pp. 1323–1325, Feb 2012.

[35] J. I. Yuz and G. C. Goodwin, "On sampled-data models for nonlinear systems," *IEEE Transactions on Automatic Control*, vol. 50, no. 10, pp. 1477–1489, Oct 2005.

[36] S. A. Davari, D. A. Khaburi, F. Wang, and R. M. Kennel, "Using full order and reduced order observers for robust sensorless predictive torque control of induction motors," *IEEE Transactions on Power Electronics*, vol. 27, no. 7, pp. 3424–3433, July 2012.

[37] A. Bemporad, F. Borrelli, and M. Morari, "Piecewise linear optimal controllers for hybrid systems," in *Proceedings of the 2000 American Control Conference. ACC (IEEE Cat. No.00CH36334)*, vol. 2, 2000, pp. 1190–1194 vol.2.

[38] ——, "Model predictive control based on linear programming - the explicit solution," *IEEE Transactions on Automatic Control*, vol. 47, no. 12, pp. 1974–1985, Dec 2002.

[39] R. Mikail, I. Husain, Y. Sozer, M. S. Islam, and T. Sebastian, "A fixed switching frequency predictive current control method for switched reluctance machines," *IEEE Transactions on Industry Applications*, vol. 50, no. 6, pp. 3717–3726, Nov 2014.

[40] L. Tarisciotti, P. Zanchetta, A. Watson, J. C. Clare, M. Degano, and S. Bifaretti, "Modulated model predictive control for a three-phase active rectifier," *IEEE Transactions on Industry Applications*, vol. 51, no. 2, pp. 1610–1620, March 2015.

[41] T. M. Wolbank, R. Stumberger, A. Lechner, and J. Machl, "Novel approach of constant switching-frequency inverter control with optimum current transient response," in *SPEEDAM 2010*, June 2010, pp. 803–808.

[42] M. Rivera, S. Kouro, J. Rodriguez, B. Wu, V. Yaramasu, J. Espinoza, and P. Melila, "Predictive current control in a current source inverter operating with low switching frequency," pp. 334–339, May 2013.

[43] E. Gutierrez, S. Kouro, C. A. Rojas, and M. Aguirre, "Predictive control of an h-npc converter for single-phase rooftop photovoltaic systems," in *2015 IEEE Energy Conversion Congress and Exposition (ECCE)*, Sept 2015, pp. 3295–3302.

[44] R. Teodorescu, *Grid Converters for Photovoltaic and Wind Power Systems*. Wiley, 2011.

Annex

RL load design

In order to design the three phase systems, the following criteria is used As a base structure, it is considered that the DC-link voltage, V_{dc} is equal to 600V, which is a common standard for grid connection. On the same line, the grid voltage is considered to be a perfect sinusoidal of amplitude $\hat{V}_g = 220\sqrt{2}$V, and a frequency of $\omega = 50$Hz. When analyzed in $\alpha\beta$ coordinates, the voltage amplitude generated by the converter must be equal to the grid voltage plus the voltage drop in the load

$$V_s = V_g + I(R + j\omega L)\,, \tag{6.1}$$

$$\hat{V}_s = \sqrt{\left(\hat{V}_g + \hat{I}R\right)^2 + \hat{I}^2\omega^2L^2}\,, \tag{6.2}$$

$$\measuredangle V_s = atan2\left(\hat{I}\omega L, \hat{V}_g + \hat{I}R\right) + \measuredangle V_g \tag{6.3}$$

For a PWM controlled converter, the output voltage amplitude is equal to

$$\hat{V}_s = m\frac{V_{dc}}{2} \tag{6.4}$$

Therefore, the maximum voltage the converter can produce consistently is equal to $V_{dc}\frac{1}{\sqrt{3}}$, which is achieved by applying a modulation index of $2/\sqrt{3} = 1.1547$ and a Min-Max injection.

For a system of power $P = \frac{3}{2}\hat{V}_g\hat{I}_r$, it is considered that the system should be able to allow an output current of at least 10% more than the reference, to allow the controller to compensate for ripple, noise and other disturbances. Therefore, for these parameters, the maximum values of R and L, for a purely resistive load and a purely inductive load

respectively, are

$$R_{max} = \frac{\hat{V}_s - \hat{V}_g}{\hat{I}_r/0.9} \tag{6.5}$$

$$L_{max} = \frac{\sqrt{\hat{V}_s^2 - \hat{V}_g^2}}{\omega \hat{I}_r/0.9} \tag{6.6}$$

For the system illustrated in section 5.2.4, the base modulation index is designed based on a purely inductive machine with $L_0 = 10$ mH,

$$m = \frac{\sqrt{\hat{V}_g^2 + \hat{I}_r^2 \omega^2 L_0^2}}{V_{dc}/2} \, . \tag{6.7}$$

Therefore, to maintain the same modulation index and the same output current for different values of R, the value of L must be computed as follows.

$$\hat{V}_s^2 = \left(\hat{V}_g + \hat{I}_r R\right)^2 + \hat{I}_r^2 \omega^2 L^2 \tag{6.8}$$

$$m^2 \tfrac{V_{dc}^2}{4} = \hat{V}_g^2 + 2\hat{V}_g \hat{I}_r R + \hat{I}_r^2 R^2 + \hat{I}_r^2 \omega^2 L^2 \tag{6.9}$$

$$\hat{V}_g^2 + \hat{I}_r^2 \omega^2 L_0^2 = \hat{V}_g^2 + 2\hat{V}_g \hat{I}_r R + \hat{I}_r^2 R^2 + \hat{I}_r^2 \omega^2 L^2 \tag{6.10}$$

$$\hat{I}_r^2 \omega^2 L^2 = \hat{I}_r^2 \omega^2 L_0^2 - 2\hat{V}_g \hat{I}_r R - \hat{I}_r^2 R^2 \tag{6.11}$$

$$L = \frac{\sqrt{\hat{I}_r^2 \omega^2 L_0^2 - 2\hat{V}_g \hat{I}_r R - \hat{I}_r^2 R^2}}{\hat{I}_r \omega} \tag{6.12}$$

Polinomial Regresion

The polynomial regression is the approximation of a dependent variable Y, that is function of an independent variable X, by a polynomial expression of the form

$$Y = b_0 + b_1 X + b_2 X^2 + ... + b_m X^m \, , \tag{6.13}$$

$$Y = \mathbf{X} B \, , \tag{6.14}$$

$$\mathbf{X} = \begin{bmatrix} 1 & x_1 & x_1^2 & ... & x_1^m \\ 1 & x_2 & x_2^2 & ... & x_2^m \\ 1 & x_3 & x_3^2 & ... & x_3^m \\ \vdots & \vdots & \vdots & \ddots & \vdots \\ 1 & x_n & x_n^2 & ... & x_n^m \end{bmatrix} \quad , \quad B = \begin{bmatrix} b_0 \\ b_1 \\ b_2 \\ \vdots \\ b_m \end{bmatrix} \, , \tag{6.15}$$

$$\tag{6.16}$$

where b_i, $i \in \{0, ..., m\}$, are the coefficients of said polynomial, and X and Y are both vectors of length n. In this expression, the use of X^q simply represents that each element of X is risen to the power q. If the degree of the polynomial is set to 1, then the process is referred to as linear regression. The values of b_i that best approximate these set of point is are computed as

$$B = \left(\mathbf{X}^T\mathbf{X}\right)^{-1}\mathbf{X}^T Y \ , \tag{6.17}$$

Publications

The following are the papers authored or coauthored by me that has been published during the PhD.

Journal Papers

- M. Aguirre, S. Kouro, C. A. Rojas, J. Rodriguez and J. I. Leon, "Switching Frequency Regulation for FCS-MPC Based on a Period Control Approach," in IEEE Transactions on Industrial Electronics, vol. 65, no. 7, pp. 5764-5773, July 2018. doi: 10.1109/TIE.2017.2777385

- C. A. Rojas, M. Aguirre, S. Kouro, T. Geyer and E. Gutierrez, "Leakage Current Mitigation in Photovoltaic String Inverter Using Predictive Control With Fixed Average Switching Frequency," in IEEE Transactions on Industrial Electronics, vol. 64, no. 12, pp. 9344-9354, Dec. 2017. doi: 10.1109/TIE.2017.2708003

Conference Papers

- M. Aguirre, S. Kouro, J. Rodriguez and H. Abu-Rub, "Model predictive control of interleaved boost converters for synchronous generator wind energy conversion systems," 2015 IEEE International Conference on Industrial Technology (ICIT), Seville, 2015, pp. 2295-2301. doi: 10.1109/ICIT.2015.7125436

- M. Aguirre, C. A. Rojas and S. Kouro, "Cascade-free model predictive control of a grid-tie multilevel photovoltaic system," IECON 2016 - 42nd Annual Conference of the IEEE Industrial Electronics Society, Florence, 2016, pp. 6734-6739. doi: 10.1109/IECON.2016.7793684

- H. Renaudineau, M. Aguirre and S. Kouro, "Single-phase dual-mode time-sharing PV string inverter," 2017 IEEE Southern Power Electronics Conference (SPEC), Puerto Varas, 2017, pp. 1-6. doi: 10.1109/SPEC.2017.8333613

- J. W. Zapata, S. Kouro, M. Aguirre and T. Meynard, "Model predictive control of interleaved dc-dc stage for photovoltaic microconverters," IECON 2015 - 41st Annual Conference of the IEEE Industrial Electronics Society, Yokohama, 2015, pp. 004311-004316. doi: 10.1109/IECON.2015.7392771

- C. A. Rojas, J. I. Yuz, M. Aguirre and J. Rodriguez, "A comparison of discrete-time models for model predictive control of induction motor drives," 2015 IEEE International Conference on Industrial Technology (ICIT), Seville, 2015, pp. 568-573. doi: 10.1109/ICIT.2015.7125159

- E. Gutierrez, S. Kouro, C. A. Rojas and M. Aguirre, "Predictive control of an H-NPC converter for single-phase rooftop photovoltaic systems," 2015 IEEE Energy Conversion Congress and Exposition (ECCE), Montreal, QC, 2015, pp. 3295-3302. doi: 10.1109/ECCE.2015.7310124